Interaction Between the AAA+ ATPase p97 and Its Cofactor Ataxin3 in Health and Disease

By Maya V. Rao

November 2017

A Dissertation Presented to the Faculty of Drexel University College of Medicine in partial fulfillment of the Requirement for the Degree of Doctor in Philosophy in Molecular and Cell Biology and Genetics

ACKNOWLEDGEMENTS

Writing this acknowledgement may prove more challenging than the actual dissertation. I've stared at a blank page for quite a while now; how does one truly convey all the love (both tough and tender), the support, inspiration, and never-ending patience that were the people in my life through these past years, without meandering aimlessly through worn-out clichés? (I wish I could cite a suitable reference here.) But today's submission day and I'm out of time, so here's my feeble attempt. It seems most appropriate to begin with Pat. Pat should be a separate acknowledgement chapter in this thesis, but I'll have to settle for an abstract. Thank you, Pat, for teaching me truly independent thought, for helping me realize my complex love for proteins and structural biology. Thank you for being an excellent professor, both in the classroom and in the lab, and an equally excellent baking enthusiast, the type that uses his students as guinea pigs for gorgeous baking experiments. Thank you for navigating through my nonsense, scientific and otherwise, for all the books I borrowed, and all the coffee, and finally thank you for making this PhD a reality.

A big thanks to my committee members, for being the perfect balance of critical and encouraging, for digging me out of the many holes I fell into, and for all the little bright ideas that eventually turned out to be big and important. In retrospect, I should have scheduled more committee meetings! A special thanks to Dr. Davis for waking me up from the dreaded PhD slump, and for generally being a key component of the complex PhD pathway.

To my family, Moky, Mama and Papa, for general amazingness, for always being on the other side of the phone whenever I needed them, and for proving that distance really doesn't matter. To Nikhil, who definitely has better words for this sentence. Now he too feels the joy of new crystals in a well, and the pain of air bubbles in an SEC column. To Susu and Babs, for being Susu and Babs. Everyone should have a Susu and Babs. They know what I mean. To friends in different parts of the country, Pia, Amrita, Ragini and Yomi, my getaways from PhD trauma and my champions in PhD triumph. THANK YOU!

Table of Contents

List of Tables

List of Illustrations

ABSTRACT

Interaction Between the AAA+ ATPase p97 and Its Cofactor Ataxin3 in Health and Disease
Maya V. Rao
Mentor: Patrick Loll, Ph.D.

p97 is an essential ATPase associated with various cellular activities (AAA+) that functions as a segregase in diverse cellular processes, including the maintenance of proteostasis. p97 interacts with different cofactors that target it to distinct pathways; an important example is the deubiquitinase ataxin3, which collaborates with p97 in endoplasmic reticulum associated degradation. However, the molecular details of this interaction have been unclear. We have characterized the binding of ataxin3 to p97, showing that ataxin3 binds with low-micromolar affinity to both wild-type p97 and mutants linked to degenerative disorders known as multisystem proteinopathy 1 (MSP1); we further showed that the stoichiometry of binding is one ataxin3 molecule per p97 hexamer. We have mapped the binding determinants on each protein, demonstrating that ataxin3's p97/VCP-binding motif (VBM) interacts with the inter-lobe cleft in the N-domain of p97. We also probed the nucleotide dependence of this interaction, confirming that ataxin3 and p97 associate in the presence of ATP and in the absence of nucleotide, but not in the presence of ADP. Our experiments suggest that an ADP-driven downward movement of the p97 N-terminal domain dislodges ataxin3 by inducing a steric clash between the D1-domain and ataxin3's C-terminus. In contrast, MSP1 mutants of p97 bind ataxin3 irrespective of their nucleotide state, indicating a failure by these mutants to translate ADP binding into a movement of the N-terminal domain. Our model provides a mechanistic explanation for how nucleotides regulate the p97–ataxin3 interaction and why atypical cofactor binding is observed with MSP1 mutants.

CHAPTER 1: Introduction

1.1. Protein homeostasis: *Maintaining the factory*

Protein homeostasis or proteostasis (1) is the synthesis, folding, transport and degradation of cellular proteins. The precise coordination of these processes sustains the fine balance of protein build-up and breakdown, which is vital to cell survival and function. Proteins are the worker molecules that perform almost every essential cellular activity, thus efficient protein turnover is key to a normal healthy cell. The proteostasis network is formed by a complex series of tightly regulated pathways that enforce protein quality control and ensure proteome stability (reviewed in (2)). The outcome is a steady supply of proteins, perfectly folded into their native conformations and targeted to appropriate locations in the cell.

The native three-dimensional structure of the protein is critical for its proper function. Proteins are folded into their distinct structures co-translationally, as the nascent polypeptide chain emerges from the ribosome. The nature of protein folding and the cellular environment is such that misfolding and unfolding events are relatively common.

The proteostasis systems exhibit a variety of strategies to degrade and clear away terminally misfolded proteins in a timely manner. When proteins misfold, specific pathways are activated, such as the cytosolic heat shock response and the unfolded protein response in the endoplasmic reticulum (ER) or mitochondria; these systems aid in refolding proteins via chaperones like the Hsp family (reviewed in (3,4)), or stimulate their clearance via the proteolytic machinery. Failure to refold, degrade or efficiently sequester aberrant proteins causes proteotoxic stress and ultimately leads to proteostatic collapse, which is deleterious to the cell (2). Potentially toxic proteins are allowed to accumulate and the cell suffers various protein aggregation-associated disorders that are typically neurodegenerative, such as Alzheimer's, Parkinson's, and Huntington's diseases (5). Most of these manifest later in life and are strongly correlated with aging, since our body loses the ability to efficiently remove defective proteins with age.

1.1.1. Degradation pathways: *Waste management*

The selective degradation of misfolded, damaged or aggregated proteins significantly contributes to maintaining a healthy proteome. Proteome stability can be perturbed by various physiological conditions, including metabolic or developmental changes in the cell or environmental stress (6). Eukaryotic cells respond to these challenges and ensure efficient protein turn-over by coordinating two major proteolytic pathways: the ubiquitin proteasome system (UPS), and a lysosomal degradation pathway termed autophagy (Fig. 1.1).

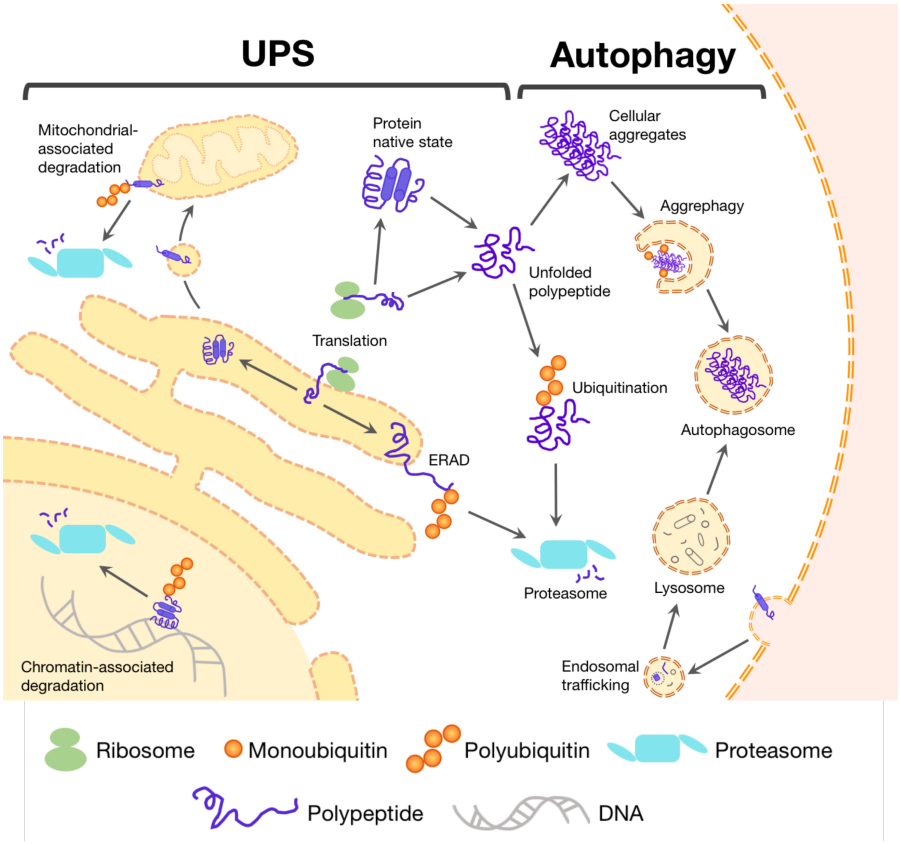

Figure 1.1 Cellular degradation pathways. The UPS and the aggresome-autophagy system are the two major routes for protein degradation in the cell. After a protein is translated in the cytoplasm, or co-translated into the ER, it undergoes multiple folding cycles to achieve its native state. Proteins that cannot reach their native fold, that unfold during cellular stress, or have accomplished their function, must be eliminated. Small and short-lived proteins are degraded by the UPS, while larger proteins, and aggregates of misfolded proteins, are handled by the autophagy system. The UPS also eliminates substrates through ER-, mitochondrial-, and chromatin-associated degradation. Figure adapted from (6,7,9).

The UPS is the primary degradation route for small polypeptides and short-lived proteins (7). The substrate protein is marked for destruction by the covalent attachment of the small protein tag ubiquitin, which then targets it to the proteasome – a barrel-shaped proteinase, within which substrates are cleaved into peptides ~2-30 residues long (8). Larger protein substrates or aggregates that could obstruct the proteasome's inner chamber are generally handled by the second proteolytic pathway, autophagy, a cellular degradation system that eliminates not only large protein aggregates, but also cytosolic components, organelles and pathogens via lysosomes (reviewed in (9-11)). In addition, the autophagy machinery recycles a large percent of old and worn-out proteins and is responsible for organelle turn-over. Both the UPS and autophagy pathways rely on crosstalk, and collaborate with each other to effectively degrade cellular proteins (9).

1.1.2. Ubiquitin proteasome system: *Stamped for the shredder*

Approximately 80-90 % of cellular proteolysis is carried out by the UPS, though this may vary based on cell type and physiological state (12). The UPS comprises two distinct, successive steps: 1) tagging, whereby aberrant protein substrates are identified and specifically tagged by the covalent attachment of ubiquitin chains, and 2) degradation, where the tagged substrates are subsequently broken down by the proteasome (13,14) (Fig. 1.1). The proteasomal machinery is a multimeric ATP-dependent protease complex, the various components of which selectively recognize and break down ubiquitin-tagged substrates. Consequently, the ubiquitin tag induces substrate processing and functions as a degradation signal or a degron (12).

Ubiquitin, a small 76-residue protein, is attached to the ε-amine of Lys side chains on the substrate via an isopeptide bond (Fig. 1.2A). Ubiquitin itself contains seven Lys residues, which can in turn be linked to additional ubiquitin molecules to form poly-ubiquitin chains. The covalent attachment of mono- and poly-ubiquitin (termed ubiquitination) is a common post-translational modification. Ubiquitination controls not only degradation events in the cell, but also various non-proteolytic processes including protein interactions, enzyme activity,

trafficking and subcellular localization, as well as larger scale events like transcription, apoptosis and cell cycle regulation (15-17). The fate of the ubiquitin-tagged substrate is specified by the position of the ubiquitin modifier, the chain length and the type of chain linkage (18). For example, K11- and K48-linked poly-ubiquitin are canonical signals for degradation, and specifically target substrates to the proteasome (13).

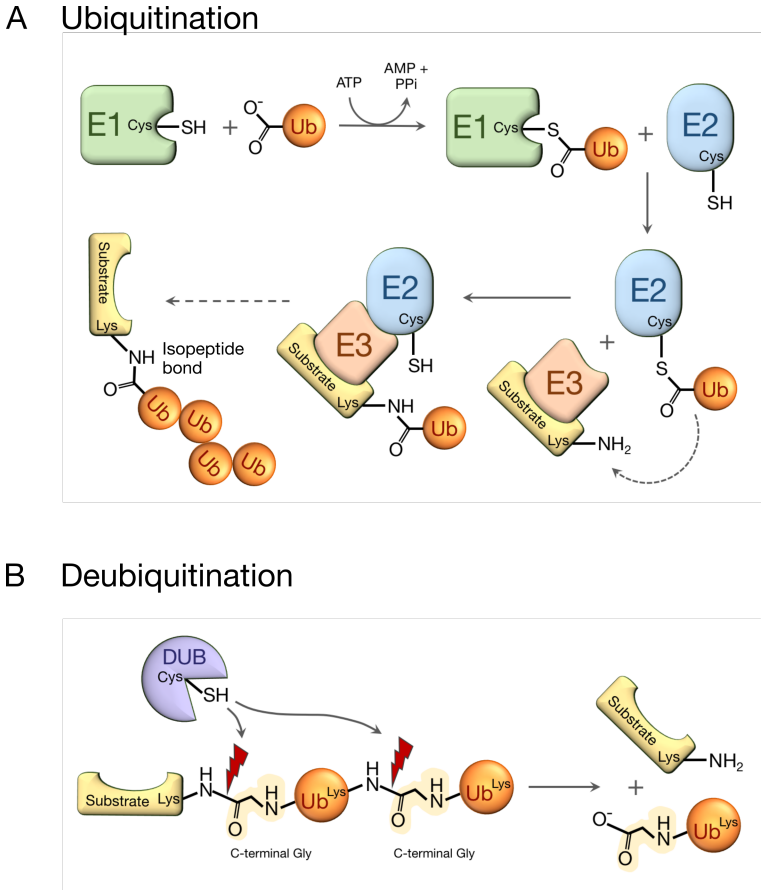

Figure 1.2 Ubiquitination and deubiquitination reactions. *A,* shows the conjugation of ubiquitin *(orange)* onto a substrate *(yellow)* lysine side chain, via an isopeptide linkage. The reaction involves a sequential three-step enzyme cascade. Ubiquitin is first activated by E1 *(green)*, which enables it to bind E2 *(blue)*, before it is finally transferred to the substrate by the E3 ligase *(pink)*. *B,* shows the cleavage of ubiquitin molecules from chains, or from the substrate it is attached to, by a DUB *(purple)*. The catalytic cysteine hydrolyses the covalent isopeptide bond between the lysine side chain and the C-terminal of ubiquitin. The site of cleavage is marked by the *red bolt*. Figure adapted from (14,18-20).

The UPS thus controls the fate of a large number of proteins and consequently demands a high degree of specificity of both the ubiquitin signal and the tagged substrate. Ubiquitination results from a sequential three-step enzyme cascade of increasing specificity (Fig. 1.2A). The ubiquitin molecule is first activated by an E1-activating enzyme, which enables it to bind to a ubiquitin-carrier protein E2, before it is finally transferred to the substrate by a ubiquitin ligase E3 (14). A minimum chain length of four ubiquitin molecules is required for the substrate to be recognized by the proteasomal machinery (13). The chain must then be trimmed or entirely cleaved prior to degradation, before the substrate can enter the proteasome. This is accomplished by peptidases referred to as deubiquitinating enzymes (DUBs) (19). DUBs reverse the ubiquitin signal attached to substrates by E1/E2/E3 enzymes (Fig. 1.2B). In the context of protein degradation, they also trim or tailor chains to achieve optimal ubiquitin-chain topology for substrate recycling or breakdown (19). On a larger scale, they regulate ubiquitin levels in the cell by processing ubiquitin precursors, recovering ubiquitin from small molecule adducts, and recycling ubiquitin chains from proteasome substrates (20).

A large proportion of UPS substrates originate in the ER, and must be extracted into the cytosol to be degraded and recycled; this component of the UPS is termed ER-associated degradation (ERAD) (21).

1.1.3. Endoplasmic reticulum associated degradation: *Extractor machines*

Secretory and membrane proteins, as well as those of the endocytic system, enter the ER by co-translation, where they complete their folding cycles and acquire various post-translational modifications. Subsequently, they are delivered to the appropriate organelle, embedded in the plasma membrane, or transported outside the cell to perform their function (21). During their folding process, some proteins fail to adopt a stable conformation. At times, more than half of the newly translated proteins may never reach maturity. The mechanisms that discriminate folded proteins from terminally misfolded proteins are unclear, and are currently thought to involve the ER-resident chaperones and co-chaperones (22). Even after multiple

folding cycles aided by chaperones, proteins that cannot be rescued must be extracted from the ER back into the cytosol, where they can be degraded and recycled by the proteasome as part of the UPS (Fig. 1.1). The ubiquitin tag on these substrates not only signals degradation, but is also required for their extraction from the ER (17,18).

The ERAD pathway is thus a quality-control strategy aimed at restoring proteostasis during an unfolding crisis, wherein the ER cooperates tightly with the UPS to identify, tag, extract, and degrade aberrant and accumulated protein substrates.

1.1.4. Autophagy: *The junk yard*

Autophagy ("self-eating") is the bulk degradative system that not only eliminates proteins, but also larger cellular constituents including whole organelles, cytosolic elements, parts of the ER, and intracellular pathogens (11). In this system, substrates are delivered to lysosomes, where they are degraded by lysosomal hydrolases. Autophagy can be categorized into three types based on how the substrate is delivered: chaperone-mediated autophagy, microautophagy, and macroautophagy (23). The last is usually referred to by the general term "autophagy" and is responsible for eliminating large protein aggregates (24) (Fig. 1.1). During autophagic degradation, substrates are sequestered by a unique organelle termed the autophagosome, which forms as a double-layered membrane structure. Fusion of this organelle with late endosomal compartments creates amphisomes, which subsequently fuse with the lysosome for digestion by acidic hydrolases (23).

Autophagy and the UPS were initially believed to be independent of each other in modes of action, core machinery and substrate specificity. However, recent studies suggest that cells function on a single proteostasis network, wherein both pathways coordinate with each other and share numerous components (reviewed in (9,12,25)). For example, autophagy is activated when the UPS is impaired or when the proteasome is inhibited (26-29), which is indicative of a compensatory mechanism. The ubiquitination process is central to both pathways, as ubiquitin-

tagged proteins are also eliminated via autophagy (12). Interestingly, autophagy can even degrade proteasomes in response to starvation and damage ((30), and reviewed in (31)).

Our studies revolve around two major players of the degradation pathways. One of them is the molecular motor p97, a key regulator of the UPS that extracts substrates from membranes and aggregates, and is also essential for autophagosome maturation (32). The other is the DUB ataxin3, thought to be a sentinel directing the degradation pathways. Ataxin3's DUB activity helps target substrates to the proteasome, and also contributes to the clearance of proteins by autophagy and aggresome formation (33-36). The two proteins directly interact with each other, and function in concert to maintain proteostasis (37,38). The research described in this dissertation is of a biochemical nature, focused on the molecular mechanism of the p97-ataxin3 interaction, and ataxin3 enzyme activity.

1.2. The AAA+ ATPase p97

The protein p97, also known as valosin-containing protein or VCP in mammals, cdc48 in yeast and plants, CDC-48 in worms, and Ter94 in flies, is an essential *A*TPase *a*ssociated with various cellular *a*ctivities (AAA+ superfamily). The presence of two highly conserved AAA domains within the protein classifies it as a Type II AAA+ ATPase (reviewed in (32)). Members of this large, functionally diverse family generally exist as double-ringed oligomers (p97 forms a hexamer), and often function as molecular motors, harnessing the energy of ATP hydrolysis to perform mechanical work in species from bacteria to humans. Other proteins in this group include the N-ethylmaleimide-sensitive fusion protein (NSF) that functions in vesicular transport processes (reviewed in (39)), the nuclear VCP-like protein (NVL) that functions in ribosome biogenesis (reviewed in (40), and the PEX1 and PEX6 proteins involved in peroxisome biogenesis (reviewed in (41)). Unlike various other AAA+ proteins, p97 does not depend on the presence of nucleotides for its hexameric assembly.

1.2.1. Structural assembly

The structure of p97 has been extensively studied for over a decade, by various techniques including X-ray crystallography (42), cryo-electron microscopy (cryo-EM) (43), nuclear magnetic resonance (NMR) (44) and small-angle x-ray scattering (SAXS) (45). Initially, negatively-stained EM samples provided basic information about the ring-like hexameric shape of the molecule (46,47). Subsequent structural efforts were limited to medium resolution (3.5–4.7 Å) images of full-length p97, with higher resolution structures of isolated domains that were indispensable in determining the architectural details of the molecule (48,49). Recently, in a study by Banerjee *et al.* (43), the latest advancements in cryo-EM technology were used to obtain near-atomic resolution structures of native, full-length p97 hexamers in multiple conformational states, and in the presence and absence of exogenous nucleotides.

1.2.1.1. Overall architecture

Fig. 1.3A depicts the domain organization of a single p97 protomer. Each protomer has a predicted molecular weight of ~90 kDa. The native, full-length p97 complex assembles as a homohexamer, with each protomer comprising an N-terminal domain (denoted hereafter as the N-domain), two tandem AAA ATPase domains termed D1 and D2, and a short, unstructured C-terminal tail (Fig. 1.3A). Within each protomer, the three domains are connected by short linkers termed N-D1 and D1-D2 loops, which lack secondary structure. The D1- and D2- domains form two coaxially-stacked hexameric rings, with an average diameter of ~130 Å. In comparison, the D2-ring appears larger and more conformationally dynamic than the D1-ring (43). The rings surround a central pore ~20 Å wide and ~70 Å in length, lined with substrate-interacting loops. The arrangement of the N-domains around the outer periphery of the D1-ring, together with the six-fold symmetry, confers a six-edged star shape to the molecule (Fig. 1.3B) (42,43).

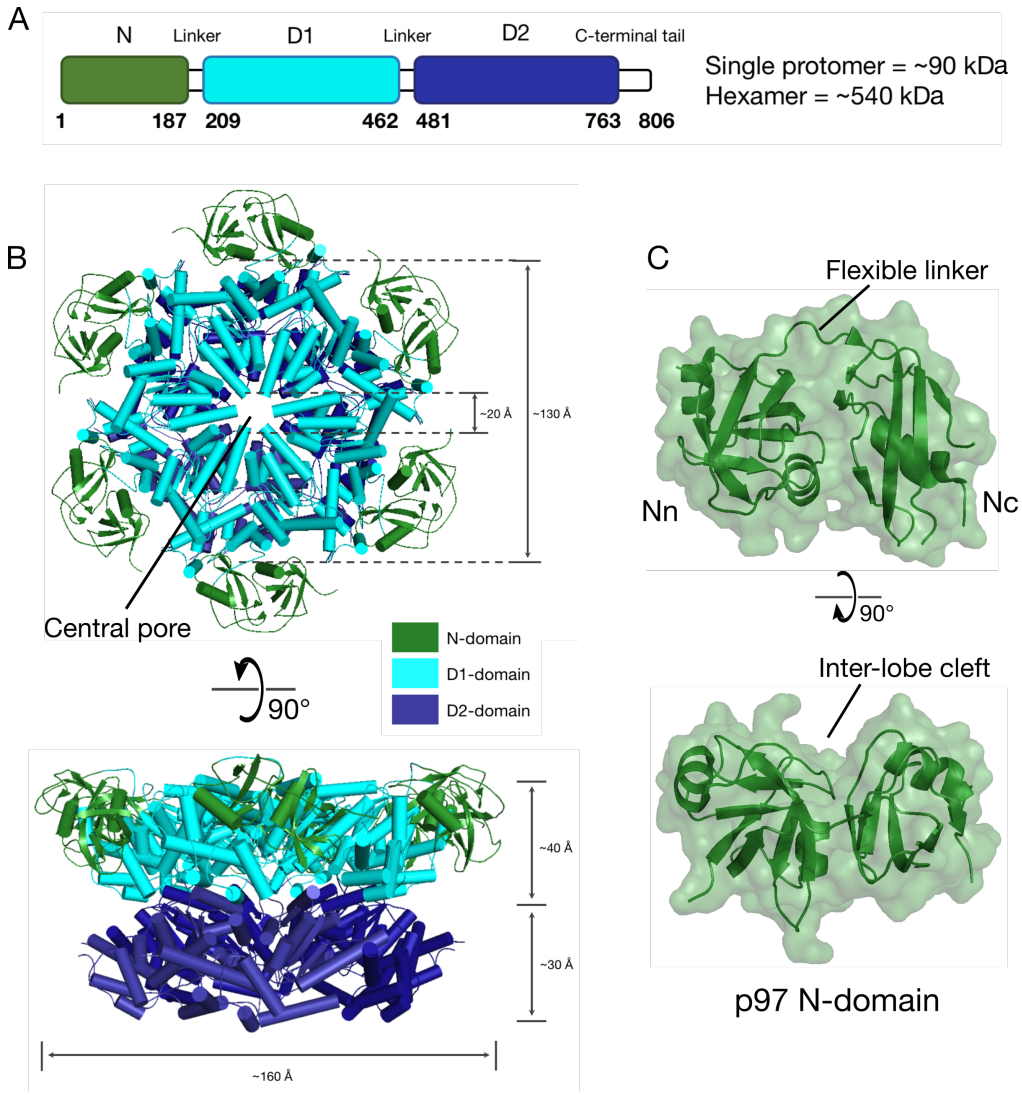

Figure 1.3 Structure of p97. *A,* is the schematic domain organization of a single p97 protomer that comprises an N-terminal domain *(green)*, D1- and D2-ATPase domains (*cyan and deep blue* respectively), two linker regions, and an unstructured C-terminal region. The scale below each domain shows the length in amino acids. *B,* is the structure of full-length hexameric p97 (PDB entry 5FTK (43) in the ADP-bound form), as viewed down the 6-fold symmetry axis from the top *(above)*, and when rotated by 90° to generate the side view *(below)*. The top view is presented with the approximate diameters of the D1-ring and the central pore, while the side view is annotated with width and height measurements. The N-domain is colored *green*, and the D1- and D2-domains are *cyan* and *deep blue*, respectively. *C,* shows a single N-domain with the Nn and Nc lobes, connected by a flexible linker. The *upper* view is rotated 90° clockwise around the in-plane horizontal axis to obtain the view *below*. The surface representation clearly shows the large inter-lobe cleft, which is a major binding pocket for numerous p97 cofactors.

1.2.1.2. The N-domain

The N-domain (residues 1 – 186) has a globular, bi-lobed structure, comprised of two sub-domains, Nn at its N-terminal and Nc at its C-terminal, connected by a flexible linker of ~6 residues. Nn has a double Ψ β-barrel structure, with six β strands forming the barrel's sides and two Ψ crossover loops. Nc has an α+β structure, with a central β-sheet of four antiparallel strands (Fig. 1.3C). A large cleft, lined with hydrophobic residues, is formed between the Nn and Nc lobes, and serves as a major binding pocket for a multitude of p97 cofactors (50) (see section 1.2.2). The N-domain is also involved in p97-substrate interactions (51).

1.2.1.3. The D1- and D2- domains

The D1 (residues 209-462) and D2 (residues 481-763) domains are aligned along a vertical axis in a head-to-tail manner within each protomer, and share a similar overall structure. Approximately 250 residues from each domain contribute to the AAA cassette that bears the active site for ATP hydrolysis. Thus, both rings have inherent ATPase activity, however D1 is less active than D2 (52). The AAA cassettes contain two sub-domains each: a larger N-terminal RecA-like α/β-fold domain that mediates hexameric ring formation and contains the active site, and a smaller C-terminal α-helical bundle domain (32). The six active sites are located at the interfaces between the adjacent protomers and are formed by Walker A and B motifs, responsible for nucleotide binding and hydrolysis respectively (52), along with an arginine-finger motif.

The classical Walker A motif (GxxxGKT, x is any residue) includes a β-strand followed by a glycine-rich loop, ending in an α-helix. A highly-conserved lysine in the loop (Lys251 in D1, and Lys524 in D2 (Fig. 1.4)) senses the state of the bound nucleotide by interacting with the terminal phosphate group. The loop is thus referred to as the "P loop". Mutagenesis of this critical lysine in either domain severely perturbs nucleotide binding (52). The Walker B motif (hhhhDE, h for hydrophobic residue) includes an aspartate that coordinates the Mg^{2+} ion, and a glutamate that is essential for ATPase activity (53) (Fig. 1.4). The arginine-finger residue (Arg359 in D1 and Arg635 in D2) projects into the active site, stabilizes the nucleotide's leaving γ–phosphate group and

stimulates ATP hydrolysis. Notably, this residue is contributed by the adjacent protomer in the ring, and is thus believed to communicate the nucleotide-state between protomers (52).

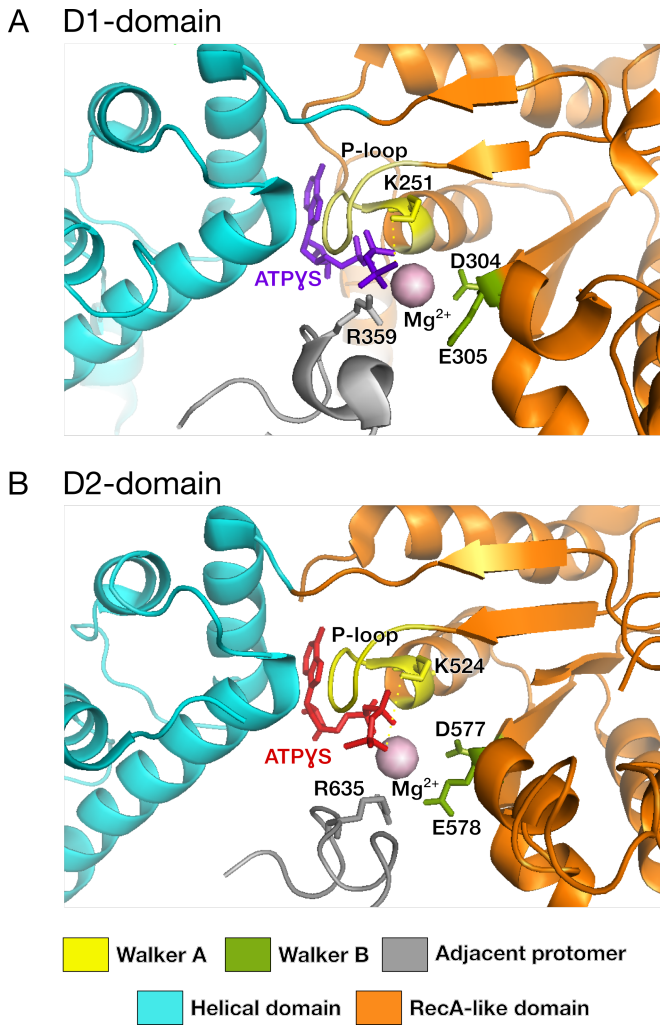

Figure 1.4 Structure of the AAA cassettes in p97 D1- and D2-domains. *A,* shows the D1-domain, and *B,* shows the D2-domain of a p97 protomer bound to ATPγS (PDB entry 5FTN (43)). The AAA cassette comprises a RecA-like domain *(orange)* and a characteristic helical domain *(cyan)*. An ATPγS, bound at the interface between the two domains, is shown in *purple* in D1, and *red* in D2, and the Mg^{2+} ion is shown in *light pink.* The Walker A motif or P-loop is depicted in *yellow,* with the conserved lysine residue shown in stick representation and labelled. The Walker B motif is shown in *green*, and the two conserved acidic residues, aspartate and glutamate, are represented by stick models and labelled. The nucleotide-binding site communicates with the adjacent protomer via the arginine finger motif *(grey)*, which contacts the bound nucleotide.

1.2.1.4. The C-terminal tail

Unlike other AAA+ members, p97 has an unstructured, highly flexible C-terminal tail (residues 764-806) that extends beyond its D2-domain. This region is involved in regulating the molecule's ATPase activity; C-terminal truncation mutants display reduced activity (54). The tail also contains phosphorylation sites that modulate the binding of a subset of p97 cofactors, as well as the protein's subcellular localization and hexamer stability (50,54).

1.2.2. p97 cofactors

Over thirty p97-interacting proteins have been identified by proteomic studies and biochemical assays, and this number is expected to increase. Just last year, in 2016, a yeast two-hybrid screen by Arumughan *et al.* (55) detected eight new cofactors for human p97. Typically, they are multi-domain proteins containing p97-binding modules along with domains that either promote interaction with other proteins, or possess enzyme activity.

Despite the abundance of cofactors, they can be categorized into a few distinct groups based on their conserved p97-binding modules. The vast majority interacts with p97's N-domain, either via domain motifs like the *u*biquitin *r*egulatory *X* (UBX) domain or the *UBX*-*l*ike (UBL) domain, or via linear peptide motifs including the *V*CP/p97-*i*nteracting *m*otif (VIM), *V*CP/p97-*b*inding *m*otif (VBM), and the SHP-binding motif. Despite considerable differences in their structures, the p97-binding modules recognize and bind in or near the same inter-lobe cleft of the N-domain. A smaller subset of cofactors recognizes the unstructured C-terminal tail, and binds via *P*NGase/*UB*A or UBX (PUB) or *P*LAP, *U*fd3p and *L*up1p (PUL) domains (reviewed in (50)).

Cofactors partner with p97 in different ways. Much of the binding mechanism is dictated by the stoichiometry and spatial arrangement of the complex. The hexameric structure potentially offers six identical binding sites for each cofactor around the ring. Typically, only one or a few of these are occupied by a single cofactor, which leaves room for others to bind. While some cofactors bind simultaneously to different protomers, others exhibit mutually exclusive binding, and some display a hierarchy in their binding patterns (reviewed in (32,50)).

Through these cofactor interactions, the N-domain couples mechanochemical ATPase activity to the unfolding or disassembly of p97 substrates. Cofactors may be roughly classified into substrate-recruiters that direct p97 to specific pathways, and substrate-processors, typically enzymes that fine-tune function within a given pathway. Diverse functions of p97-cofactor complexes, and their ability to recruit additional proteins, stem from differing symmetries and stoichiometries of these complexes (56-58).

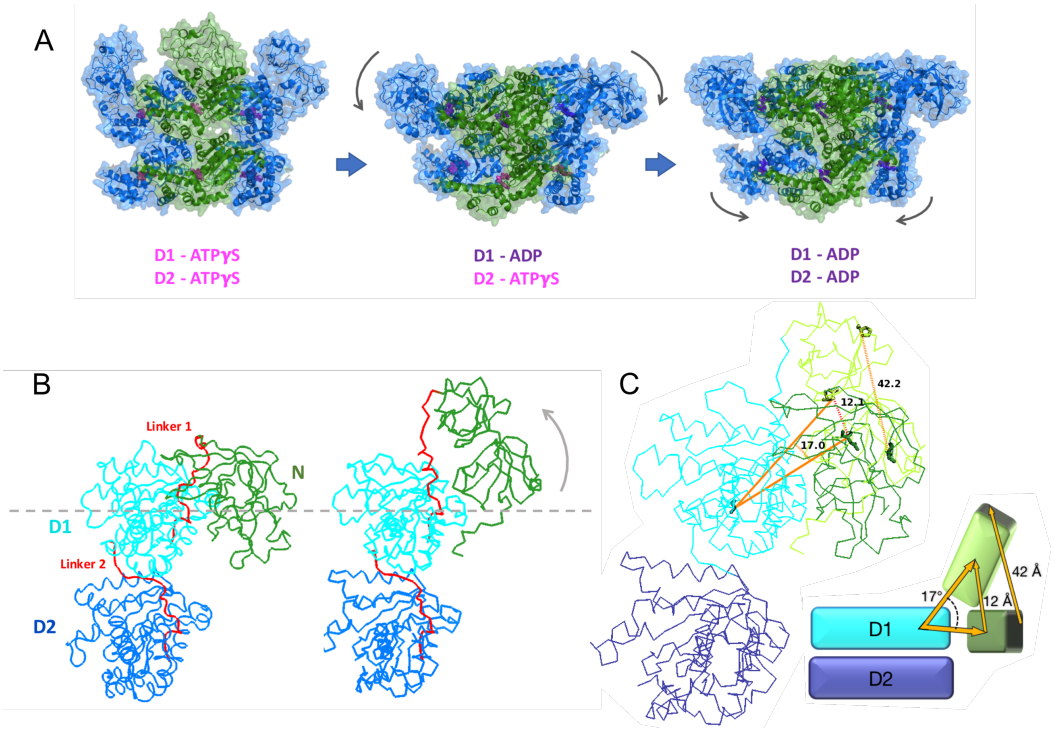

Figure 1.5 Nucleotide-induced conformational changes. *A,* shows three distinct conformations of p97 bound to various nucleotides (PDB entries 5FTN, 5FTM and 5FTK (43)). The nucleotide states of the D1 and D2 are mentioned *below* each structure. Alternate protomers are colored *green* and *blue,* and the bound nucleotide is colored *pink* for ATPγS, or *purple* for ADP. The *grey arrows* demonstrate the movements of the N- and D2-domains during the transition from the previous conformation. *B,* shows ribbon representations of the side view of a p97 protomer in the down *(left)* and up *(right)* conformations (PDB entries 5FTK and 5FTN (43)), with the N-, D1-, and D2- domains shown in *green*, *cyan*, and *deep blue* respectively, and the two linkers in *red*. The *grey dashed lines* represent the plane of the D1-ring. *C,* shows the side view of a p97 protomer, with both the up *(light green)* and down *(deep green)* conformations of the N-domain. Comparison of N-domain residues in the two conformations shows that the central D150 undergoes a hinged upward displacement of ~12 Å, sweeping an angle of ~17° (measured from G408), while a far edge residue P178 translates ~42 Å. The *inset* is a cartoon representation showing the N-domain displacement, and the location of the residues used for measurements.

1.2.3. Nucleotide-induced conformational changes

p97 undergoes dramatic intra- and inter-protomer conformational changes during its ATPase cycle, and the mechanical force generated is directed towards remodeling substrate molecules. Early attempts to study these changes by cryo-EM were limited by low resolutions of 20–30 Å, but provided evidence of moderate rotational movements attributed to the opening and closing of the central pore (48). In addition to limiting resolutions, the six ATPase domains within each ring are not synchronized during ATP hydrolysis, which adds to the challenges in studying p97 conformational dynamics. Recent advances in high-resolution cryo-EM have led to the detection of at least three well-defined, distinct conformations of p97 bound to various nucleotides (Fig. 1.5A) (43). Conformational changes involve large corkscrew-like rotational twists in D2, coupled with significant "up-down" movements of the N-domain relative to the D1-ring. N-domain movements are largely induced by the nucleotide bound in D1; ATP or ATPγS favors the "up" position, and ADP induces a "down" position (where the N-domains are coplanar to the D1-ring) (Fig. 1.5B). Comparison of the up and down structures in (43) reveals that the relative center of the N-domain (measured at D150) undergoes a hinged upward displacement of ~12 Å, sweeping an angle of ~17° (measured from G408), while a far edge residue on the N-domain (P178) translates a distance of ~42 Å (Fig. 1.5C).

These up-down conformational shifts have also been verified by SAXS analysis (59). In contrast, all crystal structures of p97 to date, with and without nucleotide analogs, reflect the ADP-bound down-state and reveal only minor structural changes (42,49,60). Perhaps crystal packing constraints limited the detection of functionally relevant conformational states. However, Tang *et al.* (59) recently crystallized a mutant form of the p97 hexamer (see section 2.5), with ATPγS bound in the D1 and all six N-domains in the up-state.

p97 exhibits complex and dynamic structural transformations. At any given time, the D1 and D2 within each of the six protomers can exist in different nucleotide-bound states, supporting the observation that these domains do not work in a concerted manner. In addition, ADP is often prebound to the D1, with typically 0.9 ADP molecules per p97 monomer (52). This may account

for the heterogeneity in the positions of the six N-domains observed in some cryo-EM experiments (43). Moreover, the six protomers around the ring also communicate with each other in a system termed the intersubunit signaling network (ISS) (50). The ISS couples the conformation of the central substrate-translocating pore to the nucleotide state of the same protomer, which is then transmitted to the adjacent protomer and thereby coordinates ATP hydrolysis in *trans* (61). The ISS is also involved in interprotomer motion transmission – the vertical transmitting of signals from the D2 to the D1, via the D1-D2 linker (62).

1.2.3.1. Conformational changes influence cofactor binding

It makes perfect sense that nucleotide-induced conformational changes, specifically those associated with D1, influence the binding of N-domain cofactors and may thus regulate the physiological functions of p97. Nevertheless, we lack mechanistic insight into such conformational control. These effects may have thus far escaped detection because most structural studies, with and without cofactors, are conducted with isolated N-domains (44,58,63-65). In both up- and down- states, the cofactor-binding cleft is available but orients differently. Since cofactors vary in shapes and sizes, it is highly conceivable that some of their binding will be obstructed by spatial restrictions in different N-domain states.

It is however clear that p97's nucleotide state determines the binding of some cofactors; for example, p47 exhibits an 8-fold decrease in affinity for ADP-bound p97 compared to its ATP-bound form (66). Conversely, cofactor-binding may provoke conformational changes and regulate ATP hydrolysis, as observed for p37 – the first known p97-activating cofactor to trigger a 11-fold enhancement of its catalytic efficiency (67).

1.2.3.2. Conformational changes influence ATPase activity

N-domain flexibility is crucial for p97's catalytic activity. The orientations of the N-domain and D1D2 linker, relative to the D1-ring, are directly correlated to ATP hydrolysis. The flexible form of the protein is competent for activity, while forms of the protein that are locked in the

coplanar or down conformations are inactive (54). N-domain movements could thereby induce transitions from an active to an inactive form as part of the hydrolysis cycle, and these transitions would generate the force required to remodel substrates and regular cofactor interactions as part of p97's cellular functions.

1.2.4. Biological functions of p97

ATP hydrolysis in the D1 and D2 is harnessed to perform mechanical work, allowing p97 to function as a segregase in processes as varied as cell-cycle regulation, transcriptional activation, DNA-damage repair, and membrane fusion (68). The protein's general mode of action is to extract polypeptides from large protein assemblies and aggregates, or from cellular structures like membranes and chromatin. p97's diverse functions have been extensively reviewed elsewhere (68-71), and can be broadly summarized into three categories.

The first, and one of p97's most significant cellular roles, is to maintain proteostasis (68), wherein the protein contributes to both proteasomal degradation and autophagy. In this context, its most widely studied function is in the ERAD pathway. Through specific interactions with various membrane-associated cofactors, p97 is recruited to the ER membrane, where it captures and extracts misfolded polypeptides. The protein can also release membrane-bound transcription factors, and extract polypeptides from the mitochondrial outer membrane to facilitate mitochondria-associated degradation (32). In addition to its segregase function, p97 also shuttles polypeptides to the proteasome. p97 function is also implicated in autophagy, as it assists in autophagosome biogenesis and maturation (72,73).

Secondly, p97 exhibits chromatin-associated functions as it releases proteins from chromatin in a manner analogous to ERAD and thus assists in chromatin-associated degradation (74).

Thirdly, biochemical and genetic evidence implicates p97 function in membrane fusion events and vesicular trafficking (75,76). In its capacity as a molecular motor, the protein facilitates the fusion of vesicles at the end of mitosis that leads to the formation of the golgi apparatus (77).

1.2.5. p97 MSP1 mutations and related disorders

As would be expected for a key component of regulatory and degradation pathways, p97 dysfunction is associated with numerous degenerative diseases. Missense mutations in p97 cause a set of heterogeneous disorders collectively termed Multisystem Proteinopathy Type 1 (MSP1), which include inclusion body myopathy, Paget disease of the bone and frontotemporal dementia (IBMPFD), and amyotrophic lateral sclerosis (78). Moreover, p97 dysfunction directly correlates to failures in proteostasis, and is also associated with a wider spectrum of diseases like familial Parkinsonism, Lewy body disease and Huntington disease (79).

1.2.6. Disease pathology

MSP1 is an autosomal-dominant, progressive and ultimately fatal disorder affecting brain, muscle and bone tissue. Despite embryonic lethality in p97 knock-out mice (80) and accelerated MSP1 pathology in homozygote p97 mutant mice (81), the pathogenic mutations are well tolerated and affect only a subset of p97 functions. Moreover, developmental abnormalities are not observed in affected individuals. This is consistent with MSP1 being a late-onset disease, and clinical pathology clearly indicates a defect in maintaining proteostasis. Pathological features of MSP1 in patient samples involve rimmed vacuoles in muscle tissue and nuclear inclusions in neurons, both which stain positive for p97 and ubiquitin (82-84). This suggests that defects in p97-mediated protein quality control networks may contribute to disease etiology.

1.2.7. Structural and functional alterations

To date, over 30 MSP1-related mutations in 17 different residues within p97 have been identified. Typically, they are located at the interface between the N- and D1- domains and within the ND1 linker, neither of which overlap with any nucleotide-binding sites or cofactor-binding pockets (67) (Fig. 2.9). This suggests that the primary basis of dysfunction in mutant p97 is faulty communication between N- and D1- domains. The effects of MSP1 mutations are evident in 1)

disrupted cellular functions, 2) altered nucleotide-binding and hydrolysis, 3) altered conformational changes, and 4) imbalanced cofactor association (reviewed in (85)).

1.2.7.1. Disrupted cellular functions

MSP1 mutations have been linked to defects in multiple proteostasis degradation pathways including the UPS, autophagy (72), and endosome-lysosomal fusion (75). A pathological hallmark of MSP is the co-localization of mutant p97 with ubiquitinated-protein inclusions, directly indicative of a defective UPS (82,83). Mutants also disrupt autophagosome and endosome maturation, leading to vacuolation, weakness and muscle atrophy (86,87). In addition, ubiquitin is often co-localized in vacuoles with other proteins like TDP-43, a substrate for both proteasomal and autophagic degradation (88). The long term degenerative effects of these mutants on brain, bone and muscle tissues are yet another indication of disrupted proteostasis, and lead to the progressive failure of different systems in the body.

1.2.7.2. Altered nucleotide binding and hydrolysis

None of the MSP1 mutations have been found in nucleotide-binding pockets, but interestingly, they still affect nucleotide-binding in the D1. ITC experiments have revealed a 2- to 5- fold decrease in the ADP binding affinity of mutant D1 compared to wild-type, which facilitates better access to other nucleotides for these mutants (59,66). Decreased prebound ADP has also been observed in ND1 fragments harboring R155H and R95G mutations (59). Furthermore, none of the mutations seem to abolish p97 ATPase activity. With a few exceptions that do not alter activity (53,89), the general effect of most MSP1-associated mutations is to significantly increase ATP hydrolysis (54,90,91).

1.2.7.3. Altered conformational changes

The structure of the MSP1-associated R155H mutant, with ADP in the D1, is very similar to wild-type p97 with all N-domains in the down state (59). However, crystal structures of two common mutants with ATPγS in the D1 show all six N-domains in the up conformation, which has been correlated with decreased ADP binding to D1 (59). This suggests that mutations do not alter p97's overall structure, but instead disrupt the up-down equilibrium of the N-domains (59,92). The disrupted conformational equilibrium is attributed to defective inter-domain communication within MSP1 mutants. Mutant D1 is less likely to be occupied by ADP to begin with, and when ADP does bind, the mutants are unable to effectively transduce the ADP-bound signal from the D1 to the N-domains. Consequently, mutant N-domains seldom adopt the down state, and this has implications in both, the function of p97, and its interaction with cofactors.

1.2.7.4. Imbalanced cofactor association

None of the identified MSP1 mutations are at p97-cofactor binding interfaces, so their effects on cofactor association are most likely indirect and subtle. Consequently, cofactor-binding experiments, comparing wild-type p97 to mutants, must be interpreted with caution. Studies using purified proteins are often inconsistent with cell-based experiments, and do not recapitulate the differences in cofactor-binding ability observed between wild-type p97 and MSP1 variants. For example, mutant p97 precipitates more Ufd1/Npl4 than wild-type in cultured cells, but not *in vitro* using pull-down assays (53,89,91). Such discrepancies in cofactor binding may be resolved by accounting for p97's nucleotide state (see section 1.2.7.2). Despite the challenges in detecting subtle differences, studies of p97 mutants have demonstrated altered interactions with various cofactors from the endocytic pathway, as well as with UPS components. Unlike wild-type p97, the R155H mutant does not form a complex with CAV1-Ubxd1 (75). Additionally, R95G and R155H mutants also bind less of the ubiquitin ligase E4B and significantly elevated amounts of ataxin3, when compared to the wild-type. This has been observed in cultured cells, as well as under pathophysiological conditions, in primary myoblasts from MSP1 patients (53).

1.3. The DUB ataxin3

DUBs are dynamic enzymes that hydrolyze the covalent isopeptide bonds between ubiquitin and a target protein, as well as between ubiquitin molecules in a chain (Fig. 1.2B). They reverse the ubiquitin signal in a manner analogous to the reversal of the kinase signal on target molecules by phosphatases (reviewed in (93-95)). However, the diverse assemblage of ubiquitin modifications on targets within a cell necessitates a certain level of specificity in DUB activity. Some DUBs may exhibit differential activity towards certain ubiquitin linkages, while some may display a size or substrate preference for the target protein conjugated to the ubiquitin C-terminal (96). Substrate specificity, as well as inherent DUB activity, is often regulated through their interactions with various binding-partners (97). Individual DUBs assemble into distinct protein complexes, or may even be part of large ubiquitin ligase complexes, in order to function as dynamic regulators of the UPS (19).

The human Josephin proteins form one the five major families of DUBs, and ataxin3 is the founding member and most widely studied of these enzymes. The other members of this family include the ataxin3-like protein (AT3L), Josephin-1, and Josephin-2, all of which exhibit DUB activity by means of a highly conserved Josephin domain that serves as the catalytic center (34,98). However, all four proteins vastly differ in their catalytic efficiencies and substrate specificities (99).

Ataxin3 has been implicated in various ubiquitin-dependent protein quality-control pathways, both in its capacity as a DUB (33,34,100), and in its ability to recognize and bind polyubiquitin chains (101,102). In its normal form, it facilitates the degradation of substrates targeted for destruction. However, a mutant form of the protein that possesses an expanded polyglutamine (polyQ) tract of pathological length aggregates and causes the neurodegenerative disorder spinocerebellar ataxia type-3 (SCA3) or Machado-Joseph disease (103-107). Thus, ataxin3 both supports normal protein clearance, and in its mutant form disrupts the same process.

1.3.1. Structural organization

Ataxin3 is composed of around 364 amino acids and has a molecular weight of 42 kDa. At its N terminus is the Josephin domain (residues 1–180 in humans; designated Josephin after Machado-Joseph disease), a globular cysteine protease module that possesses DUB activity, and is highly conserved from yeast to humans (100). Downstream of the Josephin is a relatively conserved region that contains two contiguous ubiquitin-interacting motifs (UIMs), followed by a loosely structured C-terminal tail (Fig. 2.1). The polyQ repeat region of variable length is located within the C terminus; the tract comprises 11–40 glutamine repeats in normal individuals, and is typically expanded to 55–85 repeats in disease states (reviewed in (103,108,109)). The C-terminal tail may also contain an atypical third UIM as a consequence of alternate splicing events, which give rise to multiple protein isoforms or splice variants (34,110).

Ataxin3 associates with ubiquitin and ubiquitinated substrates primarily through its UIMs (111), which exhibit cooperative binding and a preference for tetra-ubiquitin and longer chains (34). Besides these motifs, two additional distinct ubiquitin-binding sites are present within the Josephin domain (Fig. 3.1). One is the active site, and the other overlaps with a site that recognizes the UBL domain of Rad23B, a proteasomal shuttling factor (102). The Josephin can thus bind two mono-ubiquitin molecules with low affinity and no apparent cooperativity (102). Consequently, the UIMs and Josephin synergistically modulate ataxin3's DUB activity and substrate specificity. Other specific motifs in the Josephin domain and the C-terminal region facilitate binding to chromatin, transcriptional regulation, and protein-protein interactions (reviewed in more detail in (112-114)).

1.3.2. Ataxin3 chain-trimming activity

Ataxin3 DUB activity maps to the conserved Josephin domain that hosts the enzymatic cleft (Fig 3.1). The catalytic triad formed by C14, H119 and N134 demonstrates a close similarity in secondary structure and organization to the active site in papain-like cysteine proteases, including those of the ubiquitin C-terminal hydrolases (UCH) and ubiquitin-specific proteases (USP)

families (115). Ataxin3 indeed functions as a cysteine protease, albeit less efficiently than other ubiquitin proteases like USP7 and UCHL3 (98). Mutation of the crucial C14 residue abolishes its catalytic activity; this mutant is useful in studying loss-of-function effects (34,100).

The isolated Josephin domain exhibits the same DUB activity as full-length ataxin3 (34,36,98), and the protein is an endo-type DUB (116). It cleaves polyubiquitin chains of five or more subunits to produce tetra-ubiquitin, with a preference for K63- and mixed-linkage long chains (117,118). In fact, K48- and K63-linked di-ubiquitin are found to be extremely poor substrates (118). Ataxin3 thus functions as a "molecular ruler" of sorts. The UIMs play a significant role in this form of chain specificity by restricting the types of substrates that are hydrolyzed by the Josephin. Their influence is further illustrated by mutation of the UIMs, which enhances the cleavage of K48-linked substrates (117). The Josephin and UIMs thus cooperate to trim polyubiquitin chains down to an optimal length for proteasomal delivery. *In vivo* studies are consistent with these *in vitro* observations (117), and confirm ataxin3's preference for high molecular weight mixed-linkage chains; presumably the DUB prevents the accumulation of very large, aberrantly structured ubiquitin chains in the cell, through its chain-trimming activities.

Interestingly, ataxin3 is also mono- or oligo-ubiquitinated (primarily at Lys-117 in the Josephin domain) in a UIM-dependent manner *in vivo* (119), which enhances its DUB activity without altering its preference for K63-linked chains (120). This form of regulation explains why ataxin3 exhibits low catalytic efficiency *in vitro*, but is relatively more active in cells. Ubiquitination of endogenous ataxin3 is enhanced during times of cellular stress, when the proteasome is inhibited, during the unfolded protein response or when excess ubiquitin is present (103). These observations suggest that ataxin3's cellular functions in protein quality control and clearance are modulated via ubiquitination of the DUB itself.

1.3.3. Cellular functions of ataxin3

Ataxin3 is deeply involved in the clearance of misfolded, toxic and aggregated proteins, and forms a critical component of both major degradation systems, the UPS as well as aggregation-

autophagy pathways (33,34). The DUB was initially reported to 1) bind polyubiquitin chains of four or more moieties with high affinity via its UIMs (33), and 2) preferentially hydrolyze K63-linked chains, branched chains and mixed linkages (117); this correlates with the minimal length and chain type required for the proteasomal delivery of substrates (121). The synergistic action of the Josephin with the UIMs selects for substrates that are heavily or improperly ubiquitinated, and protects chains from being overly trimmed. There is also evidence that closely links ataxin3 to the ERAD pathway, in its capacity as a DUB (38). As reported in (38) and (37), the protein interacts with the p97 extractor complex, trims ubiquitin chains to their optimal topology, and facilitates the shuttling of ubiquitinated substrates to Rad23 (via association with its UBL (122)), or directly to the proteasome (through interaction with the 19S and 20S subunits (33)). In addition, ataxin3 restricts ubiquitin chains on ERAD substrates by modulating E3 ligase activity. For example, it deubiquitinates and terminates the activity of the E3 ligase CHIP when the ubiquitin chain on its substrate reaches a critical length (123).

Ataxin3 DUB activity is also required to maintain the pool of free ubiquitin in the cell for normal proteostasis. In fact, proteostatic defects are observed in mice with a mutant ataxin3 allele or worms lacking ataxin3, evident as an enhanced stress response in these animals (124,125). Interestingly, ataxin3 knockout worms also exhibit an inhibited clearance of p97 substrates (126), which links the two proteins in a model system. On the other hand, the abnormal overexpression of wild-type ataxin3 leads to the accumulation of ERAD substrates like TCRα and CD3δ (33,37,38), reminiscent of dominant negative inhibition observed in other ERAD proteins (127-129). Thus, ataxin3 DUB activity is fine-tuned and tightly regulated to facilitate the flux of proteins through the UPS.

Ataxin3 function has also been observed in other cellular contexts. The DUB can serve as a transcriptional regulator to promote or inhibit the expression of target genes (112,114,130,131), such as those that encode molecular chaperones. Studies in mice and worms demonstrate that ataxin3 is largely responsible for maintaining basal levels of chaperones at a steady state *in vivo* (125,126,132). Ataxin3-deficient fibroblasts have reduced levels of basal and stress-induced Hsp70

and its regulator Hsf1, and the loss of ataxin3 in knockout mice primarily affects Hsp70 transcription, rather than chaperone turnover (132).

Ataxin3 also binds dynein, the microtubule-based motor protein (36), and may serve as an adaptor that links polyubiquitinated substrates to dynein motor complexes, thereby facilitating retrograde transport of substrates to aggresomes. *In vitro* assays also indicate a direct interaction between ataxin3 and HDAC6 (133), and the two proteins are found co-localized with aggresomes and pre-aggresome particles (134). Moreover, ataxin3 DUB activity and ubiquitin binding are both critical for aggresome development, since neither the isolated Josephin nor UIM-deficient mutants can rescue the decreased aggresome formation observed in ataxin3 depleted cells (36). Such observations, along with other studies (35,133-135) clearly indicate a role for ataxin3 in the aggresome-autophagy pathway.

Autophagy is an important degradation pathway for large assemblies of aggregated, misfolded proteins, in situations where the UPS and chaperone systems have failed. This pathway is especially involved in the clearance of polyQ expanded, aggregation-prone proteins like huntingtin, forms of tau and alpha-synuclein, and interestingly the mutant form of ataxin3. The DUB, therefore, not only participates in aggresome formation, but its pathological expanded form misfolds, aggregates and serves as a substrate to be cleared by autophagy (136-138). This portrays ataxin3 as a "Jekyll-and-Hyde" protein, which in its normal form suppresses neurodegeneration and cytotoxicity from polyQ disease proteins via its DUB activity, but in its expanded mutant form disrupts protein clearance pathways.

1.3.4. PolyQ-expanded ataxin3: Disease and dysfunction

Ataxin3 is encoded by the gene responsible for SCA3 (also termed Machado-Joseph disease), an autosomal-dominant neurodegenerative disorder that is caused by an anomalous expansion of the polymorphic polyQ tract, located at ataxin3's C terminus (103,108,109). As a rare, hereditary disorder, SCA3 is characterized by a pathologically expanded number of CAG trinucleotide repeats at the transcript level, which codes for polyQ (139), and is likely formed by slippage

during DNA replication. The result is a toxic form of ataxin3, which is prone to misfolding and aggregation. The expanded polyQ may impair protein clearance via one or a combination of the following ways: 1) misfolded ataxin3 forms toxic oligomers and blocks its own recognition and degradation by the proteasome, 2) the expanded polyQ alters ataxin3's native activity and interactions in p97-mediated protein degradation (loss-of-function mutant), causing a functional disruption of the UPS and ERAD and proteotoxic stress, 3) cleavage of ataxin3 produces unstable, toxic fragments containing the polyQ tract, and 4) the aberrant interaction of mutant ataxin3 with specific transcription factors causes errors in transcription (gain-of-function mutant) (103). In any case, mutant ataxin3 interferes with cellular quality-control pathways and is the main cause of neurodegeneration. As discussed above, wild-type ataxin3 behaves in an opposite manner by promoting protein clearance and is neuroprotective. This pattern has been extensively verified in a fruit fly model by overexpression experiments. Native ataxin3 clearly suppresses neurodegeneration in a DUB-dependent manner, and pathogenic ataxin3 with 50–78Q repeats induces neurodegeneration (135,140-142). However, ataxin3 was not found to suppress neurodegeneration in an analogous manner in mammalian models (143).

1.4. Significance of the p97-ataxin3 interaction

1.4.1. Regulation of the ERAD pathway

The ER is a major site of protein synthesis, folding and assembly in eukaryotic cells. The ERAD pathway serves as the primary quality-control system that eliminates misfolded, aggregated or toxic proteins (21), and thus preserves ER proteostasis. The pathway is formed by a series of steps that export aberrant substrates out of the ER for degradation by the UPS (144), however, the exact sequence of events is unclear. It is known that the targeted substrates are deglycosylated, ubiquitinated, and finally extracted into the cytosol to be broken down by the proteasome (21,145), and that for each of these steps, various proteins and protein complexes are recruited and assembled around the target substrate.

Aberrant substrates are first targeted to their site of extraction at the ER membrane, presumably by ER resident chaperones (146). A subset of these substrates associates with the Derlins, a class of highly conserved membrane proteins that are thought to form a channel in the membrane (147-149). Other components of the ERAD complex are also recruited to these focal points in the membrane. p97 is recruited to the ER membrane by its association with integral membrane proteins including Derlin-1/2, SEL1L/Ubx2, and VCP-interacting membrane protein (VIMP) (147,150-153). These proteins also recruit the Hrd1p/Hrd3p E3 ligases that ubiquitinate the substrate (150,154). The assembly of the retrotranslocation complex, containing both the motor elements and the ubiquitination machinery, tightly couples substrate ubiquitination to extraction.

Ubiquitination is thought to occur on the cytosolic side of the ER membrane, after a portion of the substrate emerges from the channel. In this way, the ubiquitin signal that is essential for extraction (144,155), can be recognized and processed by p97 and its cofactors, and may even activate the ATPase's function. p97 forms a subcomplex with the Ufd1/Npl4 heterodimer; since both p97 and Ufd1 can bind ubiquitin (156), they then synergistically interact with and extract the ubiquitinated substrate (156-158).

Both extraction and proteolysis in ERAD are dependent on the ubiquitin machinery; these are the enzymes that conjugate ubiquitin onto, and detach ubiquitin from substrates. The ubiquitin chain not only recruits p97, but also targets proteins to the proteasome. However, the chain must be trimmed or removed before the substrate can enter either the extraction or degradation apparatus (159). The cleavage is carried out by DUBs like ataxin3.

Ataxin3 acts in conjunction with p97 to regulate the flux of proteins through ERAD (37,38). The DUB is thought to trim ubiquitin chains on ERAD substrates, and may even form a part of the retrotranslocation complex. The two proteins interact directly, both in cells (37,38,53,113,160), and when expressed recombinantly *in vitro* (38,113,160-162), and have been observed together in various multi-protein complexes at the ER membrane (38). Inhibiting ataxin3's DUB activity compromises p97-mediated protein degradation (37,38). In addition, when ataxin3 is overexpressed in cells, it reduces p97's association with Ufd1 and polyubiquitin, and inhibits the

extraction and degradation of substrates, possibly through a dominant negative effect (37). This suggests that unregulated binding between p97 and ataxin3 could alter the physiological regulation of the ERAD, especially in the context of disease-related mutants for either protein, and could thus contribute to disease pathogenesis. Indeed, p97 MSP 1 mutants precipitate significantly increased amounts of ataxin3 in HEK293T cells, and under physiological conditions, in myoblasts from MSP 1 patients (53).

The precise function of ataxin3 has not been characterized, but its chain trimming activity is thought to influence p97-dependent extraction in several ways. The DUB may trim the polyubiquitin chain on a substrate to a specific length required to A) activate p97, or B) enter the central pore of p97 for extraction (163). C) Modulation of the chain by ataxin3 may facilitate recognition and transfer of the substrate from the ER membrane-bound ligase to the p97-extraction complex (164). D) After substrates have been extracted into the cytosol and appropriately re-ubiquitinated, ataxin3 may aid in their transport to the proteasome. The DUB could either release them to a ubiquitin receptor like the Bag6 holdase complex, or a shuttling factor like Rad23 (33), or directly transport them to the proteasome (165). Ataxin3 may also edit the polyubiquitin chain on these substrates to maintain the appropriate degradation signal (159).

1.4.2. Role in longevity and DNA repair pathways

p97 and ataxin3 also collaborate in cellular processes other than ERAD. Briefly, their synergistic functioning regulates longevity and aging in worms, via the insulin – insulin-like growth factor-1 (IGF-1) signaling pathway. Ataxin3 cooperates with p97 to mediate the ubiquitination status of substrates within this pathway, and its DUB activity is essential for both, the stress response and for normal lifespan (126).

The two proteins have also been implicated in DNA repair pathways. They function together, along with other processivity factors like the E4 ligase Ufd-2, within ubiquitination hubs that form after homologous recombination has been initiated at double-stranded break sites (166).

PolyQ expanded ataxin3 impairs the accumulation of p97 and its association with other DNA repair proteins, leading to defective p97 function and an increase in unrepaired breaks (167).

A majority of these studies are at their initial stages, and reflect recent findings on alternate roles for the p97-ataxin3 interaction. Much remains to be elucidated about their concerted biology, both within and outside the ERAD pathway.

The work presented in this dissertation, aims to advance the understanding of the p97-ataxin3 interaction into more mechanistic and molecular realms. By employing complementary biophysical and biochemical techniques, we established an interaction model that may prove applicable to other p97 cofactors and has potential consequences for protein quality-control pathways. In addition, we have provided new insights into the regulation of ataxin3 DUB activity.

CHAPTER 2: Nucleotide-induced Conformation Changes Regulate the p97-Ataxin3 Interaction

The work described in this chapter has been published in (168).

Maya V. Rao‡, Dewight R. Williams§, Simon Cocklin‡, and Patrick J. Loll‡1

‡Department of Biochemistry and Molecular Biology, Drexel University College of Medicine, Philadelphia, PA 19102.
§LeRoy Eyring Center for Solid State Science, Arizona State University, Tempe, AZ 85287.

Author contributions: M.V.R. and P.J.L. designed the experiments. D.R.W. and M.V.R. performed the negative-stain electron microscopy and M.V.R. conducted the remainder of the experiments. S.C. contributed reagents, provided access to SPR instrumentation, and helped design some of the research. M.V.R and P.J.L. analyzed the data and wrote the manuscript.

2.1. Introduction

The protein p97, also known as valosin-containing protein or VCP, is an essential *A*TPase *a*ssociated with various cellular *a*ctivities (type II AAA+ family) (169). p97 forms a hexamer, with each protomer comprising an N-terminal domain, D1- and D2- ATPase domains, and an unstructured C-terminal region (Fig. 2.1A). The D1- and D2-domains form two coaxially-stacked rings, with the N-domains arranged around the periphery of the D1 ring (42,43).

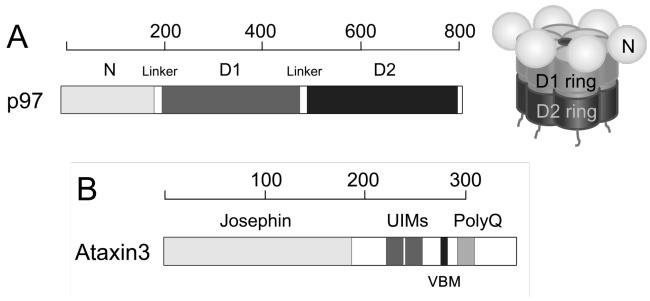

Figure. 2.1. Schematic representation of p97 and ataxin3. *A,* Structure of p97. At *left* is shown the domain organization of the p97 protomer. Each protomer comprises an N-terminal domain shown in *light gray*, D1- and D2- ATPase domains shown in *dark gray* and *black* respectively, and an unstructured C-terminal region. At *right* is shown a cartoon of the assembled hexamer, using the same shading. The D1- and D2- domains form two coaxially-stacked rings around a central pore, with the N-domains arranged along the periphery of the D1 ring. *B,* Domain organization of ataxin3 showing the Josephin domain, two ubiquitin-interacting motifs (UIMs), the p97/VCP-binding motif (VBM), and the polyglutamine (polyQ) repeat region. The linkers, UIMs, VBM, and polyQ regions are not drawn to scale. The scales above each domain representation show length in amino acids.

ATP hydrolysis in the D1- and D2-domains is harnessed to perform mechanical work, allowing p97 to function as a segregase in processes as varied as cell-cycle regulation, transcriptional activation, DNA-damage repair, and membrane fusion (32,71). One of p97's most significant cellular roles is to assist in maintaining proteostasis, and the protein contributes to both proteasomal degradation and autophagy (9,68,170-172). As would be expected for a key component of regulatory and degradation pathways, p97 dysfunction is associated with numerous degenerative disorders (78,79). Missense mutations in p97 cause a set of heterogeneous disorders collectively termed Multisystem Proteinopathy Type 1 (MSP1), which include inclusion body myopathy, Paget disease of the bone and frontotemporal dementia (IBMPFD), and amyotrophic lateral sclerosis (82,173,174). In cell culture, inhibiting or knocking down p97 induces endoplasmic reticulum (ER) stress, and triggers the unfolded protein response, with a concomitant buildup of poly-ubiquitinated substrates (175-180). p97 protects against the toxic effects of aggregation-prone proteins and localizes to cytosolic aggregates (113,181,182). It extracts misfolded and toxic substrates from such aggregates, as well as from macromolecular complexes and cellular membranes, in quality-control processes associated with chromatin and mitochondria (183-186) (reviewed in (145,187)).

p97's involvement in diverse cellular processes is coordinated by a multitude of cofactors that regulate its activity. These cofactors are roughly categorized into substrate-recruiters, which direct p97 to specific pathways, and substrate-processors, which are typically enzymes that fine-tune p97 function (188). The assembly of p97-cofactor complexes drives the subcellular localization of p97, its specificity for substrates, and the ultimate fate of these substrates (189). An important substrate-processing cofactor is ataxin3, a member of the Machado-Joseph disease class of deubiquitinating enzymes (DUBs) (103). Ataxin3 is intimately involved in the clearance of misfolded proteins, playing significant roles in the ubiquitin-proteasome system (33,34,38) and the aggregation-autophagy system (35,136,137,190). Through its ubiquitin-related activities, it suppresses neurodegeneration and cytotoxicity from various polyglutamine-disease proteins (135,140,142). In particular, ataxin3 collaborates with p97 in the process of ER-associated degradation (ERAD) (164), in which proteins that are misfolded or otherwise marked for

destruction are removed from the ER and targeted to proteasomes. In addition, ataxin3 and p97 cooperate outside ERAD in other processes involving protein degradation, such as the control of protein levels involved in the DNA damage response (166). In general, ataxin3 seems to facilitate degradation of proteins targeted for destruction. For example, ataxin3-knockout animals feature increased levels of poly-ubiquitinated proteins and increased levels of the stress response (124,125,191). Interestingly, a mutant form of ataxin3 containing an expanded polyglutamine tract gives rise to aggregates of misfolded protein, and causes the neurodegenerative disorder spinocerebellar ataxia type-3 (SCA3, also known as Machado-Joseph disease; (104-107,192,193)). Therefore, it appears that ataxin3 can both support normal protein degradation, and (in its mutant form) disrupt this same process.

The p97-ataxin3 interaction was first observed via immunoprecipitation from cell extracts (33,113,194). Subsequent studies revealed that p97 and ataxin3 are found together in multi-protein ERAD complexes at the ER membrane and that the proteins also interact *in vitro* (37,38,113,193,194). Overexpression of a catalytically-inactive form of ataxin3 strongly inhibits the processing of ERAD substrates, while overexpression of the wild-type enzyme has a less pronounced, but still inhibitory effect, possibly due to a dominant-negative effect (37,38). The functionality of this interaction has been demonstrated in worms, where p97 and ataxin3 operate synergistically to promote degradation of key substrates (126). The p97-ataxin3 interaction is perturbed by mutations in p97 associated with MSP-1, as significantly elevated amounts of ataxin3 are associated with the mutant p97, as compared to wild-type protein (53).

The molecular details of how p97 interacts with cofactors such as ataxin3 are only now being elucidated. It is becoming clear that different cofactors assemble into complexes with differing stoichiometries (57,58,195). It is also apparent that cofactor binding is influenced by major conformational changes within p97, which are driven by nucleotide binding and hydrolysis (43,54,61). Most p97 cofactors interact with the protein's N-domain (196), which is significant because the N-domain can undergo significant "up-down" motions relative to the D1 ring (43). These conformational changes are largely induced by the nucleotide bound in the D1-domain, with ATP favoring the "up" position, while ADP induces a "down" position. The up-down

equilibrium is disrupted in MSP1 mutants (59,197), in which all six N-domains preferentially adopt the up-state, regardless of the nucleotide present; this behavior correlates with decreased ADP binding to the D1-domain in these mutants (66,67). Even though the MSP1 mutations affect nucleotide binding, they are not located at nucleotide-binding sites, nor at cofactor-binding interfaces. Instead, they are mostly found in the N-domain, with some occurring in the D1-domain and the N-D1 linker (79), suggesting that they might affect cofactor binding by perturbing the N-domain conformation and/or inter-domain communication.

In order to understand the precise interplay between ataxin3, p97, and p97's ATPase cycle, a detailed analysis of binding is required. In this study, we characterized the p97-ataxin3 interaction for wild-type p97 and three common MSP1 mutants, localizing the determinants of binding for each partner and revealing that the dependence of binding upon nucleotide state is starkly different for the wild-type and mutant p97 proteins. We suggest a model in which ataxin3 binding is controlled by a nucleotide-induced shift of the N-domain conformation, which leads to steric displacement of ataxin3 in the ADP-bound state. This model has potential consequences for protein quality-control pathways in both normal and disease states, and may prove applicable to other p97 cofactors.

2.2. Experimental Procedures

2.2.1. Reagents

Enzymes for cloning were purchased from New England Biolabs (Ipswich, MA). PCR primers were purchased from Integrated DNA Technologies Inc. (Coralville, IA) and sequencing of constructs was performed by Genewiz (South Plainfield, NJ). All chemicals were from Sigma-Aldrich (St. Louis, MO) unless otherwise stated, and media components were purchased from Fisher Scientific. Chromatography columns were obtained from GE Healthcare, and all surface plasmon resonance sensor chips and chemicals were purchased from BioRad (Hercules, CA). The Rho1D4 monoclonal antibody was obtained from the University of British Columbia (Vancouver, Canada), and the 5nm Ni-NTA-Nanogold® was purchased from Nanoprobes Inc. (Yaphank, NY).

2.2.2. Cloning and Mutagenesis

Human p97 and ataxin3 proteins were cloned into the pETHSUL vector (198), to generate N-terminal hexahistidine (His_6)-tagged SUMO fusion constructs, under T7 promoter control. p97 was amplified by PCR from cDNA (Open Biosystems; clone ID 6502535). Ataxin3 was amplified from clones kindly provided by Randall Pittman and Henry Paulson; our ataxin3 sequence corresponds to that given in Kawaguchi *et al.* (107), except that the 26-residue polyglutamine tract corresponding to residues 292-317 was replaced by eleven glutamines. Constructs produced using the pETHSUL vector included one extra glycine at the N-terminus (not included in the numbering scheme). The following constructs were used in this work: full-length p97 (amino acids (aa) 1-806), p97 N-domain (aa 1-187), p97ND1 (aa 1-480), full-length ataxin3 (aa 1-345), ataxin3 Josephin domain (aa 1-190), ataxin3 Josephin + UIMs (aa 1-263), ataxin3ΔC (aa 1-292), and ataxin3ΔN (aa 220-345). The pProEX-HTb vector (Invitrogen, Carlsbad, CA) was also used to generate a full-length, N-terminally His_6-tagged ataxin3 construct (aa 1-361). The ataxin3 mutant ^{282}ANAA^{285} and all p97 mutants (Y143A, L72A, R53A, G54W, K251A, K524A, K251A/K524A, R155C/N387C, R155H, L198W, A232E, L198W/R155C/N387C, A232E/R155C/N387C) were generated by one-step PCR-mediated site-directed mutagenesis (199). The C-terminal 1D4 epitope was introduced into the full-length p97 pETHSUL construct by one-step insertion mutagenesis (199). The C-terminal His_6-tagged full-length p97 was cloned as a SUMO-p97 fusion insert into the pETCH vector (198), by Xba1/Xma1 digestion and ligation. Primer sequences and additional details are provided in Appendix 2 Supplemental Data section. Cloning, mutagenesis, and plasmid amplification were performed using the *Escherichia coli* Mach1 strain (Invitrogen). The human gp78 peptide (^{622}VTLRRRMLAAAAERRLQKQ^{640}) was purchased from Biomatik (Wilmington, DE).

2.2.3. Protein Expression and Purification

Detailed information about the preparation of various proteins is given in Appendix 2 Supplemental Protocols. Briefly, all proteins were expressed in *E. coli* Rosetta (DE3) cells (Novagen), by induction with 1 mM isopropyl-β-D-thiogalactopyranoside at an A_{600} of 0.5–0.8,

followed by overnight incubation at 24 °C. Proteins were then purified by subtractive metal affinity chromatography on a HiTrap IMAC HP column (198), followed by size-exclusion chromatography (SEC) on a HiPrep Sephacryl S-300 HR column. The ataxin3 constructs required an additional anion-exchange chromatography step using a HiTrap Sepharose Q HP column. All proteins were concentrated to 8–10 mg/ml using an Amicon® stirred cell (Merck Millipore), shock-frozen in liquid nitrogen, and stored at –80°C.

2.2.4. Surface Plasmon Resonance (SPR)

All SPR experiments were performed on a BioRad ProteOn XPR36 at 25°C using ProteOn GLC sensor chips, unless otherwise stated. The full-length p97 hexamer was captured on the chip in an oriented manner, by employing the Rho1D4 epitope–antibody system (200,201). The Rho1D4 monoclonal antibody was first immobilized to a density of ~3,500 Response Units (RU) on the chip using amine coupling, by injecting 0.1–0.5 mg/ml of the antibody for 7 min, using PBS (Alfa Aesar, Haverhill, MA), pH 7.4 and 0.005% Tween® 20 (VWR, Radnor, PA) as the running buffer. 1D4-tagged full-length wild-type p97 and mutants were captured as ligands, to densities of 100–150 RU, on the antibody-coated surfaces. Various concentrations of analytes, including ataxin3 and ataxin3 fragments with and without nucleotides, were passed over the chip at 150 µl/min, for the maximum possible contact time of 163 s. All interaction experiments were performed in a running buffer containing 25 mM Tris, pH 8.0, 200 mM KCl, 5 mM $MgCl_2$, 0.1 mM tris(2-carboxyethyl)phosphine (TCEP) (Gold Biotechnology Inc., Olivette, MO), 0.005% Tween® 20. Some experiments involving the p97 R155C/N387C variant included 7 mM DTT instead of TCEP, as indicated in the text. The surface was regenerated completely with three injections of freshly prepared 10 mM NaOH and 1% *N*-octyl-β-D-glucopyranoside (Anatrace, Maumee, OH), at 100 µl/min for 18 s, before the next round of 1D4-tagged ligand capture. Additionally, full-length ataxin3 was used as an analyte for the p97 N-domain, which was directly immobilized on the sensor chip by amine coupling (500 RU), and for the His_6-tagged full-length p97 hexamer, which was captured on a ProteOn HTG sensor chip (200–300 RU) (Appendix 2 supplemental Fig. S1).

Sensorgrams were processed and double referenced and the data were fit to an equilibrium binding model using GraphPad Prism 7.0 to derive the binding affinity. Detailed information on all SPR experiments and data analyses are available in the Appendix 2 Supplemental Protocols.

2.2.5. Isothermal Titration Calorimetry (ITC)

ITC measurements were conducted at 25 °C on a Nano ITC calorimeter (TA Instruments). Proteins were extensively dialyzed against 20 mM sodium phosphate, pH 7.0, 200 mM KCl, 5 mM β-mercaptoethanol (βME), and degassed for 15 min before each experiment. Full-length ataxin3, ataxin3ΔC, or ataxin3ΔN (400–855 μM) were placed in the syringe, and titrated as ligands into the sample cell containing 45 μM full-length p97 or 60–80 μM p97 N-domain. The first technical injection of 0.4 μl was followed by 25 injections of 2 μl into the sample cell (300 μl), using 250 rpm stirring and a 200 s delay between successive injections. At least three titration experiments were performed for each ligand, and the data were corrected for heats of dilution by injecting the same ligand concentration into a matched buffer. Corrected data were analyzed with a one-site binding model and nonlinear least-squares fitting to derive the K_D, using the NanoAnalyze 3.5.0 software package.

2.2.6. *In Vitro* Binding Assay

For competition pull-down assays, His_6-tagged ataxin3 was immobilized on Ni Sepharose Fast Flow beads (GE Healthcare) by mixing 50 μl of a 50% slurry with 100 μl of His_6-ataxin3 (5 mg/ml), for 5 min at room temperature (RT), and washing off unbound protein. The beads were then incubated at RT for 5 min with 80 μM p97ND1 or p97ND1 pre-incubated with 800 μM of the competing gp78 peptide (4 °C for 20 min + RT for 5 min). Ni Sepharose Fast Flow beads alone were used as a control. All assays were performed in 50 mM Tris, pH 8.0, 250 mM KCl, 5% glycerol, 5 mM $MgCl_2$ and 5 mM βME. The beads were centrifuged at 5,000 × *g* for 30 s in a 0.2 μm Nanosep® MF centrifugal filter (ODM02C34; PALL Laboratory) and additionally washed four times with

400 μl of buffer. Bound proteins were eluted in 100 μl buffer containing 300 mM imidazole after a 5 min incubation at RT, and analyzed by 12% (v/v) SDS-PAGE.

2.2.7. ATPase Assays

The ATPase activities of wild-type and mutant p97 proteins (Appendix 2 supplemental Figs. S6A, S7, and S8) were measured spectrophotometrically using an NADH-coupled system (202). The decrease in absorbance at 340 nm associated with oxidation of NADH was measured at 0.5 min intervals over 40 min on a DU800 spectrophotometer (Beckman Coulter). The rate of ATP hydrolysis was calculated from the change in A_{340}/min. The assay was performed at RT, in standard buffer (25 mM Tris, pH 8.0, 200 mM KCl, 5 mM $MgCl_2$), containing 2 mM ATP, 3 mM phosphoenolpyruvate, pyruvate kinase (20 units/ml), lactate dehydrogenase (20 units/ml), NADH (200 μg/ml), and 5 μM protein, in a final volume of 85 μl.

2.2.8. Electron Microscopy (EM)

The complex of full-length ataxin3 + p97 was prepared by incubating 5 μM of purified p97 hexamer (~3 mg/ml) with an 11-fold molar excess of ataxin3 at 4 °C for 15 min. The complex was further purified by SEC on a HiPrep Sephacryl S-300 HR column in 25 mM Tris, pH 8.0, 200 mM KCl, 5 mM $MgCl_2$, 0.5 mM DTT (Appendix 2 supplemental Figs. S3B and S4). The fraction corresponding to the complex peak was diluted 20-fold (final concentration ~25 μg/ml) to achieve sufficient dispersion of individual particles and applied to freshly glow-discharged 400 square mesh copper EM grids (Electron Microscopy Sciences, Hatfield, PA), coated with Formvar/carbon film. The grids were stained with 2% uranyl acetate and excess liquid was blotted away with filter paper. Micrographs were collected on a FEI Tecnai T12 (120 kV, LaB_6 filament) microscope, equipped with a Gatan UltraScan1000 CCD camera (2k × 2k pixels), using an indicated magnification of 52,000×, a defocus range between −0.7 to −1.5 μm, and an electron dose of 20 $e^-/Å^2$. A total of 20,256 particles were selected with the EMAN Boxer (203). Two-dimensional (2D) classification generated in the RELION software (204,205) resulted in 50 class-average images.

For the chemical crosslinking, a mixture of 5 μM p97 hexamer and 55 μM His_6-tagged ataxin3 was incubated with EM-grade glutaraldehyde (0.05% final concentration) at 4 °C for 10 min, in 20 mM HEPES, pH 8.0, 150 mM KCl, 2.5 mM $MgCl_2$. The N-terminally His_6-tagged ataxin3 construct was used because the VBM is near ataxin3's C-terminus (see Fig. 2.4). The crosslinking reaction was terminated with Tris, pH 8.0 (25 mM final concentration). Unbound p97 was then removed by immobilized metal-affinity chromatography, which retained the His_6-ataxin3-p97 complex. After elution, unbound His_6-ataxin3 was removed by centrifugation at 5,000 × *g* for 15 min using a 100-kDa-cutoff Amicon® Ultra-15 centrifugal filter (Merck Millipore). After a final round of gel filtration as described above, the complex fraction was diluted 25-fold (final concentration ~10 μg/ml), loaded onto grids, and stained with pH-neutralized 1% uranyl formate. 7,171 images were collected and processed as above, to give 50 class-average images.

For the Nanogold-labelling, the His_6-ataxin3-p97 complex (prepared as described above) was incubated with a five-fold molar excess of 5 nm-diameter Ni-NTA-Nanogold particles at 4 °C for 10 min. Excess Nanogold was removed by centrifugation at 3,000 × *g* for 15 min using a 10-kDa-cutoff Amicon® Ultra-0.5 centrifugal filter (Merck Millipore). The mixture was further purified by gel filtration using a Yarra SEC-3000 column (Phenomenex, Torrance, CA), in 25 mM Tris, pH 7.5, 200 mM KCl, 5 mM $MgCl_2$, 0.5 mM DTT, and the complex fraction was directly applied to grids (~3 μg/ml), stained with 2% uranyl formate, and imaged. See Appendix 2 supplemental Fig. S3B for sample preparation workflow and SEC chromatograms for all EM experiments.

2.3. Results

2.3.1. p97 interaction with ataxin3

It has previously been demonstrated that GST-fused ataxin3 can pull down p97 from cell lysates, as well as from a solution of purified p97 (37,113). To quantitatively characterize this interaction, we used SPR, focusing first on the interaction between the full-length proteins. A C-terminal 1D4 epitope (201) was used to immobilize the p97 hexamer in an oriented manner on a

sensor chip. Ataxin3 was found to bind with an equilibrium dissociation constant (K_D) of 3.7 ± 0.9 μM (Fig. 2.2A).

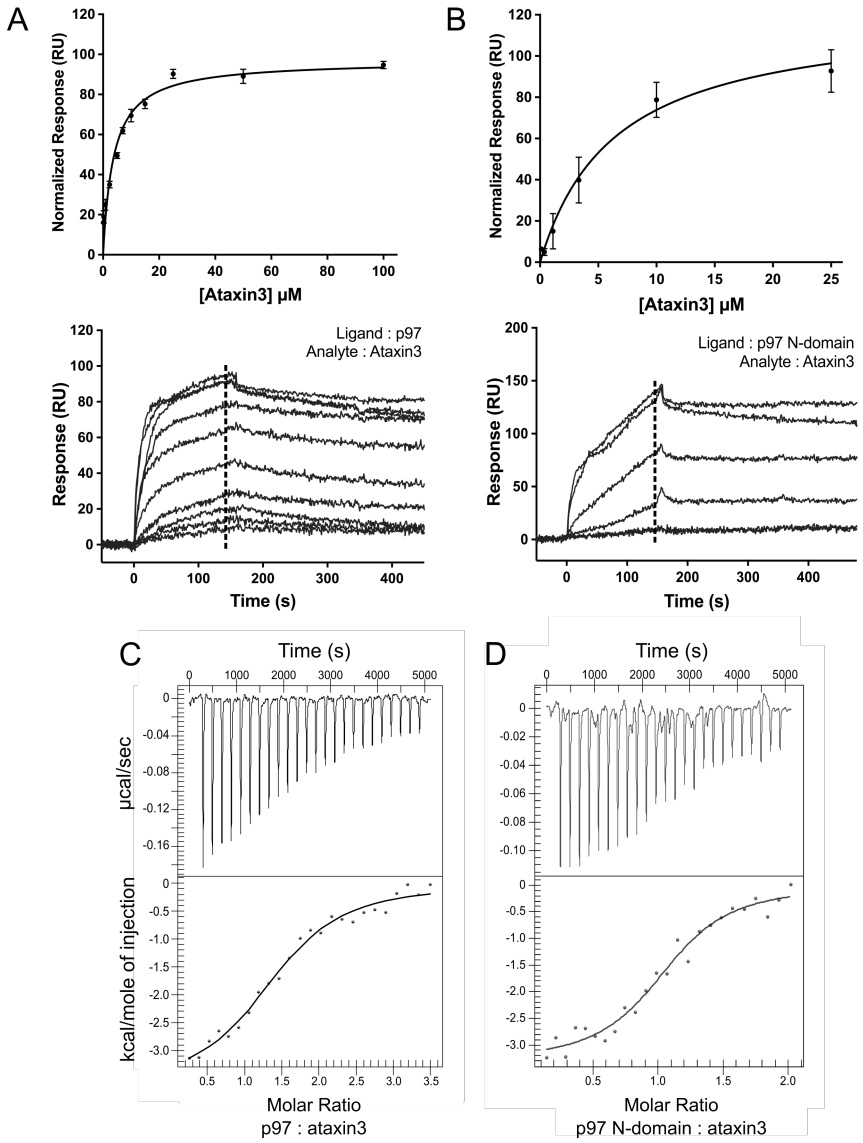

Figure 2.2. p97 interacts directly with ataxin3. *A* and *B,* Ataxin3 binding to p97 as measured by SPR. *A,* full-length ataxin3 binding to full-length p97 or *B*, full-length ataxin3 binding to the p97 N-domain. The upper panels show normalized equilibrium binding responses, fit to a one-site binding model; the lower panels show representative sensorgrams. The *dashed lines* represent the response range used to determine the equilibrium fit (for both *A* and *B, n* ≥ 3 for each concentration). *C* and *D,* Ataxin3 binding to p97 as measured by ITC; *C,* full-length p97 or *D,* the p97 N-domain. The *upper panels* show the raw data for injection of full-length ataxin3 into a cell containing either full-length p97 or the p97 N-domain, and the *bottom panels* show the integrated heat data as a function of the p97/ataxin3 mole ratio (*closed circles).* The solid lines represent the best fit of a one-site model to the data.

A similar K_D value (2.2 ± 0.2 μM) was derived using a different type of sensor chip and immobilization chemistry, indicating that the binding observed is not tag-specific (see Appendix 2 supplemental Fig. S1, A and B). Since most p97 cofactors interact with the protein's N-terminal domain, we next tested the binding of ataxin3 to the p97 N-domain fragment, obtaining a K_D of 6.4 ± 1.5 μM (Fig. 2.2*B*). This is comparable to the affinity observed with full-length p97, and suggests that the N-domain is sufficient for ataxin3 binding. We then verified these results using ITC, an orthogonal technique that should be free of any artifacts and surface effects associated with SPR. The calorimetry experiments yielded K_D values of 8.4 ± 0.1 μM and 4.5 ± 0.2 μM for ataxin3 binding to full-length p97 and the p97 N-domain respectively (Fig. 2.2, *C* and *D*), in good agreement with the SPR data. In addition, we derived stoichiometries of 1.38 ± 0.01 and 1.1 ± 0.2 ataxin3 molecules bound per full-length p97 hexamer and N-domain respectively. The binding data are summarized in Appendix 2 Table 1. Thus, we were able to confirm a direct interaction between p97 and ataxin3, with low-micromolar affinity, centered on p97's N-terminal domain.

2.3.2. EM analysis of the p97-ataxin3 complex

As a homohexamer, p97 can potentially bind up to six cofactor molecules. Our ITC experiments suggest that the binding stoichiometry of ataxin3 to the full-length p97 hexamer is near 1 : 1. In order to confirm the stoichiometry, we analyzed the complex by negative-stain EM. The proteins were incubated together and passed through gel filtration and the complex-containing fractions were negatively stained and imaged. Purified p97 alone was imaged as a control. Our preliminary analyses of the complex fractions revealed an additional blurry density at the periphery of the p97 hexamer that was absent in the control (Appendix 2 supplemental Fig. S2, A and B). The blurred appearance could result from dissociation of the complex (Appendix 2 supplemental Fig. S3A), or a flexible association between the two proteins. Additionally, only around 5% of the total particles selected showed evidence for complex formation, indicating a significant amount of unbound p97 was present. Therefore, in order to stabilize and further enrich for the p97-ataxin3 complex, we crosslinked the proteins using glutaraldehyde, followed by

affinity chromatography to remove unbound p97 and a final round of gel filtration (Appendix 2 supplemental Fig. S3B). The fractions containing crosslinked p97-ataxin3 were stained with 1% uranyl formate and imaged. Around 7,100 particles were selected from individual micrographs (Fig. 2.3A) and sorted into 50 classes. Representative 2D class averages are shown in Fig. 2.3B, in which a single distinct projection is visible at one vertex of the p97 hexamer, indicated by the white arrows. We confirmed that this additional density corresponds to ataxin3 by imaging Nanogold-labelled ataxin3 in complex with p97 (Appendix 2 supplemental Fig. S5). Together with the ITC data, our EM results clearly show that one ataxin3 molecule binds to the p97 hexamer.

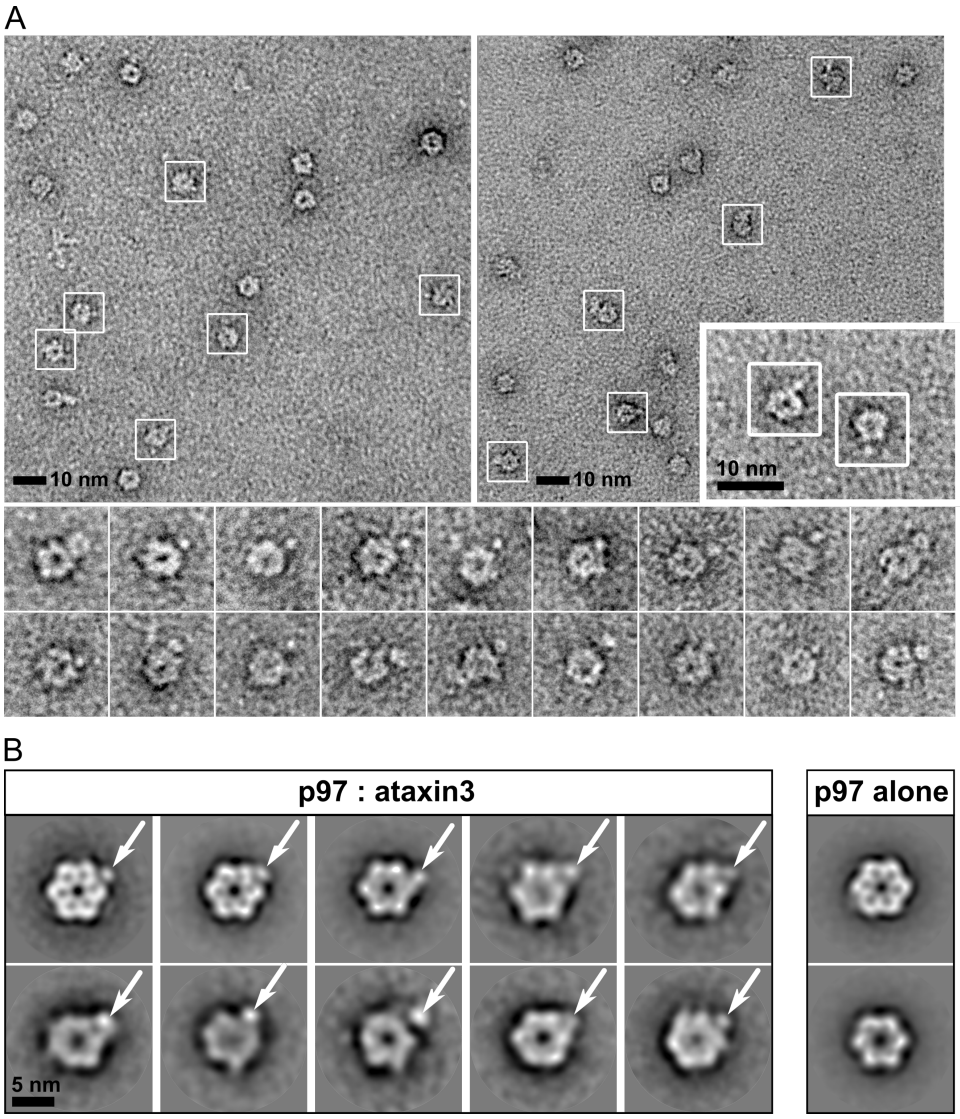

Figure 2.3. Visualization of the p97-ataxin3 complex by negative-stain EM. *A,* electron micrographs taken from different portions of the grid, showing negatively-stained hexamers of p97 crosslinked to ataxin3; *white boxes* show particles identified as complexes. The *inset* (lower right) shows a 2× magnified view of two p97-ataxin3 complexes from a third micrograph, and the *bottom panels* show additional raw images of the complex viewed down the 6-fold axis. *B*, representative 2D class averages derived from ~7,100 particles for the p97-ataxin3 complex (*left*) and p97 alone (*right*). *White arrows* indicate the bound ataxin3 molecule.

2.3.3. Analysis of the p97-ataxin3 binding interface

We next turned to identifying the portions of the ataxin3 and p97 proteins responsible for their interaction. Ataxin3 has a highly-conserved N-terminal Josephin domain that is a cysteine protease with DUB activity; the protein also contains a C-terminal polyglutamine region, two ubiquitin-interacting motifs (UIMs), and an arginine/lysine-rich p97/VCP-binding motif (VBM) (Fig. 2.1B). The VBM has previously been identified as crucial for the p97-ataxin3 interaction (113) and is well-conserved across different species (Fig. 2.4A). This motif corresponds to residues 282-285, and has the sequence RKRR. To determine if this minimal VBM is sufficient for interaction with p97, we mutated these residues to ANAA (37) and assessed the proteins' interaction by SPR, which revealed that binding was completely abolished for the mutant (Fig. 2.4D). We also tested the binding of various deletion constructs of ataxin3 (Fig. 2.4, B and C). N-terminal fragments corresponding to the Josephin domain alone or the Josephin domain plus the UIMs failed to bind to p97. However, an ataxin3 N-terminal fragment truncated after the VBM (ataxin3$_{1-292}$, denoted hereafter as ataxin3ΔC) bound p97 with the same affinity as full-length ataxin3 (Fig. 2.4D). These results were supported by ITC experiments that showed full-length ataxin3, ataxin3ΔC, and an ataxin3$_{220-345}$ C-terminal fragment (ataxin3ΔN) all bind the p97 N-domain with equal affinities (Fig. 2.4, E and F; Appendix 2 Table 1). Therefore, we conclude that ataxin3's VBM sequence is necessary and sufficient to mediate binding with p97.

To map the region of p97 that interacts with ataxin3, we first noted that in two recent crystal structures, peptides containing either a VBM motif or a related p97/VCP-interacting motif (VIM) bind in the same site, within a cleft separating the two lobes of the p97 N-terminal domain (64,206,207). Other interacting partners also bind in or near the same site; these include the UBX and UBXL domains, whose binding sites overlap the VBM/VIM cleft, despite their possessing very different structures (56,58,63,208). To test if ataxin3 utilizes the same binding cleft, we performed competition pull-down assays, using a VIM-containing peptide from the ubiquitin ligase gp78 (64). This peptide prevented His$_6$-tagged ataxin3 from pulling down the p97 fragment containing N and D1 domains (Fig. 2.5C), suggesting competition for the same site. We then mutated residues lining this binding cleft (Fig. 2.5A), and tested the mutants' abilities to bind ataxin3 using SPR.

Changing residues Tyr[143] and Leu[72] to alanine completely abolished binding, while the R53A and G54W mutations both partially reduced the interaction (Fig. 2.5, B and D). These results collectively demonstrate that the VBM of ataxin3 binds in the same inter-lobe cleft of the N-domain that is utilized by many other p97 cofactors.

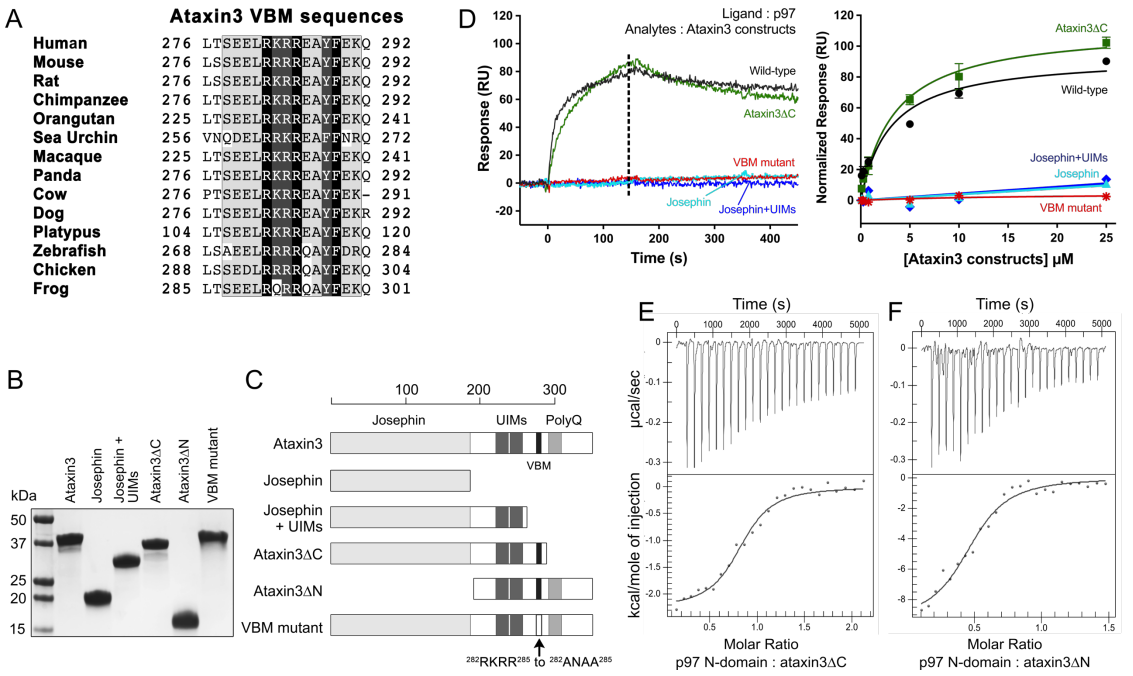

Figure 2.4. The ataxin3 VBM is necessary and sufficient for interaction with p97. *A,* alignment of the VBMs from different ataxin3 homologs showing conservation across species. *B,* SDS-PAGE gel of the different purified ataxin3 constructs used, stained with Coomassie Brilliant Blue. *C,* schematic representation of the ataxin3 constructs shown in B. *D, left,* representative SPR responses for ataxin3 constructs binding to immobilized full-length p97 (for all constructs, analyte concentration = 10 μM); *right,* normalized equilibrium binding responses for the same constructs, fit to a one-site binding model ($n \geq 3$ for each concentration). The *dashed line* in the left panel represents the response range used to determine the equilibrium fit. *E,* and *F,* ITC raw and fitted data for the binding of the p97 N-domain to ataxin3 deletion constructs. *E*, injection of ataxin3ΔC into the p97 N-domain; *F,* injection of ataxin3ΔN into the p97 N-domain.

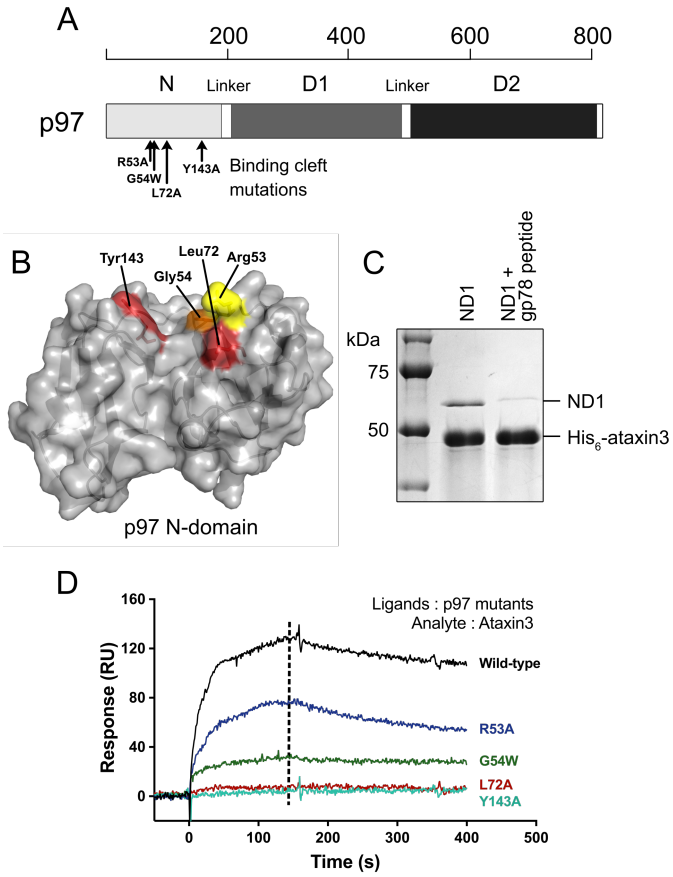

Figure 2.5. The inter-lobe cleft of the p97 N-domain forms the ataxin3 binding site. *A,* schematic representation of a p97 protomer showing the approximate positions of mutated residues *(black arrows)* in the N-domain. *B,* surface representation of the p97 N-domain (PDB entry 3TIW (64)) showing the binding cleft that separates the two lobes, and the residues lining the cleft that were mutated for binding experiments. Residues in *red* are the most crucial for ataxin3 interaction, since their mutation completely abolishes binding. Mutating the residues in *orange* and *yellow* partially reduces binding, thus these residues contribute moderately to the interaction. *C,* competition pull-down assays involving His_6-tagged ataxin3 and the p97 ND1 construct, incubated in the presence or absence of a VIM-containing peptide from gp78. *D,* representative SPR responses for 10 μM ataxin3 passed over immobilized wild-type or mutant p97 ($n \geq 3$ for each). The *dashed line* represents the time for which the response values were compared.

2.3.4. Effect of nucleotides on the p97-ataxin3 interaction

In the p97 ATPase cycles, nucleotide hydrolysis is accompanied by major conformational changes in the hexamer (42,48); hence, it is reasonable to suspect that ataxin3 binding would be sensitive to the nucleotide-binding state, and indeed, evidence is available to support this idea (113). To quantify this effect, we measured the binding of ataxin3 to p97 in the presence of various nucleotides. As shown in Fig. 2.6A, p97 binds ataxin3 in the presence of ATP, ATPγS, and AMP-PNP, as well as in the absence of added nucleotide. In contrast, ADP significantly inhibits the interaction, with an IC_{50} of 5.5 ± 1.1 μM (Fig. 2.6, A and B).

There are two nucleotide binding sites per p97 monomer, one each in the D1- and D2-domains (Fig. 2.6C); the D1-domain binds ADP approximately ten-fold more tightly than the D2-domain (52,59,177,209). In p97 preparations, a fraction of the D1-domains is typically occupied by ADP that is carried through the purification (52). Thus, even when no nucleotide is added, some ADP is likely present; added nucleotide is expected to saturate unoccupied sites and compete for the pre-occupied sites. To determine which site ADP acts through to disrupt the p97-ataxin3 interaction, we generated mutations in the Walker A motifs that selectively perturb nucleotide binding in each domain, introducing the K251A mutation in the D1-domain and the K524A mutation in the D2-domain. The mutant proteins form normal hexamers and exhibit decreased ATPase activity, especially the D2 mutants (Appendix 2 supplemental Fig. S6), which is consistent with previous findings (52). We used SPR to test the interaction of these mutants with ataxin3 in the presence of 0, 10 and 100 μM ADP (Fig. 2.6, D to H). In the absence of ADP, all the mutants bound ataxin3 with the same affinity as wild-type p97 (Fig. 2.6D). When ADP was included in the binding assay, the mutant in which the D2-domain was disrupted behaved like wild-type p97, displaying an ADP-dependent inhibition of ataxin3 binding (Fig. 2.6, E and G). However, mutants in which the D1-domain was disrupted (K251A and K251A/K524A) were still able to interact with ataxin3, even in the presence of 100 μM ADP (Fig. 2.6, F and H). Thus, ADP's inhibition of the p97-ataxin3 interaction appears to be mediated largely through nucleotide binding to the D1-domain.

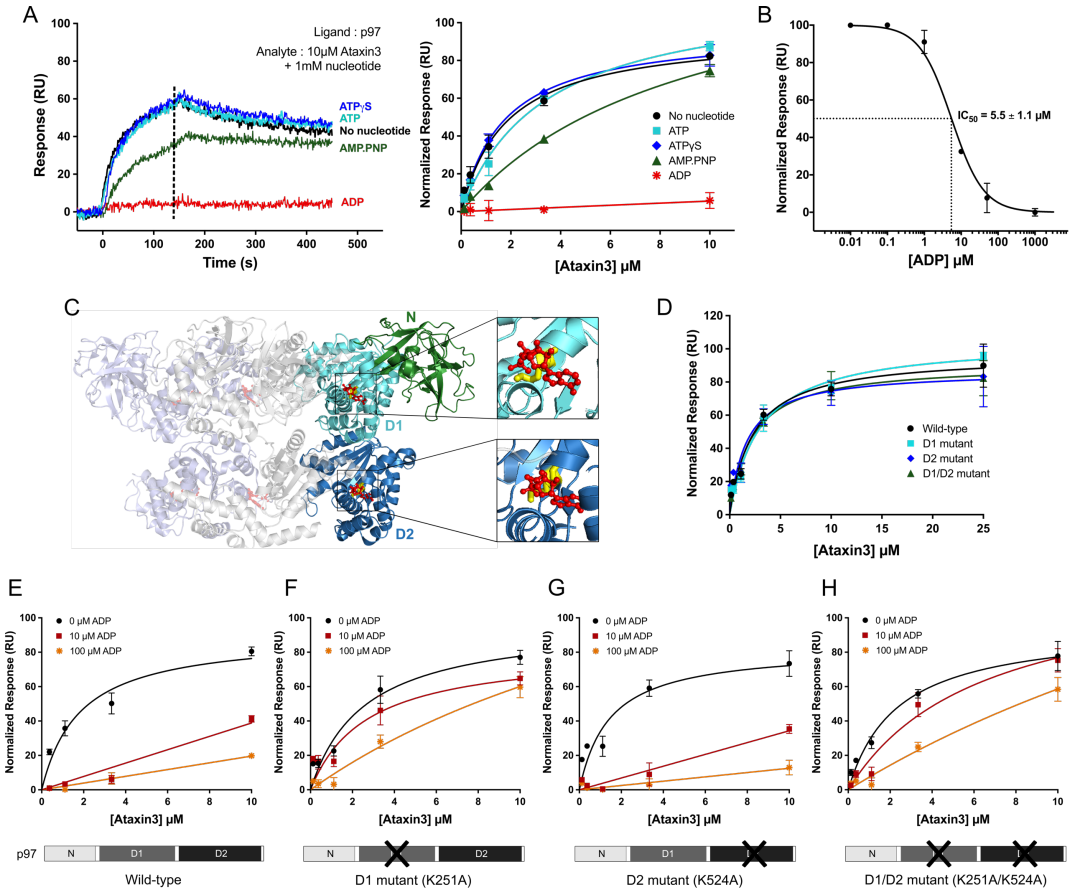

Figure 2.6. ADP inhibits the p97-ataxin3 interaction by binding to the D1-domain. *A, left,* SPR responses for 10 μM ataxin3 binding to immobilized full-length p97, in the presence of different nucleotides (1 mM), or in the absence of added nucleotide; *right,* normalized equilibrium responses, with and without 1 mM of the indicated nucleotide. The *dashed line* represents the response range used to determine the equilibrium fit. *B,* Inhibition of ataxin3 binding to immobilized full-length p97 by ADP. Ataxin3 concentration was 10 μM; the IC_{50} value was calculated from the nonlinear least-squares regression fit, represented by the *solid line*. *C,* ribbon representation of the side view of full-length hexameric p97 bound to ADP (PDB entry 5FTK (43)); for clarity's sake, only three of the six protomers are shown. Two protomers are colored *light blue* and *light gray*, and the third is colored *green*, *cyan*, and *deep blue* (denoting the N-, D1-, and D2-domains respectively). ADP is shown in *red* (ball and stick form), and two conserved Walker A residues crucial for ADP binding are shown in *yellow* (Lys-251 in the D1-domain and Lys-524 in the D2-domain). *D,* normalized equilibrium SPR responses for ataxin3 passed over immobilized wild-type p97 and the Walker mutants. *E – H,* effect of ADP on ataxin3 binding to immobilized p97. *E,* wild-type p97; *F,* D1 mutant; *G,* D2 mutant; and *H,* D1/D2 double mutant. For each p97 construct, ataxin3 binding is shown in the presence of 0, 10, and 100 μM ADP. For all SPR experiments shown, $n \geq 3$ for each concentration; equilibrium binding curves are fit to single-site binding models.

2.3.5. A conformationally-locked form of p97 cannot bind ataxin3

We next probed the mechanism by which ADP binding inhibits the p97-ataxin3 interaction. Recent cryo-EM structures of p97 reveal that when ADP occupies the D1-domain, the N-domain is positioned along the side of the hexamer, coplanar to the D1 ring (43); this conformation is referred to as the "down-state" (59). In contrast, in the presence of ATP, the N-domain moves above the hexamer, to adopt the "up-state." To test whether this conformational change affects ataxin3 binding, we generated the R155C/N387C mutant of p97. These two residues form a disulfide bond under oxidizing conditions, which tethers the N-domain to the D1-domain, mimicking the down-state, even in the absence of ADP (54) (Fig. 2.7A). In the disulfide-locked form, this mutant has very low ATPase activity; activity can be restored by addition of reducing agent (Appendix 2 supplemental Fig. S8). Under oxidizing conditions, ataxin3 did not interact with the R155C/N387C double mutant; however, under reducing conditions (+ DTT), the interaction was restored (Fig. 2.7B). The interaction of wild-type p97 with ataxin3 served as a control for any non-specific effects of the reducing agent (Fig. 2.7C). These results suggest that the down-state conformation does not allow for ataxin3 binding, and that ADP inhibits the p97-ataxin3 interaction by driving the N-domain into the down-state.

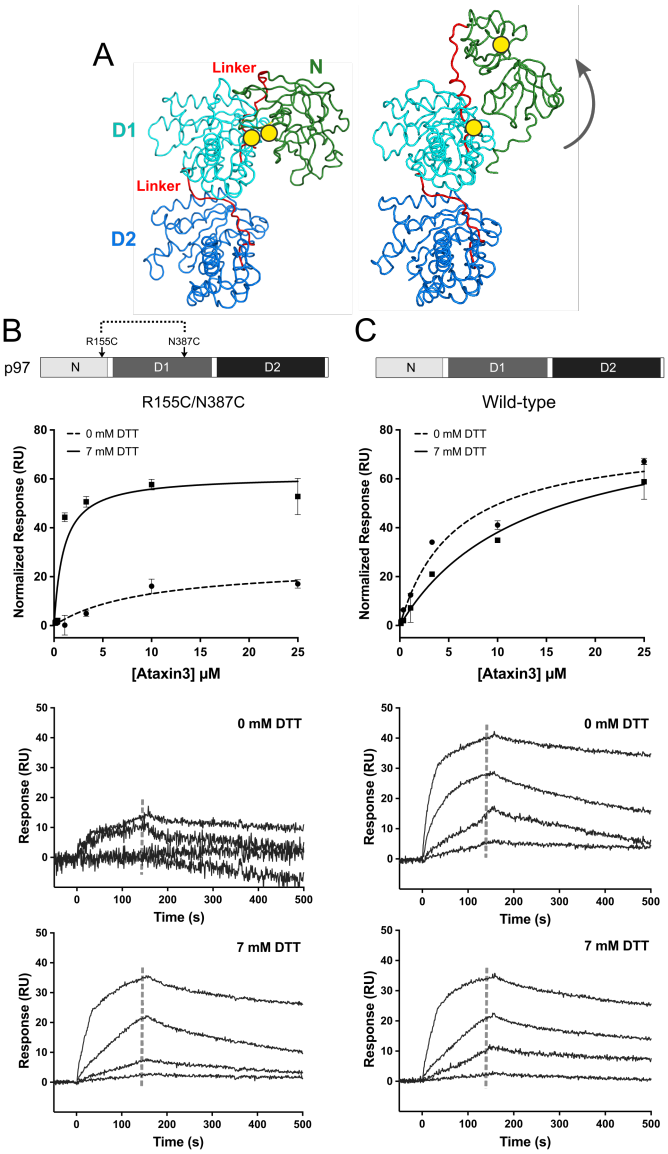

Figure 2.7. A conformationally-locked form of p97 cannot bind ataxin3. *A,* ribbon representations of the side view of a p97 protomer (PDB entries *left,* 5FTK and *right,* 5FTN (43)), with the N-, D1-, and D2- domains shown in *green*, *cyan*, and *deep blue* respectively, and the two linkers in *red*. The *yellow circles* mark the positions of the R155C and N387C mutations that form a disulfide bond under oxidizing conditions (– DTT), locking the N-domain in the down-state *(left)*. When the disulfide bond is reduced (+ DTT), the N-domain is flexible and free to move to the up-state (*right*), as indicated by the *gray arrow*. In *B* and *C,* the *top panels* show normalized SPR equilibrium responses fit to one-site binding models, and *bottom two panels* show binding to immobilized p97 with and without 7 mM DTT. *B,* R155C/N387C double mutant; *C*, wild-type p97 ($n \geq 3$ for each concentration). The *gray dashed lines* in the sensorgrams represent the response range used to determine the fit.

2.3.6. Ataxin3 binding is sterically hindered in the down-state conformation of p97

Crystal structures are available for the p97 N-domain bound to VBM and VIM peptides (Protein Data Bank ID codes 5EPP and 3TIW respectively) (64,206). When these structures are superimposed on the structure of the full-length p97 hexamer in the down-state, the peptides are oriented with their C-termini projecting directly toward the D1 ring of the hexamer (Fig. 2.8A). In ataxin3, there are approximately 60 residues located downstream of the VBM (Fig. 2.4C); hence, if the ataxin3 VBM adopts the same binding pose as that observed in 5EPP and 3TIW, these 60 residues at the protein's C-terminal end would sterically clash against the D1 ring when the p97 hexamer is in the down-state conformation (Fig. 2.8B). This suggests an explanation for why ataxin3 fails to bind when p97 is in the ADP (down-state) form. To test this hypothesis, we assessed the binding properties of the C-terminal truncation ataxin3ΔC. Unlike the full-length protein, ataxin3ΔC was still able to bind to p97 in the presence of ADP, and could also bind to the R155C/N387C double mutant under both oxidizing and reducing conditions (Fig. 2.8, C and D; Appendix 2 supplemental Fig. S9A). These results are consistent with a steric clash between the ataxin3 C-terminal region and p97's D1-ring in the down-state conformation, providing a structural rationale for the effects of ADP upon the p97-ataxin3 interaction.

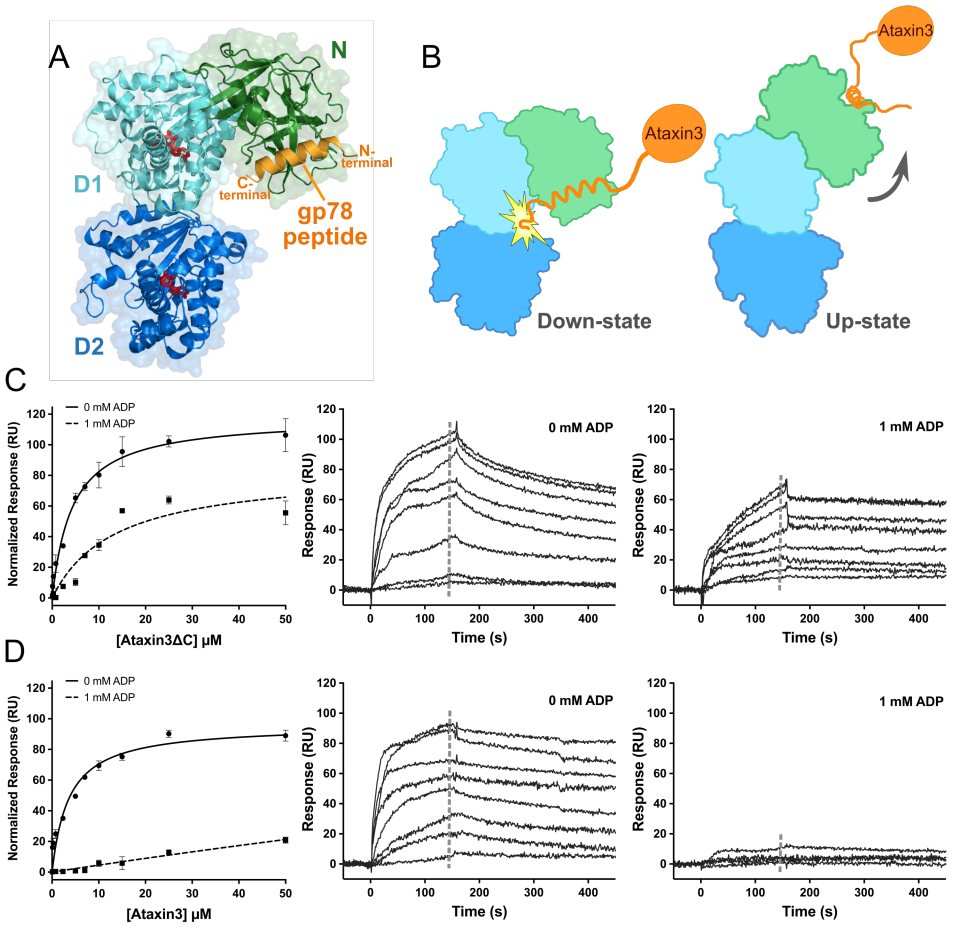

Figure 2.8. Ataxin3 binding is sterically hindered in the down-state conformation of p97. *A,* superposition of the structure of the p97 N-domain bound to the gp78 VIM peptide (PDB entry 3TIW (64)), and the structure of one protomer of full-length p97 in the ADP-bound form (PDB entry 5FTK(43)). The N-, D1-, and D2- domains are shown in *green*, *cyan*, and *deep blue* respectively, the gp78 VIM peptide in *orange*, and ADP in *red*. The N- and C- terminal ends of the peptide are labelled in *orange*. *B,* diagram depicting the predicted steric clash of ataxin3's C-terminal against the D1-domain in the down-state conformation, and unobstructed binding in the up-state. The orientation and color scheme for the p97 subunit are as in *A,* and ataxin3 is shown in *orange*. *C,* and *D,* binding of full-length ataxin3 and ataxin3ΔC to immobilized full-length p97, with and without 1 mM ADP. *Left panels* show normalized SPR equilibrium responses fit to one-site binding models, and *center and right panels* show representative sensorgrams ($n \geq 3$ for each concentration). The *gray dashed lines* in the sensorgrams represent the response ranges used to determine the equilibrium fits.

2.3.7. ADP does not affect the binding of p97 MSP1 mutants to ataxin3

MSP1 mutations in p97 alter the equilibrium between the down and up conformations of the N-domain (54,59,210). These mutations also increase p97's ATPase activity (54,91) and lower ADP affinity for the D1-domain (59,210). Moreover, the binding of MSP1 mutants to cofactors is perturbed relative to that of the wild-type protein, as seen both in cells (53,91,211) and when using purified proteins (53,66). Because many of these cofactors bind in the same inter-lobe cleft in the N-domain that is used by ataxin3, we sought to determine whether the interaction with ataxin3 is altered for MSP1 mutants.

The pathogenic MSP1 mutations in p97 are principally located in the N-domain, the N-D1 linker, and the D1-domain. We chose to study one mutation from each of these three regions, namely R155H, L198W, and A232E (Fig. 2.9, A and B). The Arg^{155} mutation is the most prevalent and widely-analyzed, and A232E has been linked to early-onset and more severe myopathy and dementia (212). L198W was initially detected in MSP1 tissue samples containing rimmed vacuoles and cytoplasmic inclusions (174), and its effect on N-domain dynamics has been investigated by NMR (197). None of these mutations are at nucleotide-binding sites, or in the binding cleft for cofactors (Fig. 2.9B). All three mutant proteins had unaltered oligomeric states and elevated ATPase activities as compared to wild-type p97 (Appendix 2 supplemental Fig. S7) (54,67). We immobilized them on an SPR sensor chip, using the same oriented-attachment strategy as for wild-type p97, and measured their interaction with ataxin3 with and without ADP. In the absence of ADP, all three mutants bound ataxin3 with affinities similar to that of wild-type p97 (Fig. 2.9C). However, in the presence of ADP the mutants still interacted with ataxin3, unlike the wild-type protein (Fig. 2.9D). ADP did not inhibit the interaction with ataxin3, even at concentrations well above the reported K_D values for the binding of ADP to the D1-domain (52,59,177,209). In wild-type p97, binding of ADP to the D1-domain triggers the down-state conformation, disrupting the ataxin3 interaction; thus, our results indicate that in the MSP1 mutants, ADP binding fails to induce the down-state, and therefore does not inhibit the ataxin3 interaction. To test this, we introduced the L198W and A232E mutations into the disulfide-locked R155C/N387C variant of p97. Both the L198W and A232E versions of the R155C/N387C mutant bound to ataxin3, even

under oxidizing conditions (Appendix 2 supplemental Fig. S10, A and B), suggesting that Cys-155 and Cys-387 are never in close enough proximity to form a disulfide bond and lock the protein in the down-state. In line with previous findings (59,85,197), it appears that the mutants rarely adopt the down-state, favoring instead a conformation placing the N-domains in the "up" position.

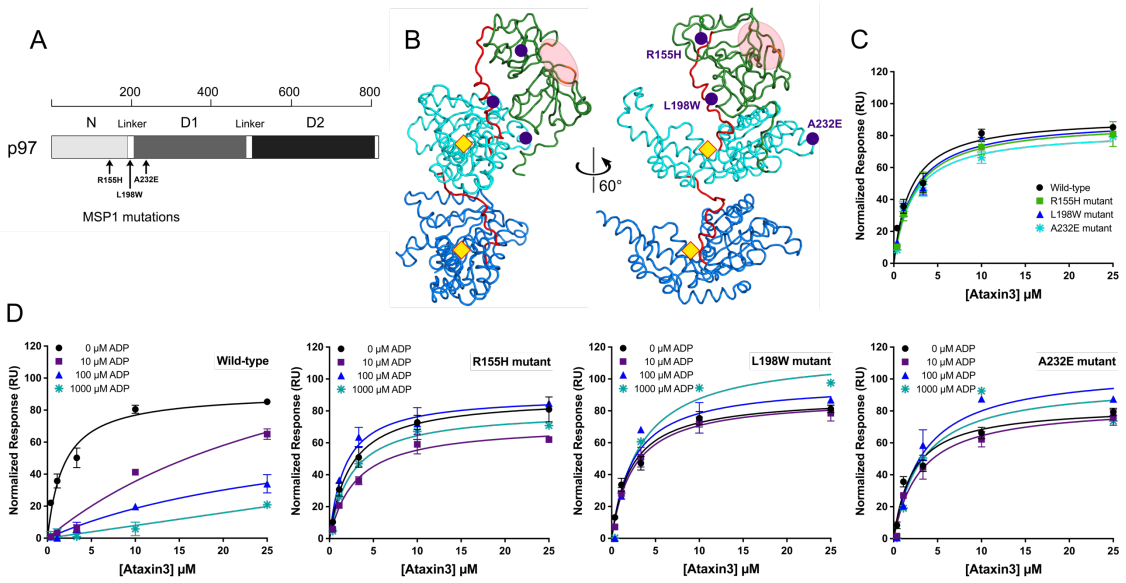

Figure 2.9. ADP does not inhibit ataxin3 binding to p97 MSP1 mutants. *A,* schematic representation of p97 showing the approximate positions of the three MSP1-related mutations *(black arrows)*. *B,* ribbon representations of the side view of a p97 protomer (PDB entry 5FTN (43)), with the N-, D1-, and D2- domains shown in *green*, *cyan*, and *deep blue* respectively, and the two linkers in *red*. The *purple circles* mark the positions of the R155H, L198W and A232E MSP1 mutations in the N-domain, N-D1 linker and D1-domain respectively. The *yellow diamonds* represent the approximate D1 and D2 nucleotide-binding sites, and the *light pink ellipse* highlights the cofactor binding cleft. The view on the *left* is rotated 60° anti-clockwise around the in-plane vertical axis to obtain the view on the *right*. In *C* and *D,* normalized equilibrium SPR responses are shown for ataxin3 binding to immobilized wild-type p97 and each of the MSP1 mutants. Panel *C* shows ataxin3 binding to wild-type and mutant p97 in the absence of ADP. Panel *D* shows the effects of 0, 10, 100, and 1000 µM ADP on ataxin3 binding to wild-type p97 and the three MSP1 mutants R155H, L198W, and A232E ($n \geq 3$ for each concentration).

2.4. Discussion

Using both SPR and ITC, we have shown that ataxin3 binds p97 with an affinity in the low-micromolar range. This is comparable to affinities reported for other p97 cofactors, which typically range from approximately 0.5 to 20 μM for intact proteins and isolated VIMs, and from approximately 50 to 70 μM for isolated VBMs (Appendix 2 supplemental Table S3). Our affinity measurements are also consistent with ITC studies that measured the binding of the ataxin3 VBM peptide to the p97 N-domain, reporting a K_D of 15.6 μM (161). In contrast, our measurements are not consistent with a previous report in which SPR was used to derive a substantially higher affinity estimate for the p97-ataxin3 interaction (K_D ~1 nM) (162). However, as we have shown in this work, the p97-ataxin3 system presents challenges when using SPR to measure binding affinities, and if mass transport and rebinding events are not accounted for appropriately, the affinity and binding kinetics will not be calculated correctly (see Appendix 2 supplemental protocols, SPR experimental details and Figs. S12 and S13). The experiments described in reference (162) feature high ligand immobilization density, low analyte flow rates, and short dissociation times, all conditions likely to promote surface-induced artifacts, which are reflected in poor global fits to the kinetic data. Hence, the apparent disagreement between our affinity measurements and those reported in the earlier paper may simply reflect differences in data analysis, and not a genuine difference in the behavior of the proteins.

We have also shown that ataxin3 associates with p97 in a stoichiometry of one ataxin3 molecule per p97 hexamer. Binding stoichiometries vary considerably for different p97 cofactors; for example, the p97 hexamer binds to a single Ufd1/Npl4 heterodimer and a single molecule of the deubiquitinating enzyme Otu1, but three molecules of p47 (57,58,213). Binding of only a single ataxin3 molecule per hexamer may leave room for the binding of other cofactors, or alternately, binding of one ataxin3 molecule may prevent interaction with other cofactors. For example, overexpression experiments in cell culture suggest that the binding of ataxin3 and Ufd1 to p97 is mutually exclusive (37). It is currently still unclear how the binding of a single ataxin3 cofactor to the p97 hexamer is sensed by the remaining five protomers, but it seems reasonable to speculate

that the sensing mechanism would entail conformational changes involving the N-terminal domains.

Our experiments do reveal how conformational changes control the nucleotide-dependent recognition of p97 by ataxin3. p97 binds many different cofactors, some of which have antagonistic functions; therefore, cofactor binding must be carefully controlled. This control may be exerted through different mechanisms, such as post-translational modification (214) or upregulation of cofactor levels (78). In the case of ataxin3, binding is clearly regulated by the nucleotide binding state of the p97 hexamer, as demonstrated by pull-down experiments using cell lysates and recombinant proteins (113). A similar, albeit less pronounced, nucleotide-based control of binding has also been reported for the cofactor p47 (66). We have probed nucleotide control of ataxin3 binding to p97 using purified proteins, confirming that the two proteins associate in the presence of ATP or the absence of nucleotide, but not in the presence of ADP. We propose a mechanism to explain this behavior, drawing upon recent cryo-EM studies that reveal that different nucleotides give rise to distinct p97 conformations in which the N-terminal domain moves relative to the D1-ring (43). Taken together with our data, these experiments suggest that an ADP-driven downward movement of the N-terminal domain dislodges ataxin3 by causing a steric clash between the D1-domain and ataxin3's C-terminus. Since ataxin3 uses a binding site on the N-terminal domain that is also used by other p97 cofactors, this steric dislodgement mechanism may also occur with other cofactors, depending upon their geometry of binding.

This model helps to explain how recognition of ataxin3 is altered in MSP1 mutants of p97. In cells, MSP1 mutants bind significantly elevated amounts of ataxin3 as compared to wild-type p97 (53). We show that the mutant proteins' affinities for ataxin3 are unchanged; however, whereas ADP abolishes ataxin3 binding to wild-type p97, it does not inhibit ataxin3 binding for the mutants. Hence, the elevated ataxin3 binding observed in cells can be explained by a failure of the mutant p97 proteins to release ataxin3, even after ATP has been hydrolyzed to ADP. This atypical ataxin3 binding reflects defective inter-domain communication in the MSP1 mutants, which makes them unable transduce the ADP-bound signal from the D1 to the N-domain. The failure to release ataxin3, even in the presence of ADP, could perturb normal processing of ubiquitinated

substrates, possibly by preventing other cofactors from binding; for example, MSP1 mutants that bind elevated levels of ataxin3 bind reduced amounts of the ubiquitin ligase E4B (53). Additionally, an increased residence time on p97 might disrupt ataxin3's normal patterns of sub-cellular localization, since residues within ataxin3's VBM form a functional nuclear localization sequence (215). Binding to p97 may mask this sequence and reduce nuclear levels of ataxin3. Notably, ataxin3 is not the only cofactor for which binding is perturbed in the MSP1 mutants; nucleotide control of p47 binding is also altered in the mutants (66), which suggests that the ADP-driven conformational changes may be a general mechanism for regulating cofactor binding.

Ataxin3 is thought to coordinate with p97 to maintain the flux of proteins through ERAD (164); however, its specific role has not been elucidated at the molecular level. In ERAD, p97 acts as a segregase, coupling ATP hydrolysis with the removal of ubiquitinated substrates from the ER. The importance of ubiquitination is quite clear—substrates must be ubiquitinated in order for p97 to be recruited to the site of protein dislocation (156), and non-ubiquitinated substrates are not efficiently unfolded and translocated by p97 (163,216). Furthermore, if the substrate is to be targeted to the proteasome, it should remain ubiquitinated once released from p97. However, the function of deubiquitination in ERAD is less clear, and thus the part played by ataxin3 has not been immediately obvious. One possibility is that ataxin3 edits non-K48 ubiquitin linkages that will not be efficiently recognized by the proteasome; this is consistent with the report that the enzyme recognizes mixed-linkage ubiquitin chains (117). Another possibility is that ataxin3 serves to trim excessively long ubiquitin chains to a minimum length necessary for proteasomal degradation. Such an activity would allow for recycling of ubiquitin molecules; it might also ease the burden on p97, since it appears that ubiquitin chains attached to substrates must be threaded through the central pore of the p97 hexamer, along with the substrate (163). Such a trimming activity for ataxin3 would be consistent with its observed substrate specificity, which is skewed toward longer ubiquitin chains. In fact, ataxin3 is quite inefficient at cleaving tetra-ubiquitin and smaller chains (99), which coincides with the minimum size required for efficient proteasome targeting (121). Thus, one possible model is that p97 is first recruited to a ubiquitinated substrate by the cofactors Ufd1/Npl4, after which ataxin3 binds (possibly triggering release of Ufd1/Npl4).

The ataxin3 then can trim excessive ubiquitin chains and/or remove incorrect linkages as the substrate is being translocated. Our EM results suggest that the linkage between ataxin3 and p97 is a flexible one, which could allow for continuous processing of ubiquitin chains even as the substrate is being threaded through the pore. Once the p97 catalytic cycle is finished and ATP is hydrolyzed to ADP in the D1-ring, the ataxin3 would be released. Given that the D1-ring only needs to undergo one or a few hydrolysis cycles in order for an entire substrate to be processed (163), ataxin3 may be able to fully complete its task during a single ATP/ADP cycle. It is also possible that ataxin3, once dislodged from p97, can re-engage with ubiquitinated substrates that have been released from p97, possibly facilitating their hand-off to shuttling factors like Rad23 and Dsk2 for delivery to the proteasome (217,218).

CHAPTER 3: Ataxin3 is Activated by Non-Covalent Interactions with Ubiquitin

3.1. Introduction

The modification of targets by ubiquitin is a powerful and versatile form of regulation. Ubiquitination can brand a protein for destruction, alter its intracellular location, or regulate its function. It is not surprising that the ubiquitin molecule is central to a diverse range of cellular processes, from transcription, translation, and signal transduction, to protein trafficking, organelle assembly, and cell cycle control (15-18). Typically, ubiquitination involves a covalent modification of other proteins. There have been reports however, of non-covalent ubiquitin control (219-221), wherein the ubiquitin signal is recognized and processed by ubiquitin-binding domains (UBDs). UBDs form transient and non-covalent interactions with both single molecules and chains of ubiquitin. Over 20 families of UBDs have been identified; most of them encode α-helical structures, including the ubiquitin-associated domain (UBA) and the ubiquitin-interacting motif (UIM) (221-223).

Most protein-protein interaction interfaces are formed by hydrophobic contacts, and the UIMs are no exception. The highly-conserved short peptide sequence of the UIM binds mono- and poly-ubiquitin primarily via hydrophobic residues that recognize the Leu-8/Ile-44/Val-70 hydrophobic patch on ubiquitin (224,225). Proteins often contain multiple copies of the UIM connected by linkers of varying lengths. These UIM repeats typically bind ubiquitin in a cooperative manner (226,227), and the binding can be specifically altered or disrupted by mutation of conserved residues within the UIM (101,119,228). Some proteins lack *bona fide* ubiquitin-binding sites like UIMs, but are still able to bind ubiquitin non-covalently. Often, these non-canonical binding sites are merely exposed hydrophobic patches or aromatic clusters on the protein surface that can facilitate short-lived, low-affinity interactions with hydrophobic residues on ubiquitin (102). This poses a challenge to identify and characterize such sites, due to the possibility of non-specific or irrelevant interactions with ubiquitin, and their scant sequence homology with other known binding interfaces.

The binding of ubiquitin to targets, both covalently and non-covalently, signals different outcomes for these targets in various pathways. DUBs are enzymes that reverse or switch off the signaling message from ubiquitin or poly-ubiquitin chains (Fig. 1.2). They function by cleaving ubiquitin from substrates, editing the length or type of ubiquitin chains, and disassembling untethered poly-ubiquitin chains to recycle ubiquitin molecules (reviewed in (97,229,230)). There are nearly 100 DUBs encoded by the human genome (230), and relatively little is known about their precise function or regulation. DUB activity may be regulated at the level of transcription or degradation, and sometimes by substrate-induced conformation changes, complex formation or post-translational modifications (97,229-231).

DUB activity is sometimes controlled by its own ubiquitination (reviewed in (232)). For example, the ubiquitination of K157 on UCH-L1 decreases its activity, while the opposite is observed for ataxin3 and Josephin1 on their K117 residues (120,233,234). To date, there are no reports of whether non-covalent ubiquitin interactions also modulate DUB activity. The possibility of this type of regulation is suggested by studies of other enzymes involved in the ubiquitin pathways. A ubiquitin-binding site on the E2 ligase UBE2B, remote from its active site, was first described in 1999 (235); since then, many other E2 and E3 ligases were found to be controlled by low-affinity interactions with ubiquitin (219). The RING domain in some E3s contacts the ubiquitin molecule attached covalently to the associated E2, which is necessary for ubiquitin transfer activity (236). Binding to ubiquitin stimulates the activity of Parkin, another important E3 ligase (237). The UbcH5 family of E2s binds ubiquitin at a site distant from the active site to promote self-assembly, and eventually, the formation of ubiquitin chains (238). It is now clear that ubiquitin is not merely a substrate, but also functions as an allosteric regulator of E2 and E3 activity. Finally, non-covalent interactions with ubiquitin can even regulate proteins unrelated to ubiquitin pathways. The tyrosine phosphatase PtpA from *Mycobacterium tuberculosis* is activated by ubiquitin binding (239), and proteolysis by the metalloprotease IDE, the insulin-degrading enzyme, is inhibited by its binding to ubiquitin (240). Here we report that the catalytic activity of the DUB ataxin3 is stimulated by a direct interaction with ubiquitin and ubiquitin conjugates.

Ataxin3 is the founding member of the Josephin isopeptidase family, and possesses an N-terminal catalytic Josephin domain, followed by two UIMs, a polyQ tract that is expanded in the neurodegenerative disorder SCA3, and a third C-terminal UIM that is only present in certain splice variants (241) (Fig. 2.1 and Fig. 3.3A) (described in detail in section 1.3). The DUB contacts ubiquitinated substrates via its first two UIMs (111), and exhibits a strong affinity for K48- and K63-linked poly-ubiquitin chains of four or more subunits; however, ataxin3 preferentially cleaves K63- and mixed-linkage chains *in vitro* (117), and has endo-type activity (116). It thus believed to function as a chain-trimming DUB. The UIMs enhance this property (34) and critically regulate ataxin3's cleavage preference, as well as its ability to bind ubiquitin (117). Other than the UIMs, there are two additional ubiquitin-binding sites on ataxin3 that reside in the Josephin domain, denoted site 1 and site 2 (Fig. 3.1) (102,115,118,122). Site 1 is the active site that orients the substrate ubiquitin molecule for cleavage by the catalytic triad, and is indispensable for DUB activity (118). Site 2 is located on the opposite face of the Josephin and overlaps with the Rad23B binding patch. This site may be involved in the release of ubiquitin or ubiquitinated substrates via competitive Rad23B interactions. Both sites promote non-covalent, low affinity binding to ubiquitin molecules as described in (102).

Ataxin3 function is implicated in ubiquitin-dependent protein quality control (see section 1.3). In its capacity as a DUB, it significantly contributes to ERAD, coordinating with the p97 ATPase to target substrates to the proteasome (37,38). Additionally, its DUB activity appears to be neuroprotective against toxic proteins (140), and is also necessary for aggresome formation (36). However, while ataxin3 clearly functions as a DUB *in vivo*, its *in vitro* activity is less efficient than that of structurally similar proteases like USP7 and UCHL3. Todi *et al.* demonstrated that ataxin3 is moderately activated by ubiquitination of its Josephin domain (120), and indeed, ataxin3 is observed to be ubiquitinated in cells (242). Additionally, its ubiquitination increases during cellular stress (120), when there is a higher requirement for its activity. The UIMs mediate the ubiquitination of ataxin3 (119), and coordinate with the Josephin by presenting ubiquitin chains to the catalytic site, and restricting the types of linkages cleaved (120).

The Josephin and the UIMs are also thought to cooperate with each other in other ways, linking ubiquitin recognition and binding to proteolysis. The UIMs may recruit ataxin3 to ubiquitinated substrates, orient these substrates relative to the Josephin, or fine-tune the Josephin's editing function. Here we report a robust modulation of ataxin3 DUB activity via the UIMs and the ubiquitin-binding sites on the Josephin. We demonstrate that ubiquitin, and more specifically His_6-tagged ubiquitin, directly stimulates enzymatic activity for both full-length ataxin3 and the isolated Josephin domain; this magnitude of stimulation far exceeds that observed as a result of ataxin3 ubiquitination (120), and has not been reported previously. Our results suggest that the cellular functions of ataxin3 may be regulated via non-covalent, transient interactions with ubiquitin.

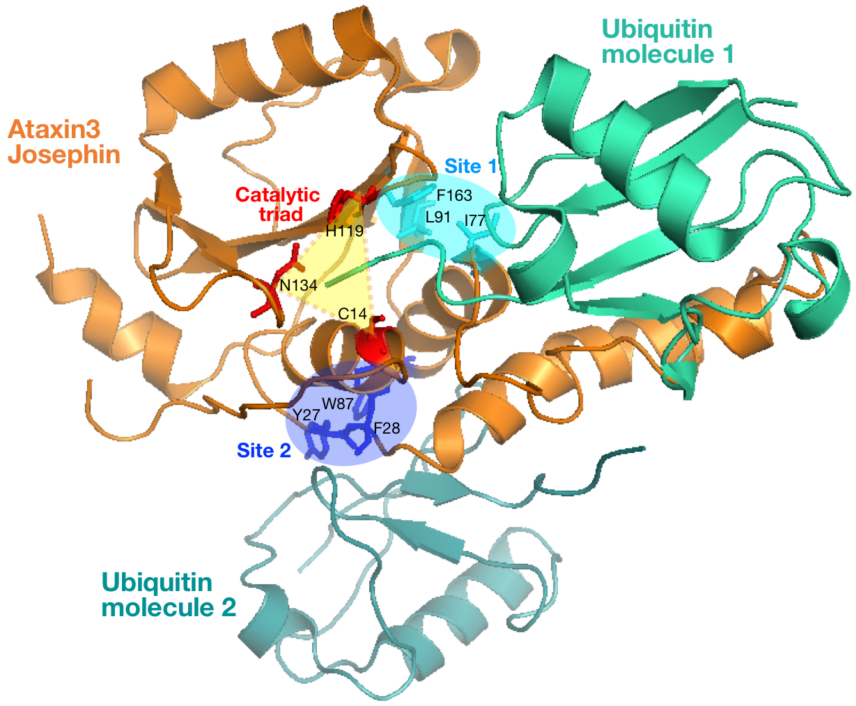

Figure 3.1 Structure of the ataxin3 Josephin domain bound to two ubiquitin molecules. (PDB entry 2JRI (102)) The Josephin is shown in *orange*, and the two ubiquitin molecules are depicted in *light green* and *teal*. The key residues in the ubiquitin-binding site 1 *(cyan ellipse)* are shown in *cyan,* and those in site 2 *(deep blue ellipse)* are shown in *deep blue*. The catalytic triad is highlighted by the *yellow triangle* and the three crucial residues are shown in *red*. The C-terminal end of ubiquitin molecule 1, which would be hydrolyzed by the active site residues, is visible within the catalytic triad *yellow triangle.*

3.2. Experimental Procedures

3.2.1. Reagents

Enzymes for cloning were purchased from New England Biolabs (Ipswich, MA). PCR primers were purchased from Integrated DNA Technologies Inc. (Coralville, IA) and sequencing of constructs was performed by Genewiz (South Plainfield, NJ). All chemicals were from Sigma-Aldrich (St. Louis, MO) unless otherwise stated, and media components were purchased from Fisher Scientific. Chromatography columns were obtained from GE Healthcare, and the ubiquitin-AMC was purchased from Boston Biochem (Cambridge, MA).

3.2.2. Cloning and mutagenesis

Human ataxin3 proteins were cloned into the pETHSUL vector to generate N-terminal His_6-tagged SUMO fusion constructs, under T7 promoter control (see section 2.2.2 for ataxin3 construct details), and ubiquitin was cloned into the pRSETA and pETCH vectors (99,198). The following constructs were used in this work: full-length ataxin3 (aa 1-345), ataxin3 Josephin domain (aa 1-190), ataxin3 site-2 mutant (aa 1-345), ataxin3 UIM mutant (aa 1-345), ubiquitin (aa 1-76), and ubiquitin-His_6 (aa 1-86). The site-2 mutant (W87K) and the UIM mutant (S236A/S256A) were generated by one-step PCR-mediated site-directed mutagenesis (199), using full-length pETHSUL-ataxin3 as the template. The C-terminal His_6-tagged ubiquitin was cloned into the pETCH vector (198) by Xba1/Xma1 digestion and ligation. Primer sequences and additional details are provided in Appendix 3 supplemental tables 1 and 2. Cloning, mutagenesis, and plasmid amplification were performed using the *Escherichia coli* Mach1 strain (Invitrogen).

3.2.3. Protein expression and purification

Detailed information about the preparation of ataxin3 constructs is given in section 2.2.3 and Appendix 2 supplemental protocols. The site-2 and UIM mutants were expressed and purified by the same protocol as wild-type ataxin3.

The ubiquitin constructs were expressed in *E. coli* Rosetta (DE3) cells (Novagen). The transformed cells were grown in auto-inducing media ZYP-5052 (243), after which, the cells were harvested by centrifugation at 5,000 × *g* for 30 min. The cell pellets were then resuspended in water and flash-frozen. Preceding purification, the pellets were rapidly thawed under running water and resuspended in 1× PBS, pH 7.4, 10 mM $MgCl_2$, and 1 μg/ml DNAse and RNAse. All cells were lysed by at least two passes through an Emulsiflex-C5 homogenizer (Avestin, Ontario, Canada) at approximately 173 MPa. Following clarification at 18,000 × *g*, the cell lysate was treated with 0.5% v/v perchloric acid, and stirred for 30 min at room temperature. The precipitated slurry was then centrifuged again at 18,000 × *g*. For the untagged ubiquitin construct, the supernatant was dialyzed against 20 mM sodium acetate, pH 5.2, and loaded onto a HiTrap SP HP column equilibrated in the same buffer, for cation-exchange chromatography. Ubiquitin was eluted over 20 column volumes of buffer at the same pH, using a 0–300 mM gradient of NaCl. The pooled fractions were concentrated to 20–25 mg/ml using an YM3 Centricon device, and aliquots were flash frozen and stored at –80°C. For the $UbHis_6$ construct, the protein was first dialyzed against 50 mM sodium phosphate, pH 8, 250 mM NaCl, 20 mM imidazole, and loaded onto a HiTrap Chelating HP column, for isolation by immobilized-metal affinity chromatography. After elution over a 20–300 mM gradient of imidazole, the protein was further purified by cation-exchange chromatography, and concentrated as described above.

3.2.4. Fluorometric UbAMC assays

Assays were performed on a Fluoromax-3 spectrofluorimeter (Jobin Yvon Horiba), at room temperature, in a buffer containing 50 mM Tris, pH 7.5, 250 mM NaCl, 5 mM DTT, in a total reaction volume of 200 μl. Fluorescence (excitation: 345 nm, emission: 445 nm) was measured at 5 s intervals for 10 min. For experiments with full-length ataxin3 (wild-type and mutants), 1 μM UbAMC substrate and 20 nM enzyme were used. For experiments involving the isolated Josephin domain, the substrate and enzyme concentrations were 2 μM and 50 nM respectively. The concentration of ubiquitin or ubiquitin-His_6 used in all reactions was 75 μM. The initial reaction

rates were calculated from linear fits of the fluorescence vs. time data. All rates are reported as an approximate fold increase over basal wild-type hydrolysis rate.

3.3. Results

3.3.1. Ubiquitin and ubiquitin-His_6 stimulate ataxin3 DUB activity

There is increasing evidence that the function of the E1/E2/E3 machinery in attaching ubiquitin to substrates, and assembling poly-ubiquitin chains, is regulated by the binding of ubiquitin itself at noncatalytic sites on these enzymes (219). It is possible that such interactions also control the detachment of ubiquitin from substrates by DUBs. Since ataxin3 specifically associates with ubiquitin and ubiquitin chains (34,101,102,117), we hypothesized that these interactions might regulate its enzymatic activity.

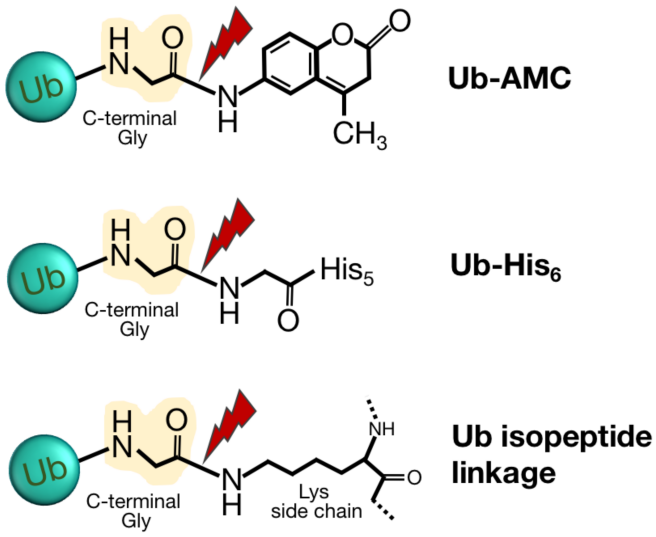

Figure 3.2 Linkages in different ubiquitin substrates. Comparison of the structures of Ub-AMC, $UbHis_6$, and the true isopeptide linkage in the vicinity of the scissile bond. The ubiquitin molecule is depicted by the *teal sphere.* The site of DUB cleavage is indicated by the *red bolt*.

Ataxin3 DUB activity has been extensively studied *in vitro* (34,99,100,116,117,120), and has been characterized previously using the artificial DUB substrate ubiquitin-7-amino-4-methoxycoumarin (Ub-AMC), which consists of the fluorophore AMC conjugated to the C-terminal of ubiquitin by an amide linkage (Fig. 3.2). Ub-AMC is weakly fluorescent, but exhibits increased fluorescence when hydrolyzed to free AMC; this facilitates a sensitive and continuous monitoring of substrate cleavage by the DUB under consideration. Using this assay, we first measured the DUB activity of purified wild-type ataxin3 alone, under steady-state conditions (using 20 nM ataxin3 with 1 μM Ub-AMC substrate), and calculated an initial Ub-AMC hydrolysis rate of 5.5 ± 1.3 fM/sec (Fig. 3.3B). We then tested the effect of a large excess of mono-ubiquitin (75 μM) on ataxin3 DUB activity, using both native and His_6-tagged ubiquitin constructs (hereafter denoted Ub and $UbHis_6$ respectively). The addition of Ub caused a 3-fold increase in the hydrolysis rate, while $UbHis_6$ greatly stimulated DUB activity and induced a 40-fold increase in hydrolysis (Fig. 3.3B); such a robust up-regulation of DUB catalysis has not been described previously. We performed the experiments in the absence of ataxin3 to control for any spurious fluorescence from Ub or $UbHis_6$, and detected no increase in the signal (Appendix 3 Fig. 1). In addition, we observed no stimulation of DUB activity with a His_6-tagged control protein MBP-His_6, added to the reaction at the same concentration as Ub and $UbHis_6$ (Appendix 3 Fig. 2). Interestingly, $UbHis_6$ also functions as a DUB substrate for ataxin3 (Fig. 3.2), and the fusion protein is slowly cleaved to release the His_6-tag, but this hydrolysis cannot be detected in our fluorescence assay.

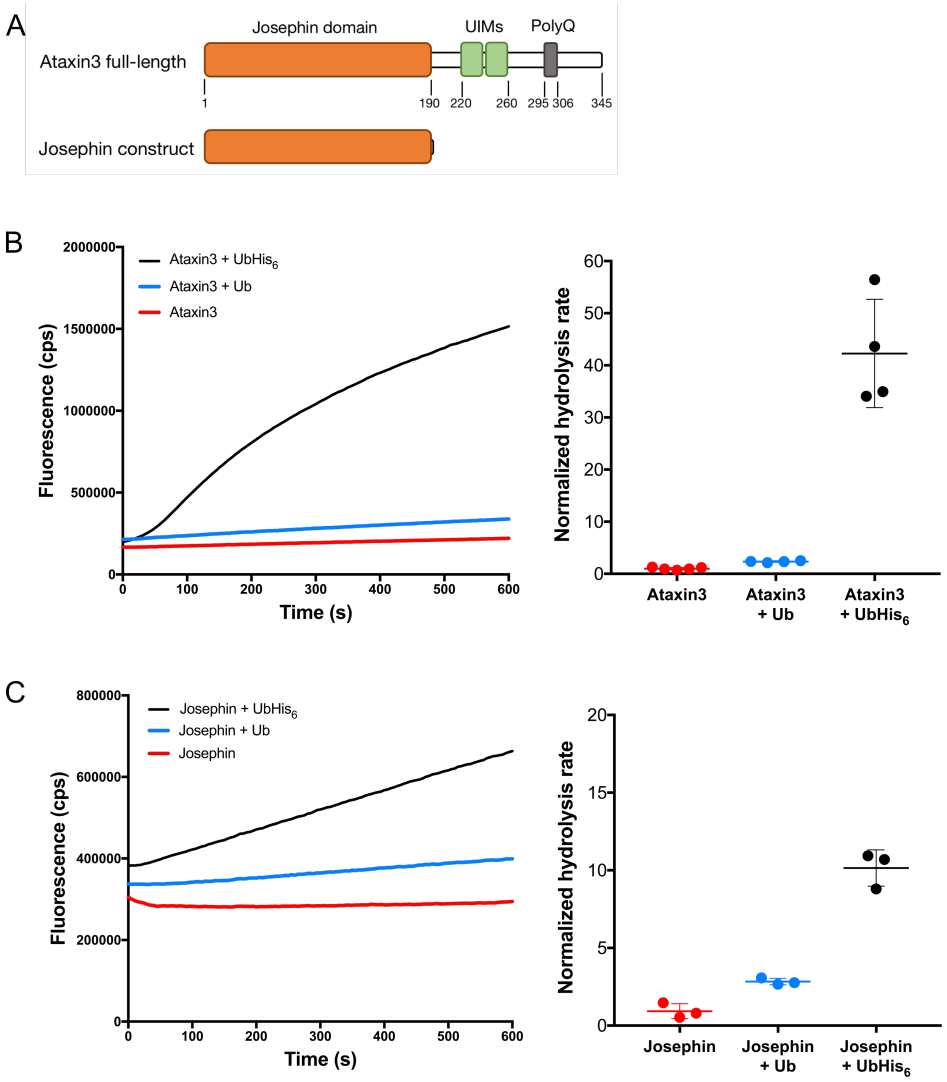

Figure 3.3 Ubiquitin constructs stimulate full-length ataxin3 and the isolated Josephin domain. *A,* schematic representation of full-length ataxin3 and the Josephin construct showing the Josephin domain *(orange)*, two UIMs *(green)*, and the polyQ repeat region *(grey)*. The scale below the full-length representation shows length in amino acids. *B and C,* stimulation of ataxin3 by Ub *(blue)* and $UbHis_6$ *(black)* as measured by Ub-AMC cleavage assays; *B,* full-length ataxin3, or *C,* the isolated Josephin domain *($n \geq 3$ for each reaction)*. The *left panels* are representative plots showing the increase in fluorescence over time, and the *right panels* show the initial reaction rates normalized to the basal hydrolysis rate *(red)*.

3.3.2. Effect of Ub and $UbHis_6$ on the isolated Josephin domain

We then investigated the effect of Ub and $UbHis_6$ on the isolated Josephin. The Josephin domain hosts the enzymatic cleft and thereby forms the catalytic center of ataxin3. We tested the activity of the isolated Josephin domain construct (using 50 nM enzyme and 2 μM Ub-AMC), and found that it hydrolyzes Ub-AMC at the rate of 2.7 ± 1.8 fM/sec (Fig. 3.3C). On adding Ub and $UbHis_6$, the reaction rate was increased 3-fold and 10-fold respectively (Fig. 3.3C), a similar, albeit less pronounced stimulation as that observed for full-length ataxin3.

Thus, $UbHis_6$ induces a 40-fold increase in full-length activity, but only a 10-fold stimulation for the isolated Josephin domain. There are two ubiquitin-binding sites (denoted site 1 and site 2; Fig. 3.1) that reside in the Josephin domain (102). However, since the Josephin domain lacks the C-terminal half of the protein, along with all the binding motifs therein, it is likely that one of those missing sites may account for the observed differences in stimulation. Indeed, the motifs that promote ataxin3 binding to ubiquitin chains, the UIMs, are absent in the Josephin construct (Fig. 3.3A).

We hypothesize that $UbHis_6$ binds to multiple ubiquitin-binding sites on ataxin3, and thereby enhances ataxin3 DUB activity. As characterized previously by ITC, mono-ubiquitin binds sites 1 and 2 in the Josephin with affinities of 47 ± 13 μM and 43 ± 10 μM respectively (102). An apparent K_D of 97 ± 17 μM was also derived for ubiquitin binding to the isolated UIMs, through NMR titration experiments (226), although this may be a rough estimate of a much more complex interaction. Such low affinity interactions, however, are consistent with that observed in other DUBs and ubiquitin-binding domains (244,245), especially in the case of transient ubiquitin function where the molecule is not a permanent binding partner. The concentrations of Ub and $UbHis_6$ in our assays were calculated based on the above-mentioned affinities, in order to saturate all binding sites.

3.3.3. Multiple ubiquitin-binding sites modulate ataxin3 activity

We next sought to test our hypothesis, specifically whether $UbHis_6$ stimulates ataxin3 activity directly by binding to the multiple non-covalent ubiquitin-binding sites. Nicastro *et al.* reported the solution structure of the Josephin bound to two ubiquitin molecules (102) that revealed both the location of these binding sites, and the residues involved in their interactions with ubiquitin (Fig. 3.1). Site 1 is the DUB active site and exploits an induced fit mechanism to bind ubiquitin, involving a flexible helical hairpin. This site is critical for positioning the substrate adjacent to the catalytic triad. Site 2 is on the opposite side of the Josephin domain as the catalytic cleft, and overlaps with the Rad23B binding site. Mutation of specific residues in either site selectively abrogates their interaction with ubiquitin (I77KQ78K for site 1 and W87K for site 2) (102,118).

We reasoned that a site-1 mutant would not be useful for our analyses, since it does not possess any measurable DUB activity (118,246). Instead, we generated and tested the site-2 mutant of full-length ataxin3 (Fig. 3.4A). Adding $UbHis_6$ to the reaction stimulated a 13-fold increase in the hydrolysis rate of the site-2 mutant, a much-reduced stimulation compared to that observed with the wild-type (Fig. 3.4B). In addition, a distinct lag phase was noticeable for the cleavage reaction, which was either absent or too short-lived to be detected for the wild-type (Fig. 3.4B). The site-2 mutant also demonstrated an overall lower basal rate of hydrolysis as compared to the wild-type. This is consistent with earlier studies using K48-linked penta-ubiquitin and mixed-linkage tetra-ubiquitin chains as substrates (118). However, in those studies, the site-2 mutant exhibited a 70% reduction in the basal rate of chain cleavage as compared to the wild-type, while our mutant is 90% less active as measured using the Ub-AMC assay.

After testing the ubiquitin-binding site on the Josephin domain, we next analyzed the contribution of the UIMs. The two short tandem motifs consist of a conserved core sequence eeexLxxAxxxSxxe (e = negatively charged residue, x = any residue) (Fig. 3.4A) (247), and bind ubiquitin in a cooperative manner (226). Mutation of the conserved serine residues to alanines in both UIMs considerably diminishes binding to tetra-ubiquitin (101) and to ubiquitinated proteins

(119). Given that the affinity of the UIMs for mono-ubiquitin is already low (226), the S–A mutations should successfully abolish any binding to our $UbHis_6$ protein. We thus generated the full-length ataxin3 UIM mutant (S236A/S256A) (Fig. 3.4A), and tested for the stimulation of its activity. $UbHis_6$ stimulated the UIM mutant activity to an even smaller extent than that observed for the site-2 mutant (Fig. 3.4C); the calculated hydrolysis rate was only 6-fold higher compared to the 40-fold stimulation observed in the wild-type. The basal activity of the UIM mutant was also found to be lower than that of the wild-type, and the initial lag phase was even more pronounced as compared to that observed with the site-2 mutant.

Since neither the site-2 nor UIM mutations affect the expression or stability of the protein (101,102), it is unlikely that our observations are due to structural defects in the mutant enzymes. From our experiments, it is evident that both the Josephin site 2 and the UIMs contribute to the stimulation of ataxin3's basal DUB activity, induced by the binding of $UbHis_6$ at these sites. Moreover, the large increase in hydrolysis rate observed for the wild-type is greater than the individual stimulation in each mutant, which suggests a synergistic effect of the two sites.

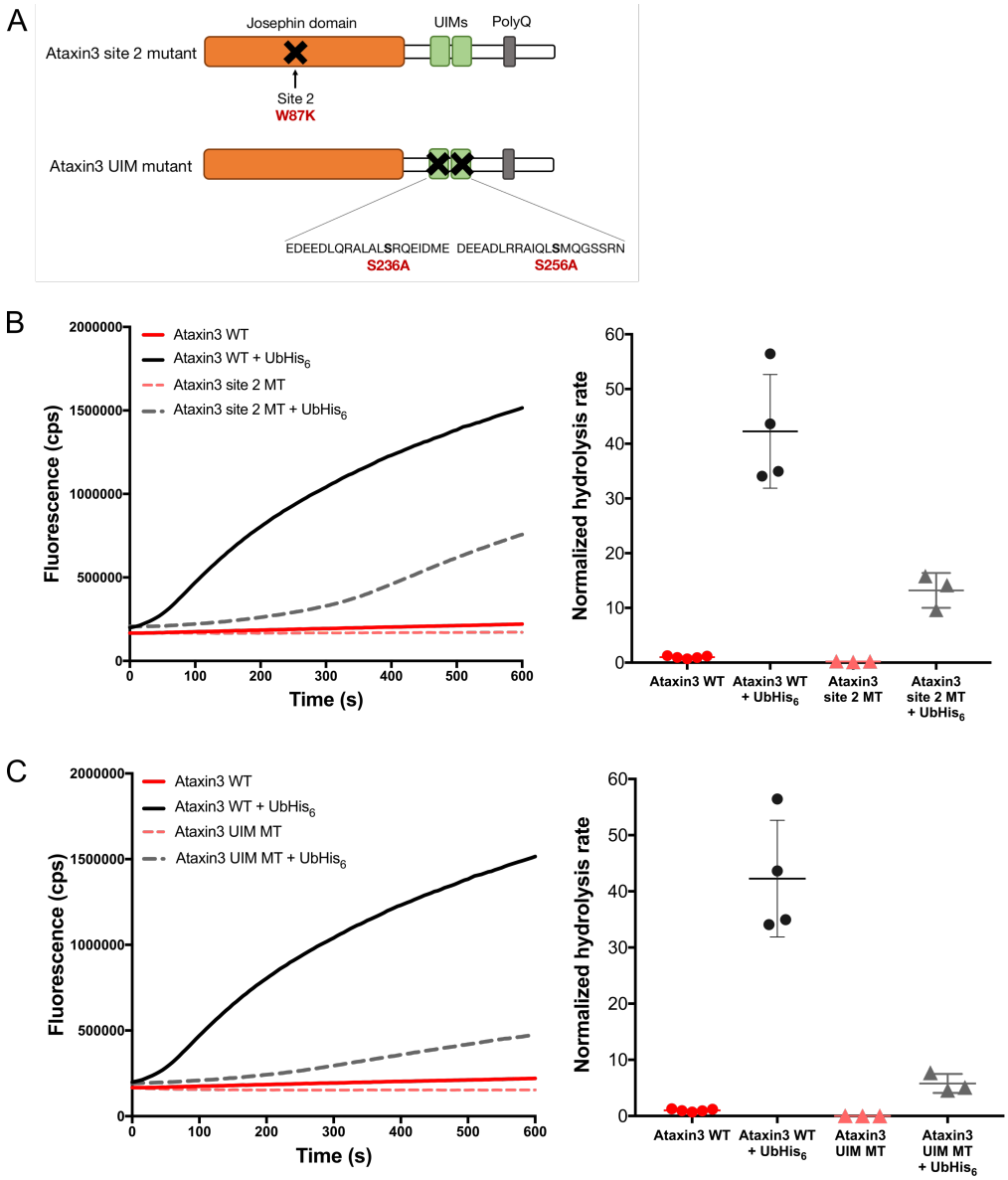

Figure 3.4 Reduced stimulation of ubiquitin binding-site mutants. *A,* schematic representations of the ataxin3 site 2 mutant *(above)*, and UIM mutant *(below)*, using the same color scheme as Fig. 3.3A. The residue mutations for both constructs are mentioned in *red*, and the site of each mutation is depicted with a *black cross*. In the UIM mutant, the critical Ser residue within each UIM sequence is indicated in *bold face*. *B and C,* stimulation of wild-type (WT) and mutants (MT) by $UbHis_6$ as measured by Ub-AMC cleavage assays; *B,* ataxin3 WT and site 2 MT, or *C,* ataxin3 WT and UIM MT *($n \geq 3$ for each reaction)*. The *left panels* are representative plots showing the increase in fluorescence over time, and the *right panels* show the initial reaction rates normalized to the basal hydrolysis rate of the wild-type. The wild-type data shown in *B*, and *C*, is the same as that shown in Fig. 3.3B.

3.3.4. UbHis$_6$ also enhances ataxin3 SRT mutant activity

Ataxin3 activity differs significantly from that of its homolog AT3L, with the latter exhibiting considerably higher cleavage of a variety of substrates (99). When specific residues in ataxin3 are mutated to the corresponding residues in AT3L, the DUB activity of the resulting chimera is much enhanced and nearly equal to that of AT3L (99); these mutations comprise S12F, R59L and T60A, which together form the triple SRT mutant. None of these residues lie in the enzymatic cleft or at any known ubiquitin-binding site, although the Ser-12 residue is adjacent to the active site and may enhance substrate affinity (Fig. 3.5A).

In order to test whether Ub and UbHis$_6$ would further stimulate its activity, we generated the SRT mutant in the full-length ataxin3 construct (Fig. 3.5B). Consistent with previous results, we observed a large increase in basal SRT mutant activity, with a hydrolysis rate of 165.6 ± 9.4 fM/sec, which corresponds to a 30-fold increase over basal wild-type activity (Fig. 3.5C). On adding Ub and UbHis$_6$, the rate was further increased, measured as a 45- and 60-fold stimulation respectively (Fig. 3.5C).

Thus, the basal DUB activity of the SRT mutant, which is already significantly enhanced, can be further stimulated by the ubiquitin constructs up to around the same maximum as that of the wild-type.

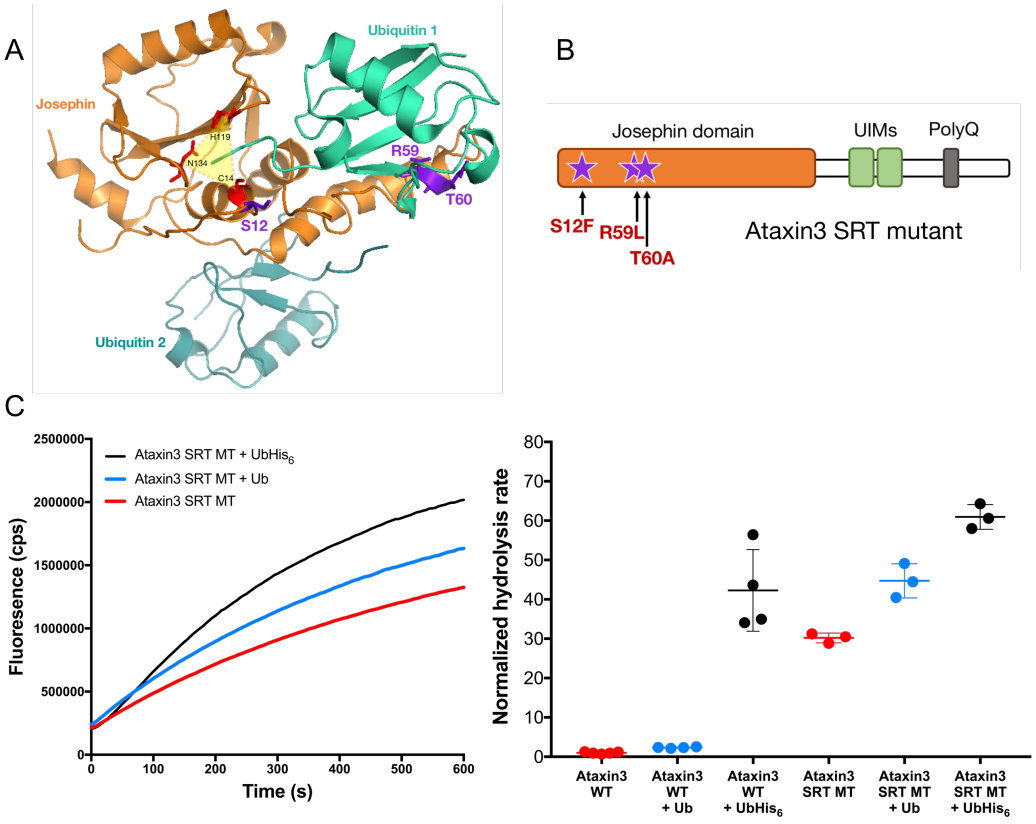

Figure 3.5 Stimulation of ataxin3 SRT mutant by ubiquitin constructs. *A,* structure of the ataxin3 Josephin/ubiquitin complex (PDB entry 2JRI), using the same color scheme as Fig. 3.1. The three residues that are mutated are shown in *purple*. R59 and T60 are on the helical hairpin, and S12 is near the active site cysteine. *B,* schematic representations of the ataxin3 SRT mutant. The three mutations are mentioned in *red*, and the site of each mutation in the Josephin domain is indicated with a *purple star*. *C,* stimulation of the SRT mutant by Ub and $UbHis_6$, as measured by Ub-AMC cleavage assays *($n \geq 3$ for each reaction)*. The *left panel* is a representative plot showing the increase in fluorescence over time for the SRT mutant alone (red), and with Ub *(blue),* and $UbHis_6$ *(black).* The *right panel* shows the initial reaction rates in the presence and absence of ubiquitin constructs, for the wild-type (WT), and the SRT mutant (MT), normalized to the basal hydrolysis rate of the WT. The WT data shown is the same as that shown in Fig. 3.3B.

3.4. Discussion

Using a continuous assay based on the fluorogenic substrate Ub-AMC, we have shown that the DUB activity of full-length ataxin3 is stimulated by non-covalent interactions with either Ub or $UbHis_6$. Although these are low-micromolar affinity interactions, they are able to elicit a 3-fold increase in the rate of substrate cleavage in the presence of Ub, and a nearly 40-fold increase with $UbHis_6$. It is not clear why the stimulation by $UbHis_6$ is so much greater than that observed with Ub alone. Unlike Ub, the $UbHis_6$ construct is a substrate of ataxin3; this may be significant in the context of allosteric regulation. In fact, the scissile bond in $UbHis_6$ is more similar to the naturally occurring isopeptide linkage in physiological substrates, than the Ub-AMC bond (see Fig. 3.2), and $UbHis_6$ could conceivably compete for the active site on ataxin3, thus reducing or blocking the fluorescent signal in our assays. However, the robust increase in the signal with $UbHis_6$ indicates that the effect of the enhancement is substantial enough to overcome any competitive effects. Alternately, it may be a non-specific effect mediated by the His_6-tag, but it is unlikely due to the His_6 tag alone, given that the MBP-His_6 control does not stimulate activity. Future experiments with different ubiquitin conjugates will be useful in revealing the molecular determinants of this stimulation.

Ub and $UbHis_6$ also enhance the activity of the isolated N-terminal Josephin domain, but to a lesser extent than that observed for the full-length. This suggests that along with the Josephin site 2, the UIMs that are absent in the isolated Josephin construct are also required for the complete stimulation of ataxin3's DUB activity. We therefore generated mutants in which ubiquitin binding at one or the other of the two sites was compromised, and found that both mutants exhibited reduced stimulation by $UbHis_6$, indicating that the effects of binding in the two sites are additive. Interestingly, an initial lag phase was observed for both mutants. Lag phases are characteristic of many enzyme-catalyzed reactions; often, the lag marks a conformational change within the enzyme (248), a switch from an inactive or less active to a more active form (e.g. a conventional lag is observed during the activation of the hydrogenase class of enzymes (249)). Conformational changes may be induced by the binding of the substrate itself or by the slow association of allosteric ligands, like the binding of glucose or small-molecule activators to human glucokinase,

which is visible as a distinct lag phase (250,251). In our assays, the lag was either absent or too rapid to detect for the wild-type, and was more pronounced for the UIM mutant than for the site-2 mutant. Possibly, the UIMs convey the $UbHis_6$-bound signal to the active site more quickly or more efficiently than site 2, and when both sites are available as in the wild-type, the signal is transduced quickly enough to mask the lag phase.

Since DUBs are proteases, it is crucial that their activity and specificity be regulated, to avoid the inadvertent cleavage of non-substrate molecules in the cell. DUBs are often controlled by components of the pathways in which they function, for example, caspase-3 inactivates the DUB USP7, which functions in apoptosis (252). Several DUBs are modified by ubiquitin (253-255); this typically involves the covalent conjugation of ubiquitin, which regulates their degradation. In the case of ataxin3, ubiquitination enhances DUB activity (120), but this stimulation only corresponds to a 4-5-fold increase in activity, and is not as robust as the stimulation we observe from the non-covalent binding of ubiquitin. Based on our findings, we propose a novel form of DUB regulation, wherein the binding of Ub and $UbHis_6$ to the Josephin site 2 and the C-terminal UIMs in ataxin3 causes conformational changes that enhance catalysis.

A conformational switch has been previously suggested for ataxin3 in a mechanism involving a helical hairpin in the Josephin (19,115). The three published solution structures of the Josephin alone (PDB entries 2AGA, 2DOS and 1YZB) show the hairpin in significantly different conformations, involving closed, intermediate and open states (115,116,122). Validation calculations and SAXS measurements have since disproved the 2AGA structure (256), however, computational analyses using molecular dynamic simulations support the possibility of an analogous three-state pathway (Fig. 3.6) (257,258), and suggest that different states may be stabilized under different conditions. In structures of the Josephin-ubiquitin complex from both ataxin3 and the closely related AT3L protein (PDB entries 2JRI (102) and 3O65 (99) respectively), the hairpin is in the open conformation, which clearly accommodates the ubiquitin molecule at site 1 (Fig. 3.6).

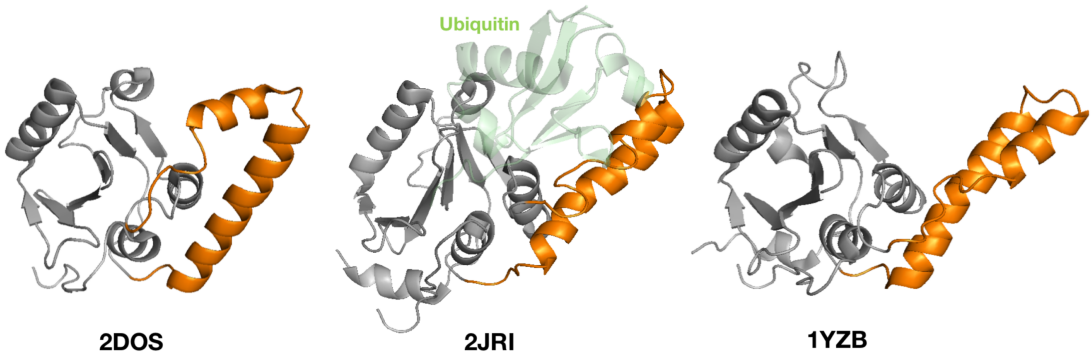

Figure 3.6 Comparison of the various ataxin3 Josephin structures. In all three structures, the Josephin is shown in *grey*, and the helical hairpin arm is shown in *orange*. The arm assumes different conformations in each of the structures; it is closer to the Josephin in 2DOS, and extended away from the Josephin, in what is termed as the "open state", in 1YZB. The 2JRI structure shows a marginal extension of the arm, as it appears to grasp the ubiquitin molecule *(semi-transparent representation colored green)* bound at site 1.

It is tempting to speculate that ubiquitin binding to site 2 either induces or stabilizes the open conformation and thus, facilitates better substrate access to site 1 (Fig. 3.7). Alternately, binding at site 2 may merely position a chain for cleavage at site 1, increase substrate affinity at site 1, or facilitate substrate hand-off to site 1. The significance of these dual binding sites is yet to be elucidated, however, the Pastore group has shown that their respective positions on the Josephin impose a linkage preference for poly-ubiquitin substrates cleaved at the active site (118).

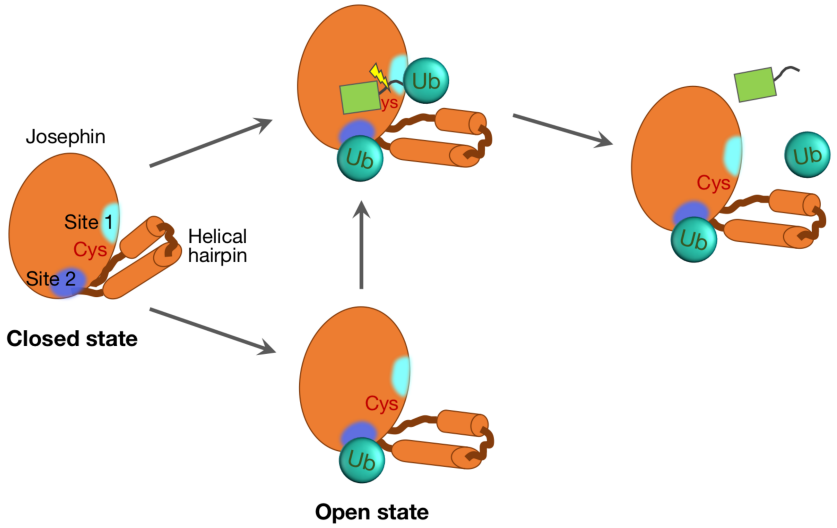

Figure 3.7 Model depicting conformational regulation of the helical arm by ubiquitin. The Josephin domain is shown in *orange*, and the ubiquitin molecules are shown as *teal spheres.* The ubiquitin-binding sites are shown in *cyan* (site 1), and *deep blue* (site 2). The helical hairpin arm is initially folded against the Josephin domain in the closed state, which is computed to be the most energetically favorable configuration (257). In this state, the arm perhaps blocks substrate access to site 1. Ubiquitin binds at site 2, and either induces or stabilizes the open state. This allows the substrate to bind at site 1, after which it is cleaved by the active site Cys residue *(red)*, and released.

We find that the Josephin site 2 and the UIMs both contribute to the stimulation of activity, suggesting a cooperative effect. Collaboration between the UIMs and the Josephin has already been demonstrated in substrate selectivity (117); it is perfectly reasonable that their coordination is extended to scenarios involving non-covalent interactions and conformational changes within the enzyme. First, the freely accessible UIMs would selectively bind K63- or mixed-linkage chains with high affinity (34,117). The UIMs themselves exhibit cooperativity and preferentially bind polyubiquitin substrates of four or more subunits *in vitro* (34). Once a chain of appropriate length is trapped, it could migrate until it encounters and binds the Josephin, via cooperative interactions involving all the binding sites (Fig. 3.8A). Alternately, occupancy of the UIMs may transduce an allosteric signal to the Josephin, stimulating a catalytically enhanced conformation at the active site (Fig. 3.8B). It is also possible that the unstructured C-terminus partially occludes the Josephin sites (259), and that binding of ubiquitin to the UIMs exposes these sites (Fig. 3.8C). Once ubiquitin interacts with the Josephin and is properly positioned for cleavage, it can be hydrolyzed at the

DUB active site, after which it must be released. The ubiquitin chain may be released via competitive interactions with Rad23 that also binds to site 2 (102). Alternately, when the chain is trimmed to less than four moieties, it may simply detach due to low affinity binding. This exemplifies ataxin3 as a polyubiquitin specific "molecular ruler" that selects and trims chains to an appropriate length, via its multiple binding sites. Indeed, the DUB effectively cleaves chains comprising more than five ubiquitins to produce tetra-ubiquitin (117,118), which correlates with the minimum signal for efficient proteasomal degradation (121).

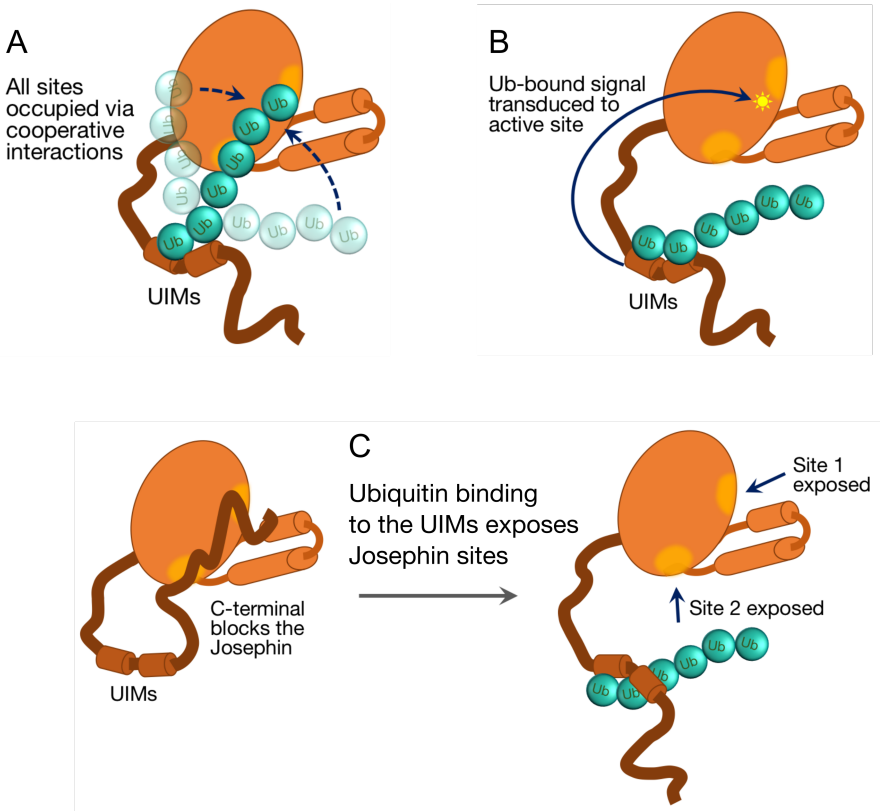

Figure 3.8 Models for coordination between the UIMs and the Josephin domain. The Josephin domain is shown in *orange*, the flexible C-terminal and UIMs in *brown*, and the ubiquitin molecules are shown as *teal spheres. A,* the UIMs first trap a poly-ubiquitin chain, which can then migrate until it encounters and binds the Josephin. *B,* the UIMs bind ubiquitin, and transduce the bound signal to the Josephin, which induces a catalytically enhanced conformation at the active site. *C,* the unstructured C-terminus partially occludes the Josephin sites, and binding of ubiquitin to the UIMs exposes these sites.

The first insight into interpreting ubiquitin signals came from the identification of the Leu-8/Ile-44/Val-70 hydrophobic patch on ubiquitin, which is necessary for its interaction with the S5a/Rpn10 proteasomal subunit (260). The same patch, along with another hydrophobic surface on ubiquitin, mediates vegetative growth and endocytic transport in yeast (261). Thus, the surface of a ubiquitin molecule is essentially made up of three-dimensional signals that are read by distinct sites or domains (e.g. the UBD) on proteins. A polyubiquitin chain would present hydrophobic surfaces from each ubiquitin moiety to such a binding domain, enabling a multivalent interaction. Non-covalent interactions involving hydrophobic interfaces are important in a biological context, since low affinity and transient binding would ensure that the interaction is readily reversible. This may be necessary to proceed to the next phase in a pathway (e.g. release of the substrate after proteasomal recognition, to facilitate its degradation), or to reversibly regulate enzymes that function in ubiquitin pathways (e.g. to activate DUBs when required, and to deactivate them later, thus preventing indiscriminate proteolysis).

Our results show that non-covalent ubiquitin interactions directly regulate ataxin3's enzymatic properties, and thus define a novel, non-traditional role for the signaling molecule. This mode of control by ubiquitin may also apply to other DUBs, further refining their cellular functions. It makes biological sense that DUB activity would be modulated through allosteric interactions with their substrates, and essentially be "turned on" when the substrate needs to be cleaved. In this way, during cellular stress, the high levels of ubiquitinated substrates that require processing would themselves upregulate DUB activity.

CHAPTER 4: Conclusions

4.1. Nucleotide-induced conformational changes regulate the p97-ataxin3 interaction

4.1.1. Summary

A remarkable aspect of p97 is its involvement in diverse cellular processes. Over the last decade, it has become clear that p97 achieves its functional diversity by employing a multitude of cofactors. These cofactors partner with p97 in unique and sometimes interdependent ways, reflecting their distinct roles in p97 function, and thus giving rise to a complex network of p97-cofactor interactions. Cofactors follow a hierarchy in their binding to p97 (63). Much of the binding mechanism is dictated by the stoichiometry and spatial arrangement of the complex. Our EM analyses of full-length proteins clearly demonstrate that only one ataxin3 molecule binds to the p97 hexamer, which leaves room for other cofactors. Alternately, the binding of ataxin3 could also prevent interaction with other cofactors. This idea is strongly supported by experiments showing mutually exclusive binding of ataxin3 and Ufd1 to p97 (37). It is unclear whether the binding of a single cofactor to p97 can induce a conformational change to rearrange the other N-domains, but such a mechanism would explain the diverse cofactor-binding patterns observed. In this case, a 1:6 ataxin3-p97 complex could certainly A) inhibit additional ataxin3 binding, and B) selectively promote or inhibit interaction with other cofactors.

Many of the p97 cofactors have antagonistic functions, which may be required at different instances within a pathway, and would eventually decide the fate of the substrate. Thus, cofactor binding must be carefully regulated. Regulation occurs in various ways, including post-translational modification (65,214) and transcriptional upregulation of cofactors (262,263). Our experiments reveal that in the case of ataxin3, binding is regulated by p97's nucleotide state. High resolution cryo-EM has revealed at least three distinct nucleotide-bound conformations that clearly place the N-domain in different positions relative to the D1 ring (43). ADP-bound p97, with the N-domains in the down state, does not interact with ataxin3 due to steric constraints, as the C-terminus of ataxin3 clashes with the D1-domain. However, interaction is restored in the ATP-bound or nucleotide-free states, where the N-domains are in the up position. These results

recapitulate cellular studies showing differential binding of ataxin3 to p97 in the presence of different nucleotides (113). Thus, ataxin3 may shuttle on and off p97, perhaps to facilitate the association of other cofactors required for processing substrates.

In addition to cofactor studies of the wild type, there are also reports characterizing MSP1 mutants of p97, and their atypical cofactor binding; however, these studies have not focused on nucleotide regulation. None of the identified MSP1 mutations are in p97's nucleotide-binding sites or cofactor interfaces, so their effects on cofactor binding are most likely indirect and subtle. Consequently, cofactor-binding experiments must be interpreted with caution. Studies using purified proteins are often inconsistent with cell-based experiments, and do not recapitulate the differences in cofactor-binding ability observed between wild type p97 and MSP1 variants (53,89,91); such discrepancies may be resolved by accounting for p97's nucleotide state. Our results have shown that although ataxin3 binds to wild type and mutant p97 with the same affinity, ADP does not inhibit its interaction with the mutants; this explains the elevated binding of mutant p97 with ataxin3 observed in cultured cells, and in patient tissue samples (53). Our findings are consistent with defective inter-domain communication in MSP1 mutants, explained as the inability of these mutants to transduce the ADP-bound signal from the D1 to the N-domain. This disrupted up-down equilibrium may also alter the binding of other cofactors, with potential consequences in protein quality-control pathways.

The p97-ataxin3 interaction is an essential component of ERAD (37,38), where p97's primary function is to extract ubiquitinated substrates from the ER; however, the precise mechanism of this process remains unclear. Conceivably, ataxin3 binds and catalyzes the trimming or the *en bloc* removal of ubiquitin chains substrates that would otherwise sterically impede their engagement or threading by p97. A similar processive function is observed in the proteasome-associated DUB Rpn11, which facilitates substrate entry into the proteasome (264). Another possibility is that ataxin3 edits non-K48 linked polyubiquitin that will not be efficiently recognized by the proteasome; this is consistent with the DUB's preference for long, mixed-linkage chains as substrates (117). Ataxin3 may also trim excessively long ubiquitin chains downstream of extraction to an appropriate length necessary for proteasomal degradation, before substrate hand-

off to shuttling factors like Rad23 and Dsk2 (217,218). Besides coordinating substrate extraction, ataxin3 may further assist p97 in engaging ubiquitinated substrates. The DUB binds ubiquitin via sites on its Josephin domain and its UIMs (33,34,119), and p97 also has a predicted polyubiquitin recognition site on its N-domain, adjacent to the ataxin3-binding cleft (57,157). The spatial arrangement of these sites may facilitate the simultaneous interaction of the polyubiquitinated substrate with both ataxin3 and p97, and thereby synergistically enhance the relative binding affinities of these interactions. Moreover, our EM studies with non-crosslinked proteins hint at the possibility of a flexible association between ataxin3 and p97. It is tempting to imagine a scenario where ataxin3 is attached to p97 by its C-terminal VBM, leaving the Josephin domain and UIMs free to move about and bind longer ubiquitin-chains. Besides ataxin3, other DUBs like Otu1, VCIP135 and YOD1 function with p97, both in yeast and mammalian cells (262,265-267), indicating an evolutionary role for DUBs in p97-dependent processes.

In vivo, even minor errors in cofactor interactions could be toxic. p97 may become trapped in ineffective complexes unable to bind other cofactors, and thus disrupt degradation pathways, causing ubiquitinated proteins to be shuttled off to autophagic vacuoles. A pathological hallmark of MSP1 is the co-localization of mutant p97 with ubiquitinated protein inclusions, indicative of a defective UPS (82,83). Disrupted autophagosomes and endosome maturation is also observed, which leads to vacuolation, weakness and muscle atrophy (86,87). It is conceivable that mutants alter the normal equilibrium between shuttling to the proteasome and autophagy. Atypical cofactor binding has also been observed in MSP1 patient myoblasts that lack protein aggregates (53,89), implying that this is an early event in pathogenesis rather than a consequence of the disease. We propose that MSP1 mutations cause subtle but ultimately fatal errors in p97 function, which is consistent with a late-onset disease. Our findings that p97 mutants do not necessarily abolish, but alter cofactor-binding patterns via dysregulated N-domain conformations, validate the complex nature of these interactions and support the proposed pathogenesis mechanism.

4.1.2. Future directions

A) We have shown that ADP binding to p97 inhibits its interaction with ataxin3. The mechanism is through the downward displacement of the p97 N-domain in the ADP-bound state that results in a steric clash between the D1 domain and the ataxin3 C-terminal. It would be interesting to examine the interaction of other cofactors in the light of p97 nucleotide states. If nucleotides regulate the binding of other cofactors to p97, we could investigate if this was through a similar mechanism as that observed for ataxin3. Analyses of published p97-cofactor complex structures (complete list in Appendix 2 supplemental Table 3), would help establish rationale for testing cofactors whose interactions with p97 are likely to be inhibited in the down state. For example, the UBL from Otu1 and the UBD from Npl4 both bind in the p97 N-domain inter-lobe cleft (44,58). The UBL and UBD domains are located at the N-terminal halves of their respective proteins. Conceivably, the C-terminal portions of these proteins may be positioned such that they clash with the D1 in the ADP-bound form of p97. The opposite orientation may produce the same effect in the case of the UBX domain from p47 (56), another cofactor that exhibits reduced binding to p97 in the presence of ADP (66).

B) We could also test the binding of other cofactors to p97 MSP1 mutants in the presence of nucleotides. Since the up-down equilibrium of the N-domain is altered in disease mutants, it is possible that atypical cofactor binding will only be detected in the context of p97's nucleotide state. In our experiments, ataxin3 binding to p97 mutants was not inhibited by ADP. Such altered ADP-inhibition has also been reported for the binding of p47 to mutant p97 (66).

C) Some cofactors like p37 and p47 play critical roles in regulating p97's ATPase activity. p37 produces an 11-fold increase in catalytic efficiency, and was the first activating cofactor to be identified. p47 shows a more complex regulation profile that is dependent on its concentration. These cofactors control ATPase activity by binding to p97's N-domain, thereby inducing conformation changes in the protein that affect nucleotide binding at the D1 (67). Since ataxin3 binds in the same N-domain cleft, and the interaction is regulated by nucleotide-

induced conformational changes, we decided to investigate the effect of ataxin3 on p97 activity. Preliminary experiments show that wild type ataxin3 stimulates ATP hydrolysis, while the VBM mutant that does not interact with p97 has no effect at the same concentrations (Appendix 1). These initial results necessitate a more in-depth kinetic analysis of the observed stimulation, over a wider range of ataxin3 concentrations. Also, it is unlikely that this effect can be explained by the same rationale postulated for p37 and p47, since the binding of ataxin3 to the N-domain is not strong enough to affect nucleotide binding; in fact, nucleotide binding inhibits the interaction. So ataxin3 likely enhances ATPase activity by some other mechanism. Moreover, p37 and p47 failed to activate p97 disease mutants (67). Since mutants typically exhibit increased activity, and the p97-ataxin3 interaction is altered in these mutants, it would be interesting to test if ataxin3 effects ATP hydrolysis in the mutants.

4.2. Ataxin3 is activated by non-covalent interactions with ubiquitin

4.2.1. Summary

The cellular functions of DUBs are regulated through a combination of specific protein-protein interactions, modulatory domains, and post-translational modifications. DUBs comprise various binding motifs, and interact with distinct partners that target them to specific pathways, confer substrate preferences, and modulate enzyme activity. We have shown that the DUB activity of full-length ataxin3 is stimulated by non-covalent interactions with Ub and $UbHis_6$, and that these low-affinity interactions are able to induce a 3-fold and a 50-fold increase in the rate of substrate hydrolysis, respectively. The ubiquitin constructs also induce a smaller, yet significant, stimulation of DUB activity in the isolated Josephin domain. Moreover, we have shown that this stimulation is through an additive effect of both the Josephin site 2 and the UIMs.

The enhancement of ataxin3 activity through ubiquitin interactions may constitute a feed-forward regulatory process in various cellular pathways. We suggest that regulation of enzymatic

activity by non-covalent substrate interactions would further refine the cellular functions of DUBs, and that binding of ubiquitin may also stimulate activity in other classes of enzymes.

4.2.2. Future directions

A) The Josephin domain of ataxin3 interacts with the N-terminal UBL domain of the proteasome-associated shuttling factor Rad23B (102). The Rad23B binding site overlaps with Josephin site 2, in fact, the W87K mutation that abrogates ubiquitin binding at site 2, also disrupts the Rad23B interaction (135). Since Ub and $UbHis_6$ stimulate ataxin3 activity via site 2, we could test the effect of Rad23B on DUB activity, at similar concentrations. We could also test if Rad23B competes for the site, and perhaps inhibits the stimulation by $UbHis_6$. Previously, full-length Rad23B was shown to reduce the ability of the Josephin domain to cleave poly-ubiquitin chains (118). Competition experiments may help define a mechanism for this form of inhibition.

B) We could test if other ubiquitin conjugates also stimulate the rate of substrate cleavage. For example, K48- and K63-linked di-ubiquitin are both substrates of ataxin3, and are cleaved with a similar efficiency as that observed for $UbHis_6$. We would use di-ubiquitin at the same concentration as $UbHis_6$ and check for stimulation of activity. This would also verify whether the stimulation is due to the substrate-like property of $UbHis_6$, or just an artifact of the His_6-tag. We could also test for stimulation in the presence of poly-ubiquitin chains with K48-, K63-, and mixed-linkages. Additionally, we could test a fusion protein comprising multiple ubiquitin moieties, linked via regular peptide bonds instead of the isopeptide linkage in chains. This would be a poorer substrate than regular chains, and would not compete significantly with the assay substrate. We would also vary the number of ubiquitin moieties in this fusion construct to test the effect of chain length on stimulation of activity.

C) To detect any structural changes in ataxin3, due to the binding of Ub and $UbHis_6$, we would perform intrinsic fluorescence measurements for ataxin3, in the presence and absence of Ub

and $UbHis_6$. The signal from the ubiquitin constructs should be negligible since they do not contain any Trp residues.

D) Our studies with Ub and $UbHis_6$ were performed at fixed concentrations of these ubiquitin constructs (see section 3.2.4 for experimental conditions). We would next test the concentration dependence of DUB stimulation, using a range of Ub and $UbHis_6$ concentrations, and verify if it correlates with reported ubiquitin binding affinities. We could also test the kinetics of DUB activity, and verify if the relation between the rate of cleavage and substrate concentration is hyperbolic or sigmoidal.

APPENDICES

APPENDIX 1: Ataxin3 Stimulates p97 ATPase Activity.

Some p97 cofactors like p37 and p47 play critical roles in regulating its ATPase activity. p37 stimulates p97's ATPase activity, and p47 shows a more complex regulation profile that is dependent on its concentration. These cofactors control ATPase activity by binding to p97's N-domain, thereby inducing conformation changes in the protein that affect nucleotide binding at the D1 (67). Since ataxin3 binds in the same inter-lobe cleft, we decided to investigate the effect of ataxin3 on p97 activity.

Using the NADH-coupled assay (see section 2.2.7) we measured the ATPase activity of p97 (at 0.5 μM monomer) in the absence and presence of an increasing concentration of wild-type ataxin3 (0–20 μM). Ataxin3 stimulated p97's activity in a concentration dependent manner, with an approximately 2.5-fold stimulation at the highest concentration tested (20 μM ataxin3; this corresponds to a molar ratio of 1:40 for the p97 monomer : ataxin3). (Appendix 1 Fig. 1). In comparison, Zhang *et al.* showed that p37 produces a 3.7-fold stimulation of ATPase activity at molar ratio of 1:20 (p97 monomer : p37) (67). We next tested if the VBM mutant that does not interact with p97 produces any stimulation at the two highest concentrations of wild-type tested, and found that addition of the mutant does not change p97 activity (Appendix 1 Fig. 2). These, preliminary experiments show that wild-type ataxin3 stimulates ATP hydrolysis, while the VBM mutant has no effect at the same concentrations.

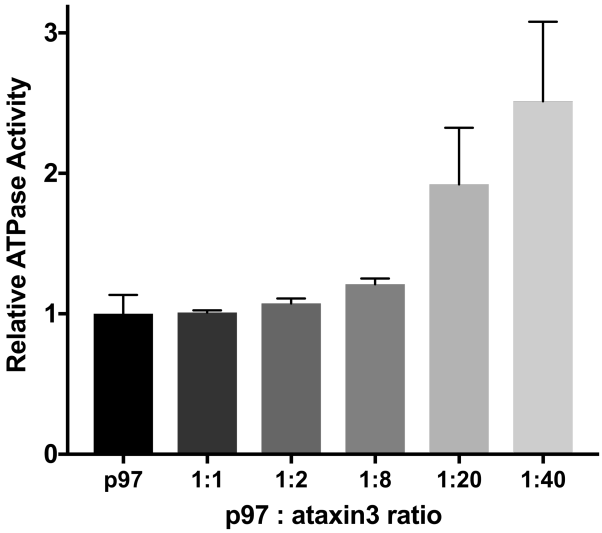

Appendix 1 Figure 1. Ataxin3 stimulates p97 activity. Graph showing the relative increase in p97 ATPase activity with increasing concentrations of ataxin3 (0–20 μM). *(n = 3 for each reaction)* p97 concentration was 0.5 μM monomer in all assays.

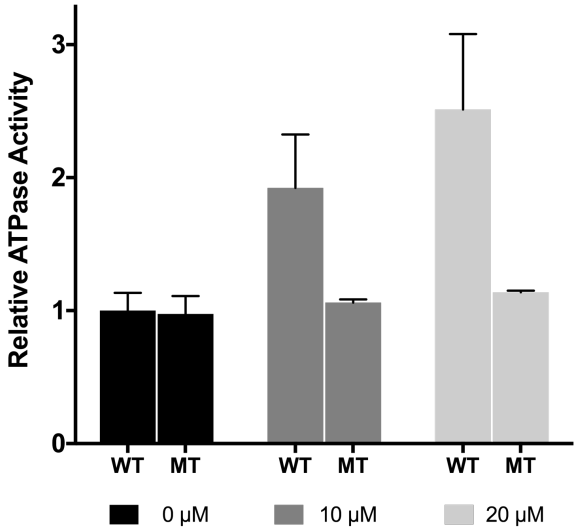

Appendix 1 Figure 2. The VBM mutant does not stimulate p97 activity. Graph showing relative increase in p97 ATPase activity with the last two concentrations of ataxin3, and no increase with the VBM mutant at the same concentrations *(n = 3 for each reaction).* Ataxin3 WT and MT concentrations are mentioned below the bars. p97 concentration was 0.5 μM monomer in all assays.

APPENDIX 2: Supplemental Protocols, Tables and Figures for Chapter 2.

Appendix 2 Supplemental Protocols

1. Protein Expression and Purification

All proteins were expressed in *E. coli* Rosetta (DE3) cells (Novagen), by induction with 1 mM isopropyl-β-D-thiogalactopyranoside (IPTG) at an A_{600} of 0.5–0.8, followed by shaking overnight at 24 °C. After roughly 21 h, the cells were harvested by centrifugation at 5,000 × *g* and the pellets were resuspended in water and flash-frozen. Attempts were made to express the p97 N-domain in *E. coli* Rosetta (DE3) cells using an auto-induction protocol (243), but this resulted in a large amount of the protein being in the pellet after the centrifugation steps, indicating denatured or aggregated protein; this was not observed when using the IPTG induction protocol. Preceding purification, the pellets were rapidly thawed under running water and resuspended in lysis buffer. All cells were lysed by at least two passes through a chilled Emulsiflex-C5 homogenizer (Avestin, Ontario, Canada) at approximately 173 MPa. For the His_6-SUMO-fusions, lysis, clarification and subtractive purification were performed as described previously (198), expect for minor changes described below.

For all the His_6-SUMO-ataxin3 constructs (full-length wild-type, full-length 282ANAA285 mutant, Josephin domain, Josephin + UIMs, ataxin3ΔC and ataxin3ΔN), the cells were lysed in 50 mM sodium phosphate, pH 8.0, 250 mM NaCl, 20 mM imidazole, 10 mM $MgCl_2$, 5 mM β-mercaptoethanol (βME), 5% v/v glycerol, 1 μg/ml each DNAse and RNAse, and protease inhibitor (Prod. #88266, Pierce ThermoFisher; 1 tablet/ 50 ml lysate). The lysates were clarified at 311,000 × *g* for 1 h and loaded onto a HiTrap IMAC HP column pre-equilibrated with 50 mM sodium phosphate, pH 8.0, 250 mM NaCl, 20 mM imidazole, 5% v/v glycerol, 5 mM βME, and eluted using a 20–300 mM gradient of imidazole. The eluted fractions were pooled and dialyzed back into 50 mM sodium phosphate, pH 8.0, 250 mM NaCl, 20 mM imidazole, 5% v/v glycerol, 5 mM βME, at 4 °C, in the presence of the doubly-tagged SUMO-specific protease Ud1 (dtUd1) (198). 200 μg of protease is sufficient to cleave the amount of fusion protein obtained from a 1-L culture. After an

overnight dialysis, the sample was applied to the same metal affinity chromatography column to remove the His_6-SUMO tag and the dtUD1 enzyme. After subtractive purification, the ataxin3 constructs were further purified by ion exchange chromatography. The proteins were first dialyzed against 50 mM sodium phosphate, pH 8.0, 50 mM NaCl, then loaded onto a HiTrap Sepharose Q HP column and eluted using a 50–1000 mM gradient of NaCl. The desired fractions were pooled and further purified by size-exclusion chromatography (SEC) on a HiPrep Sephacryl S-300 HR column equilibrated in 25 mM Tris, pH 8.0, 200 mM KCl, 5 mM $MgCl_2$, 5 mM βME. For the N-terminally His_6-tagged ataxin3 protein, the Ud1 cleavage and subtractive purification steps were omitted.

For all the His_6-SUMO-p97 constructs (full-length wild-type protein, with and without the C-terminal 1D4-tag, p97 N-domain, p97N + D1-domains, and all p97 mutants), the cell pellets were lysed in in 50 mM Tris, pH 8.0, 250 mM KCl, 20 mM imidazole, 10 mM $MgCl_2$, 5 mM βME, 5% v/v glycerol, 1 μg/ml each DNAse and RNAse, and protease inhibitor tablets (details above). Clarification and subtractive purification were performed as described for the ataxin3 constructs, except the IMAC buffer contained 50 mM Tris, pH 8.0, 250 mM KCl, 20 mM imidazole, 5 mM $MgCl_2$, 5 mM βME, 5% v/v glycerol, and the elution was over a 20–300 mM gradient of imidazole. After subtractive purification, the proteins were directly purified by gel filtration as described above. For the ITC experiments, full-length p97 was subjected to an additional ion exchange chromatography step before SEC, through a HiTrap Sepharose Q HP column, using a buffer with 100 mM HEPES, pH 7.0, 50 mM NaCl, 5 mM βME, and a 50–500 mM linear NaCl gradient. This step was to ensure the removal of any aggregated material in order to concentrate full-length p97 sufficiently for ITC. The C-terminally His_6-tagged full-length p97 was expressed as a SUMO-fusion, which helped in expression and solubility. The SUMO was later removed by cleavage with dtUd1 as described above, and the sample was purified by gel filtration. On our preparative Sephacryl S-300 column, the elution profile for full-length p97 was similar to that described by Niwa *et al.* (54) using a Superose 6 column (supplemental Fig. S11*A*). Niwa *et al.* verified that their void peak contained irreversibly aggregated material, and the additional shoulder present in their trace contained dodecameric p97 with some aggregates. To further analyze the size-exclusion

behavior of p97, we injected full-length p97 onto a Yarra SEC-3000 column (for improved separation of high molecular-weight species), and observed a smaller peak between the void peak and hexamer peak (supplemental Fig. S11*B*). This peak most likely contained higher-order oligomers and/or aggregates, and was in equilibrium with the hexamer species, since reinjection of the hexamer peak yielded the same three-peak elution profile (data not shown).

For all ataxin3 and p97 proteins, the final SEC fractions from the Sephacryl S-300 column were pooled and concentrated to 8–10 mg/ml using an Amicon stirred cell (Millipore), and then aliquoted, flash-frozen, and stored at –80 °C.

2. Surface Plasmon Resonance (SPR)

All SPR experiments were performed on a BioRad ProteOn XPR36 at 25 °C. The full-length p97 hexamer was captured as a ligand in an oriented manner employing two different strategies, A) the Rho1D4 epitope-antibody system (200,201) and B) histidine-tagged protein capture.

Rho1D4 epitope-antibody system. The Rho1D4 monoclonal antibody was immobilized on a ProteOn GLC sensor chip by amine coupling using 1× PBS pH 7.4 plus 0.005% Tween® 20 as the running buffer. The surface was first activated with a freshly prepared mixture of 1-ethyl-3-(3-dimethylaminopropyl) carbodiimide hydrochloride (EDC) and N-hydroxysulfosuccinimide (sulpho-NHS), (final concentrations 20 mM EDC : 5 mM sulpho-NHS), at a flow rate of 30 μl/min for 5 min. The 1D4 antibody was diluted in 10 mM sodium acetate, pH 5.5 (final concentration 0.1–0.5 mg/ml), and immobilized to a density of ~3,500 response units (RU) on the activated surface, at a flow rate of 30 μl/min for 7 min. Excess activated groups were blocked with 1 M ethanolamine-HCl, pH 8.5 at a flow rate of 30 μl/min for 5 min. The surface was stabilized by at least three consecutive injections of regeneration solution (freshly prepared 10 mM NaOH and 1% *N*-octyl-β-D-glucopyranoside), each at a flow rate of 100 μl/min for 18 s. For each sensor chip, one of the lanes with the immobilized 1D4 antibody was maintained as the reference surface. The buffer was switched to 25 mM Tris, pH 8.0, 200 mM KCl, 5 mM $MgCl_2$, 0.1 mM TCEP, 0.005% Tween® 20. C-terminally 1D4-tagged full-length p97 and p97 mutants were diluted into this buffer (final

concentration 5–50 μg/ml) and captured (100–150 RU) as ligands on the antibody-coated surfaces, at a flow rate of 50 μl/min for 30 s. Various concentrations of analytes, including ataxin3, the 282ANAA285 mutant, and fragments with and without nucleotides, were diluted in the Tris buffer and passed over the chip at 150 μl/min, for the maximum possible contact time of 163 s. Some experiments involving the p97 R155C/N387C variant also included either 7 mM DTT or no reducing agent, instead of TCEP, as indicated in the main text and figures. The surface was regenerated completely with three injections of freshly prepared regeneration solution, at 100 μl/min for 18 s, before the next round of 1D4-tagged ligand capture.

His_6-tagged protein capture. The ProteOn HTG sensor chip surface was first activated with 10 mM $NiSO_4$ (30 μl/min for 120 s) following the standard protocol recommended by the manufacturer. C-terminally His_6-tagged full-length p97 hexamer (final concentration 0.1–0.4 mg/ml) was captured on the chip to a density of 200–300 RU, using a flow rate of 30 μl/min for 120 s. A reference surface was generated for each chip using His_6-tagged MBP as a control protein. Full-length ataxin3 was flowed over as the analyte, at the concentrations indicated (supplemental Fig. S1), at 100 μl/min, for a contact time of 200 s. Running and dilution buffers used throughout contained 25 mM Tris, pH 8.0, 200 mM KCl, 5 mM $MgCl_2$, 1 mM βME, 5% v/v glycerol, and 0.005% Tween® 20, and the surface was regenerated with three injections of 300 mM EDTA, pH 8.5, at 30 μl/min for 800 s, before the next round of His_6-tagged p97 capture. We observed that a small amount of the ligand accumulated on the chip with each subsequent round of capture, presumably via non-specific aggregation, and the regeneration steps were thus unable to completely clear this material. However, reproducible results were obtained over as many as six rounds of p97-His_6 capture for each flow strip.

The p97 N-domain was immobilized as the ligand on a ProteOn GLC sensor chip by amine coupling, using the same protocol described above. 1D4-tagged N-domain was not used for SPR experiments, as baselines obtained with this construct displayed significant drift. The p97 N-domain was diluted in 10 mM sodium acetate, pH 5.0 (final concentration 20 μg/ml), and directly immobilized on an activated chip to a density of 400–500 RU, at 30 μl/min for 7 min. The chip was blocked with 1 M ethanolamine-HCl, pH 8.5 as described above and stabilized with at least three

injections of running buffer (30 μl/min for 1 min). The running and dilution buffers used for all p97 N-domain experiments contained 1× PBS, pH 7.4, and 0.005% Tween® 20. A reference surface was generated for each chip using the 1D4 antibody immobilized to the corresponding density. Full-length ataxin3 was flowed over as the analyte at the concentrations indicated (Fig. 2B), at 150 μl/min for a contact time of 163 s.

All binding data were first double-referenced to the control flow strip with immobilized Rho1D4 antibody alone, as well as buffer injections during the analyte step. The data were then normalized, relative to the total ligand density on the corresponding surface (Eq. 1), to account for minor differences in ligand immobilization between experiments.

$$Normalized\ analyte\ response = \frac{Observed\ analyte\ response}{Ligand\ density} \times 100 \qquad \text{Equation 1}$$

The processed data were fit to an equilibrium binding model using GraphPad Prism 7.0 to derive the binding affinity. A global 1:1 kinetic analysis of the binding data resulted in poor fits, especially at lower concentrations (supplemental Fig. S12). This deviation from ideal first-order binding kinetics may reflect the need for a more complex interaction model, or, alternatively, might indicate surface-induced artifacts. Since we had no substantial evidence to support a more complex interaction scheme (e.g., conformational changes occurring upon analyte binding or multiple binding sites), we probed the data for mass-transport effects and rebinding events, and optimized conditions to minimize these artifacts, following strategies recommended in (268). We first compared the initial association signals obtained by exposing analyte to different densities of the immobilized ligand (supplemental Fig. S13*A*). The analyte responses, when normalized to the total corresponding ligand density on that surface, produced superimposable curves across flow strips with densities < 200 RU. Ligand densities greater than 200 RU showed slower association kinetics, indicating the presence of mass transport artifacts (supplemental Fig. S13*A*). Thus, we ensured that p97-1D4 was captured to densities of 100–150 RU for all experiments; this level is low enough to minimize mass-transport effects and yet sufficiently high to maintain a good

signal/noise ratio. Additionally, a high flow rate of 150 μl/min was used for the analyte, since we detected increased mass-transport effects using lower flow rates (data not shown). We also tested for rebinding events by introducing a competitor in the dissociation phase (excess untagged p97); by binding to the dissociated analyte, this competitor will prevent rebinding to the immobilized ligand. A significantly faster dissociation was observed in the presence of the competitor (supplemental Fig. S13*B*), indicating that the system was mass-transport limited and that the true dissociation rate was probably greater than the observed rate. Based on these findings, we concluded that kinetic analyses were untrustworthy in this system, and therefore we limited our data analysis to derivations of binding affinity from equilibrium measurements, which are unaffected by mass-transport limitations.

Appendix 2 Tables

Appendix 2 Table 1. Equilibrium dissociation constant *(K_D)* values for the interaction between p97 and ataxin3 fragments

p97 constructs	Ataxin3 constructs	K_D (μM)
Full-length (1–806)	Full-length (1–345)	3.7 ± 0.9[a] ; 8.4 ± 0.1[b]
Full-length (1–806)	Ataxin3ΔC (1–292)	4.3 ± 0.6[a]
p97 N-domain (1–187)	Full-length (1–345)	6.4 ± 1.5[a] ; 4.5 ± 0.2[b]
p97 N-domain (1–187)	Ataxin3ΔC (1–292)	2.8 ± 0.1[b]
p97 N-domain (1–187)	Ataxin3ΔN (220–345)	4.0 ± 0.4[b]

[a] Values were calculated using the equilibrium binding response from 3 or more SPR experiments for each interacting pair. Data were fit to a one-site specific binding model using GraphPad Prism 7.0

[b] Values were calculated from 3 or more ITC experiments for each interacting pair. Data were fit to a one-site independent binding model using NanoAnalyze 3.5.0.

Appendix 2 Supplemental Table 1. Expression constructs and primers used in this work. Plasmids pETHSUL and pETCH have been described elsewhere (198). For all the His_6-SUMO-fusions, a single Gly residue was inserted between the protease cleavage site and the N-terminus of each protein, to increase the efficiency of cleavage by the SUMO-specific protease Ud1.

Target	**Primers (5'-3')**	**Plasmid Backbone**	**Cloning Method**
p97	1: AGATTGGTGGCATGGCTTCTGGAGCCGA TTCAAA 2: GAGGAGAGTTTAGACATTAGCCATACAG GTCATCATCATTG	pETHSUL	LIC
p97-1D4	1: AATGATGATGACCTGTATGGCACCGAAA CCTCTCAGGTGGCGCCGGCGTAATGTCTAA ACTCTCC 2: GGTGCCATACAGGTCATCATCATTGTCTT CTGTGTATACACTGCCACCTGTGCCGC	pETHSUL	Insertion mutagenesis pETHSUL-p97 template
p97-His_6	1: TTTTTTTTTTTCTAGAATGTCTGACTCCGA AGTCAATCAAG 2: TTTTTTTTTTCCCGGGGCCATACAGGTCAT CATCATTG	pETCH	Xba1/Xma1 digestion and ligation
p97 N-domain	1: AGATTGGTGGCATGGCTTCTGGAGCCGAT TCAAA 2: GAGGAGAGTTTAGACATTACTCCCCTTCG CAGTGGATCAC	pETHSUL	LIC
p97 ND1	1: AGATTGGTGGCATGGCTTCTGGAGCCGAT TCAAA 2: GAGGAGAGTTTAGACATTACCCGATGTCT TCCCAGGTTAC	pETHSUL	LIC
Ataxin3	1: AGATTGGTGGCGGTATGGAGTCCATCTTC CACGAG 2: GAGGAGAGTTTAGACTATTATTTTGGTCG ATGCATCTGTTGG	pETHSUL	LIC
His_6-Ataxin3	1: TTTTTTTTTTTCCATGGGTATGGAGTCCAT CTTCCACG 2: TTTTTTTTTTGCGGCCGCGACTAGTGAGC TCG	pProEX-HTb	Nco1/Not1 digestion and ligation
Ataxin3 Josephin domain	1: AGATTGGTGGCGGTATGGAGTCCATCTTC CACGAG 2: GAGGAGAGTTTAGACTATTATTTTGGTGT ATCCATCTCTTCGA	pETHSUL	LIC
Ataxin3 Josephin+UIMs	1: AGATTGGTGGCGGTATGGAGTCCATCTTC CACGAG 2: GAGGAGAGTTTAGACATTAGTTTCTGGAA CTACCTTGCATACTTAG	pETHSUL	LIC
Ataxin3ΔC	1: GAGAAGCAATAATCAGCAGCAACAACA ACAACAGCAACAACAGCGGGACC 2: TGCTGCTGATTATTGCTTCTCAAAGTAGG CTTCTCGTCTCTTCCGAAGC	pETHSUL	Insertion mutagenesis pETHSUL-atx3 template
Ataxin3ΔN	1: AGATTGGTGGCGGAATGTTAGACGAAGA TGAGGAGG 2: GAGGAGAGTTTAGACTATTATGTCAGATA AAGTGTGAAGGT	pETHSUL	LIC

Abbreviations: Ligation independent cloning (LIC), p97 N- and D1- domains (p97 ND1) and Ubiquitin interacting motifs (UIMs).

Appendix 2 Supplemental Table 2. Primers used for one-step site-directed mutagenesis of ataxin3 and p97 (199). pETHSUL-ataxin3 and pETHSUL-p97-1D4 were used as templates.

Ataxin3 mutant construct	**Primers (5'-3')**
^{282}ANAA^{285}	1: GAGCTTGCGAACGCGGCGGAAGCCTACTTTGAGAAGCAACAGCAGCAAC 2: AAAGTAGGCTTCCGCCGCGTTCGCAAGCTCTTCTGAAGTAAGATTTGTACCTG
p97 mutant construct	**Primers (5'-3')**
Y143A	1: CTGGAAGCGGCTCGACCCATCCGGAAAGGAGACATTTTTCTTGTCCG 2: GGTCGAGCCGCTTCCAGGAAGTACGGCTTAAGGTATACCTCGAAGAG
L72A	1: CATCGTCGCTTCTGATGATACTTGTTCTGATGAGAAGATTCGGATGAATAGAG 2: CATCAGAAGCGACGATGCAAACAGCTTCTCGTCTCTTCTTTCCTTTCAGC
R53A	1: GTTGTTCGCAGGTGACACAGTGTTGCTGAAAGGAAAGAAGAGACGAGAAGCTG 2: GTGTCACCTGCGAACAACTGCAATTCATCCATCTTGGGCTGGGACAAG
G54W	1: GTTCCGATGGGACACAGTGTTGCTGAAAGGAAAGAAGAGACGAGAAG 2: CTGTGTCCCATCGGAACAACTGCAATTCATCCATCTTGGGCTGGG
K251A	1: GAACAGGAGCTACCCTGATTGCTCGAGCTGTAGCAAATGAGACTGGAG 2: ATCAGGGTAGCTCCTGTTCCAGGAGGTCCGTAAAGCAGGATTCCTC
K524A	1: CTGTGGGGCTACTTTGTTGGCCAAAGCCATTGCTAATGAATGCCAG 2: CAACAAAGTAGCCCCACAGCCAGGAGGTCCATAGAACAGAACTCCC
K251A/K524A	K251A and K524A were used together
R155C/N387C	R155C 1: TTTTCTTGTCTGCGGTGGGATGCGTGCTGTGGAGTTCAAAGTGGTGG 2: CCACCGCAGACAAGAAAAATGTCTCCTTTCCGGATGGGTCGATACG N387C 1: AAGTGCATGAAGCTGGCAGATGATGTGGACCTGGAACAGGTAGCCAATG 2: CTGCCAGCTTCATGCACTTGGTATGGATCTGAAGAATCTCTAAGCGTCC
R155H	1: TTTTCTTGTCCATGGTGGGATGCGTGCTGTGGAGTTCAAAGTGGTGG 2: CCACCATGGACAAGAAAAATGTCTCCTTTCCGGATGGGTCGATACG
L198W	1: AGAGTCCTGGAATGAAGTAGGGTATGATGACATTGGTGGCTGCAGG 2: ACTTCATTCCAGGACTCTTCCTCATCCTCTCGTTTGATAGGCTCCC
A232E	1: CCCTCTTTAAGGAAATTGGTGTGAAGCCTCCTAGAGGAATCCTGC 2: CCAATTTCCTTAAAGAGGGCAGGATGTCTCAGGGGCAGTTCCAC
L198W/R155C /N387C	L198W primers were used with the pETHSUL-R155C/N387C mutant
A232E/R155C /N387C	A232E primers were used with the pETHSUL-R155C/N387C mutant

Appendix 2 Supplemental Table 3. Binding affinities and structures for various p97-cofactor complexes.

p97 construct	Cofactor construct	K_D	Technique	p97-interacting domain/motif	PDB entry	References
N	Ufd1 peptide	221 μM	ITC	SHP box	5B6C	(269)
N	Npl4 ULD	17.8 μM	ITC	ULD	2PJH	(44,270)
FL p97	FL Ufd1/Npl4	1.7 μM	ITC	SHP box / ULD		(63)
ND1	FL Ufd1/Npl4	2.1 μM	ITC			
FL p97	FL Otu1	0.71 μM	ITC	UBXL	4KDI, 4KDL	(58)
FL p97	FL p47	0.7 μM	ITC	UBX / SHP box	1S3S	(56,63,66)
ND1	FL p47	0.54 μM	ITC			
FL p97	FL p47	22 nM, 0.89 μM	SPR			
FL p97	FL p37	19 nM	SPR	UBX		(66)
ND1	Faf1 UBX	30 μM	ITC	UBX	3QQ8, 3QWZ	(63,270)
N	Faf1 UBX	25.6 μM	ITC			
ND1	FL SVIP	0.67 μM	ITC	VIM		(64,161)
NL	FL SVIP	5.92 μM	ITC			
N	SVIP peptide	6.6 μM	ITC			
ND1	gp78 peptide	21.3 nM	BLI	VIM	3TIW	(64,161)
N	gp78 peptide	5 μM	ITC			
ND1	ANKZF1 peptide	16.3 nM	BLI	VIM		(64)
FL p97	FL UBXD1	3.5 μM	ITC	VIM / PUB		(64)
N	RHBL4 C-terminal	68.9 μM	SPR	VBM	5EPP	(206)
N	Hrd1 peptide	47.8 μM	ITC	VBM		(161)
N	E4B peptide	46.3 μM	ITC	VBM		(161)
N	Ataxin3 peptide	15.6 μM	ITC	VBM		(161) and this study
FL p97	FL Ataxin3	3.7 ± 0.9 μM	SPR			
N	FL Ataxin3	6.4 ± 1.5 μM	SPR			
N	FL Ataxin3	4.5 ± 0.2 μM	ITC			

Abbreviations: Full-length (FL), p97 N- and D1- domains (ND1), p97 N-domain (N), Ubiquitin-fusion degradation protein 1 (Ufd1), Nuclear localization protein 4 (Npl4), Ovarian tumor domain-containing protein 1 (Otu1), Fas-associated factor 1 (Faf1), Small valosin-interacting protein (SVIP), Ankyrin repeat and zinc finger domain-containing protein 1 (ANKZF1), Ubiquitin regulatory X domain protein 1 (UBXD1), Rhomboid protease (RHBDL4), HMG-CoA reductase degradation protein 1 (Hrd1), Isothermal Titration Calorimetry (ITC), Surface plasmon resonance (SPR), Biolayer interferometry (BLI), Ubiquitin-like domain (ULD, also known as UBD), Ubiquitin regulatory X domain (UBX), UBX-like domain (UBL), peptide:N-glycanase/ UBA or UBX (PUB), p97/VCP-interacting motif (VIM), and p97/VCP-binding motif (VBM).

Appendix 2 Supplemental Figures

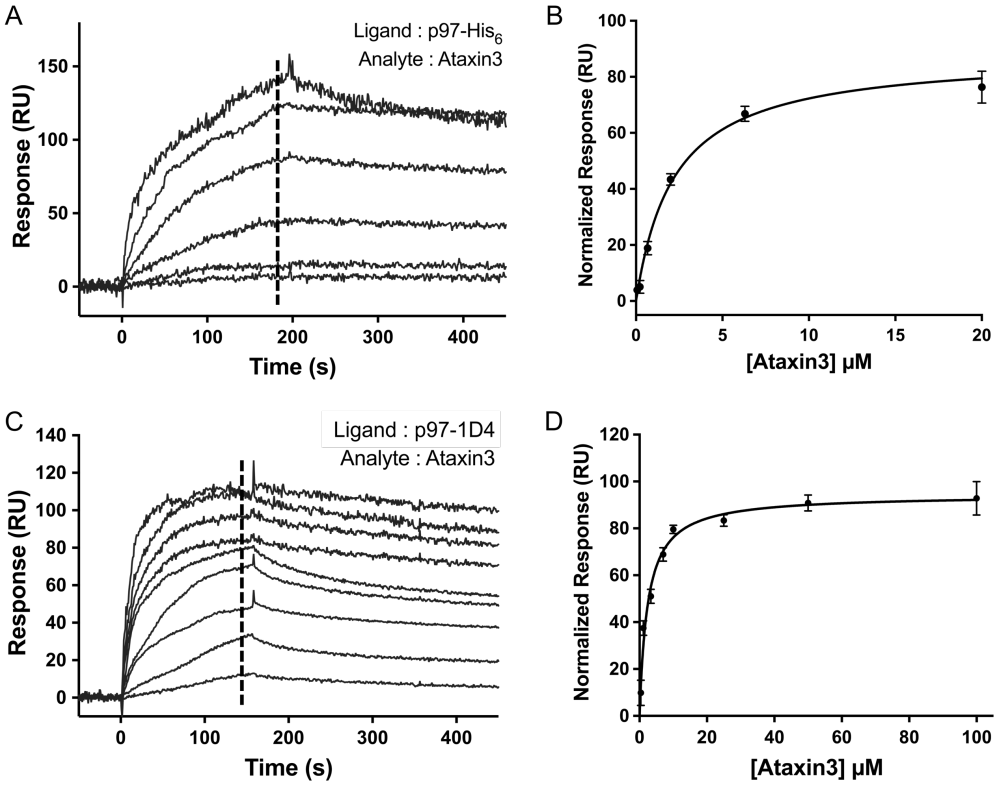

Appendix 2 Supplemental Figure S1. Alternate p97 preparations have the same affinity for ataxin3. (A) Representative sensorgram for full-length ataxin3 binding to full-length p97-His_6 (ataxin3 concentrations 0–20 µM, $n \geq 3$ for each concentration). **(B)** Normalized equilibrium response fit of the data in A to a one-site binding curve (K_D = 2.2 ± 0.2 µM). **(C)** Representative sensorgram for full-length ataxin3 binding to full-length p97-1D4 (ataxin3 concentrations 0–100 µM, n ≥ 3 for each concentration). The p97-1D4 sample was purified using an additional ion exchange chromatography step, similar to the ITC sample preparation. **(D)** Normalized equilibrium response fit of the data in C to a one-site binding curve (K_D = 2.4 ± 0.2 µM). The dashed lines in the left panels represent the response range used to determine the fit.

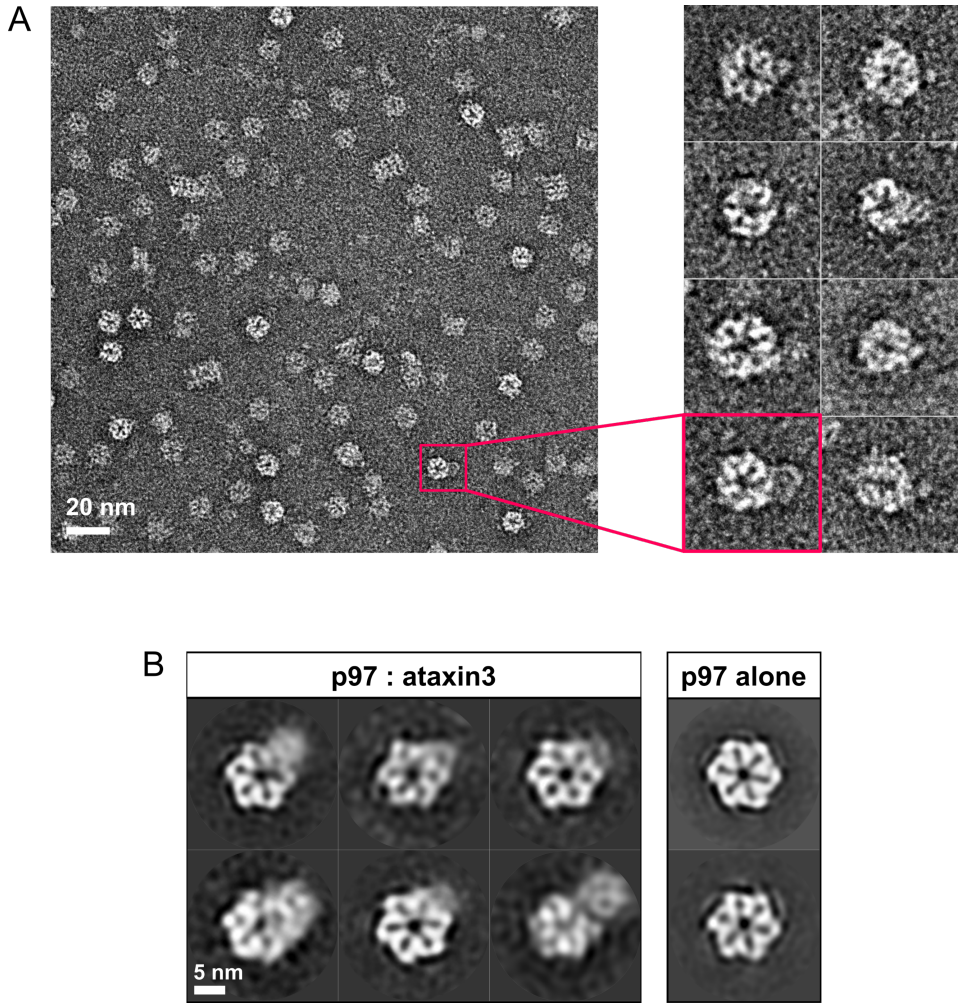

Appendix 2 Supplemental Figure S2. Negative-stain electron microscopy (EM) analyses of the p97-ataxin3 complex. (A) *Left*, electron micrograph showing negatively-stained hexamers of p97 bound to ataxin3 (non-crosslinked). The *magenta box* highlights one p97-ataxin3 complex. *Right,* raw images of the complex viewed down the 6-fold axis, shown at higher magnification. **(B)** Representative 2D class averages for the non-crosslinked p97-ataxin3 complex (*left*) and p97 alone (*right*). From the 20,256 particles selected, only ~1,300 particles were sorted into classes that show the additional blurred density corresponding to ataxin3. No side views of the p97 hexamer were observed in any samples, suggesting that the relatively flat, disk-shaped hexamer adopts a preferred orientation coplanar with the plane of the EM grid.

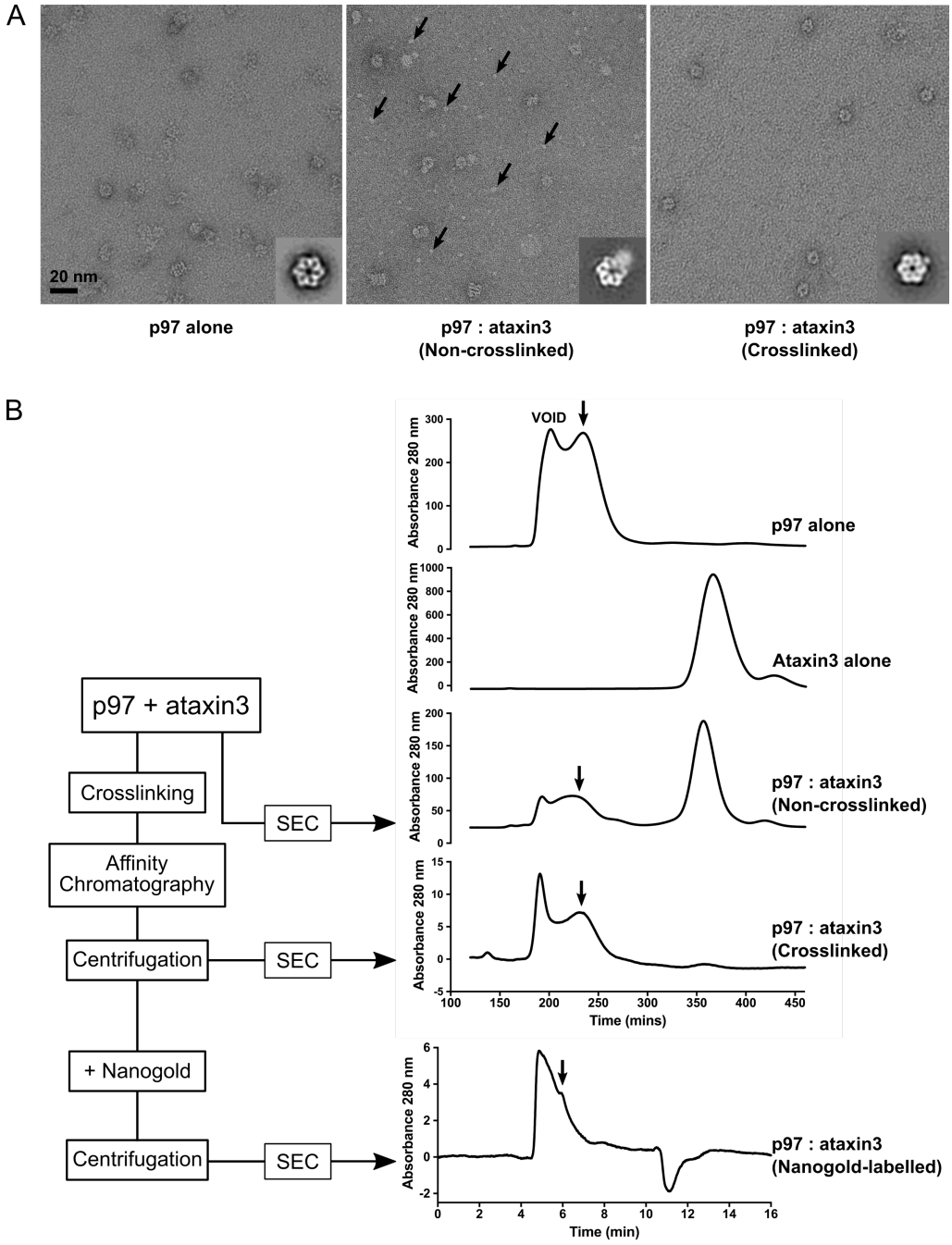

Appendix 2 Supplemental Figure S3. Comparison of non-crosslinked and crosslinked samples. (A) Negative-stained electron micrographs showing p97 alone, non-crosslinked p97-ataxin3 complexes, and crosslinked complexes. *Insets* show a representative 2D class average from each experiment. Note the presence of numerous particles in the middle micrograph (*black arrows*), of a size significantly smaller than the expected dimensions for p97; these particles are absent in the other two micrographs. These particles may represent free ataxin3, implying that the complex has dissociated either during the SEC step or during grid preparation. The blurred density seen for the non-crosslinked complexes might therefore reflect partial dissociation, which is resolved by crosslinking. **(B)** Workflow for preparation of complexes for EM, along with

SEC chromatograms for p97 alone, ataxin3 alone, and the non-crosslinked, crosslinked and Nanogold-labelled complexes. The *black arrows* indicate the fractions used for negative-stain EM. As seen from the position of the peaks, the complex peak may overlap with the p97-alone peak. In the non-crosslinked experiment, the inability to resolve these peaks may have introduced free p97 in the fraction applied to the grids, which would also account for the relatively low fraction of particles containing the complex (~5% of the total particles). The crosslinking, affinity purification, and centrifugation steps aided in removal of unbound p97 and ataxin3 (note the disappearance of the ataxin3 alone peak in the chromatogram for the crosslinked complex). The p97-alone chromatogram shows a typical purification profile similar to others described previously, with irreversibly aggregated material in the void volume peak (54). Note that a different SEC column was used for the Nanogold-labelled material as compared to the other complexes (see Methods), which explains the difference in elution times.

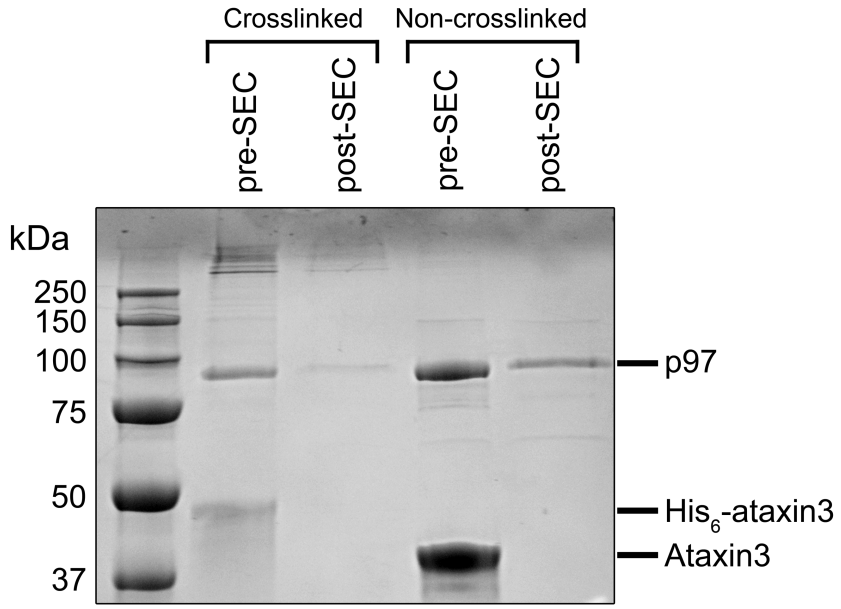

Appendix 2 Supplemental Figure S4. SDS-PAGE gel of the crosslinked and non-crosslinked EM complexes. The gel is stained with Coomassie Brilliant Blue. Lane 1 is the His_6-ataxin3-p97 complex crosslinked with 0.05% glutaraldehyde and purified by immobilized metal-affinity chromatography. Lane 2 is the crosslinked sample from lane 1 after SEC. Lanes 3 and 4 are the p97-ataxin3 complex without crosslinker before and after SEC respectively. In lanes 2 and 4, the tagged and untagged ataxin3 bands are not visible at the dilutions obtained after SEC.

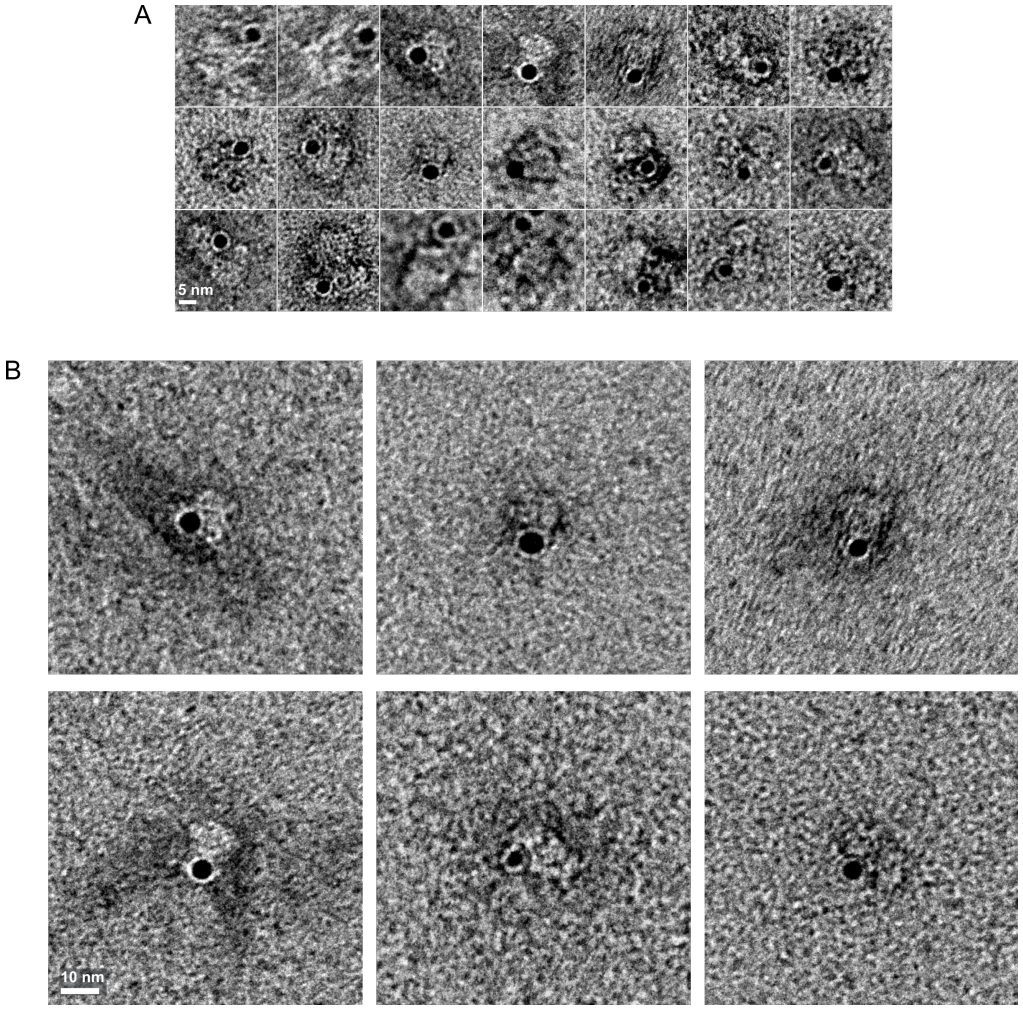

Appendix 2 Supplemental Figure S5. p97 complexed with Nanogold-labeled ataxin3. (A) Raw images of p97 complexed with Nanogold-labelled ataxin3. One single gold particle, visible as a black dot, is observed per complex. **(B)** Six additional complex images as above, shown at higher magnification.

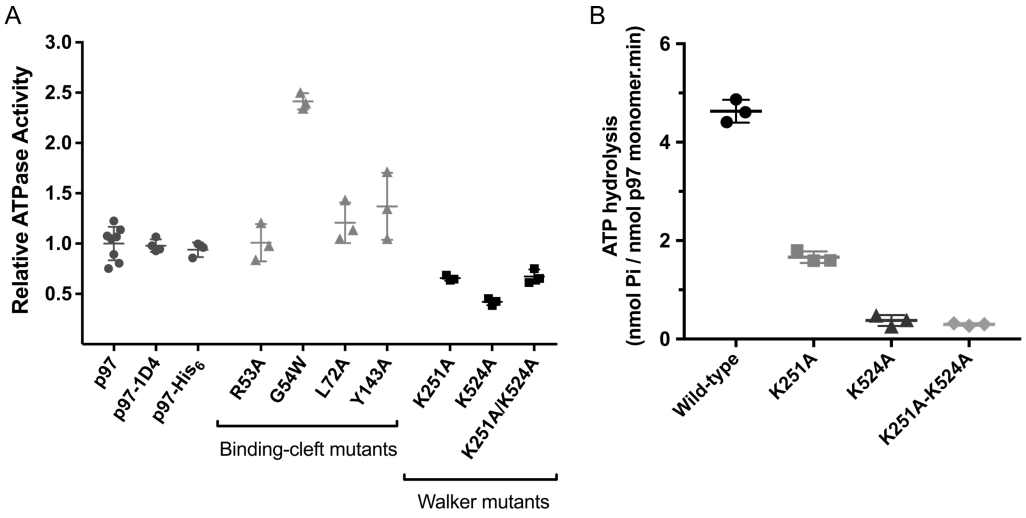

Appendix 2 Supplemental Figure S6. ATPase activities of wild-type and mutant p97. (A) ATPase activities of full-length wild-type p97 (untagged and tagged), four cofactor binding-cleft mutants, and three Walker mutants (all mutants are 1D4-tagged). The C-terminal 1D4 and His_6 tags do not affect ATP hydrolysis. G54W is not an identified MSP1 mutation and it is thus unclear why that mutant has elevated activity ($n \geq 3$ for all measurements). **(B)** We noticed that the relative activities of Walker mutants *vs.* wild-type p97, as shown in panel (A), do not follow the same trend as seen in Briggs *et al.* (8); specifically, in our hands, the K524A mutants appear to possess higher activity than previously reported. However, the activities cannot be directly compared, since different assay conditions were used. The experiments in panel (A) rely upon a coupled assay linked to NADH consumption and were performed at room temperature; in contrast, the Briggs *et al.* experiments utilize a colorimetric Malachite Green assay, performed at 37°. Therefore, to determine whether these disparities in relative activities reflect differences in the assay conditions or genuine differences in the proteins, we measured the ATPase activities of our p97 proteins using a Malachite Green assay at 37 °C, as described in (8). We found that under these conditions, the activities of our different p97 variants follow a trend that is very similar to previously published results (52,209), demonstrating that the apparent disparity in activities results from different assay conditions, and not from different behavior on the part of the proteins.

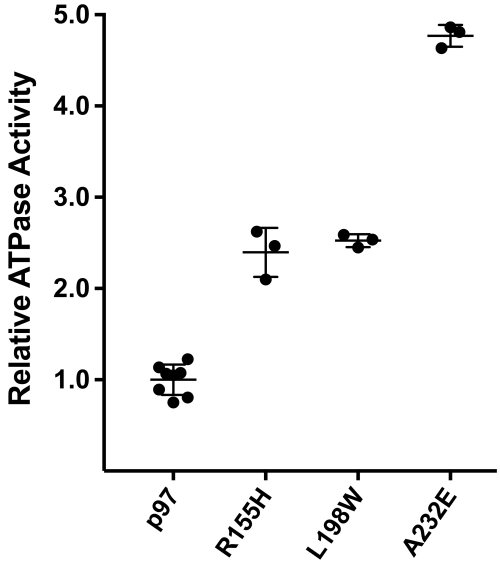

Appendix 2 Supplemental Figure S7. ATPase activities of full-length wild-type p97 and three MSP1 mutants. The mutants show increased activity as compared to the wild-type, consistent with previously published data (54,67).

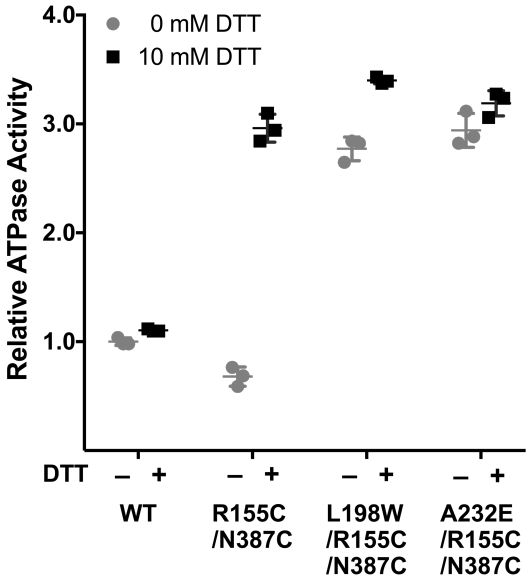

Appendix 2 Supplemental Figure S8. ATPase activity in the presence and absence of DTT. ATPase activities of full-length wild-type p97 (WT), the R155C/N387C double mutant, and the L198W and A232E MSP1 mutant versions of the R155C/N387C double mutant, all measured in the presence and absence of DTT. Note that the disulfide-locked form (– DTT) of the R155C/N387C double mutant has very low activity, which is rescued in the presence of reducing agent (+ DTT). The L198W and A232E versions of the R155C/N387C double mutant show no difference in activity with and without DTT. This suggests that in the two mutants, Cys-155 and Cys-387 are never in close enough proximity to form a disulfide bond and lock down the N-domain.

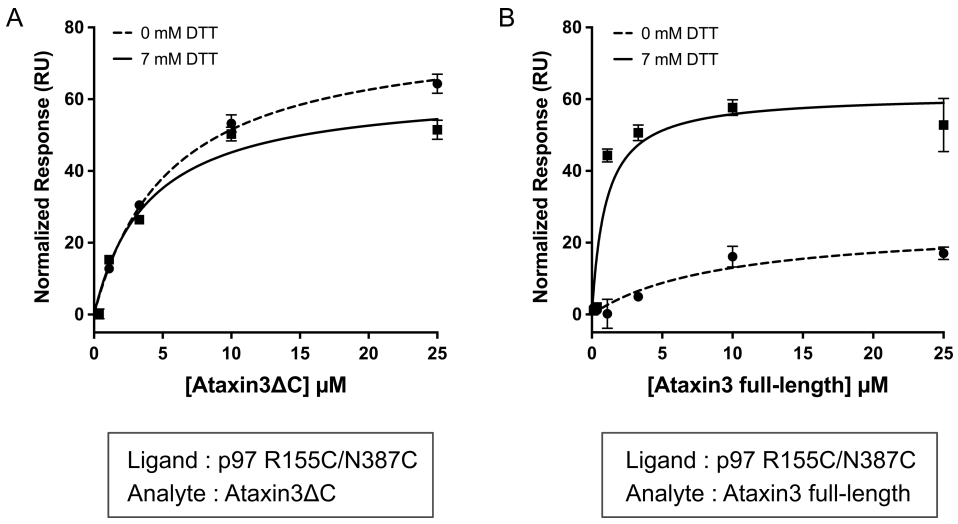

Appendix 2 Supplemental Figure S9. Ataxin3ΔC binds a conformationally-locked form of p97, unlike full-length ataxin3. Ataxin3ΔC binds equally to the disulfide-locked form (– DTT) and reduced form (+ DTT) of the R155C/N387C p97 double mutant, unlike full-length ataxin3. Normalized equilibrium binding response for **(A)** ataxin3ΔC and **(B)** full-length ataxin3 binding to the R155C/N387C double mutant, in the presence and absence of 7 mM DTT ($n \geq 3$ at each concentration for both analytes). The data shown in (B) are the same as those shown in Fig. 7*B*.

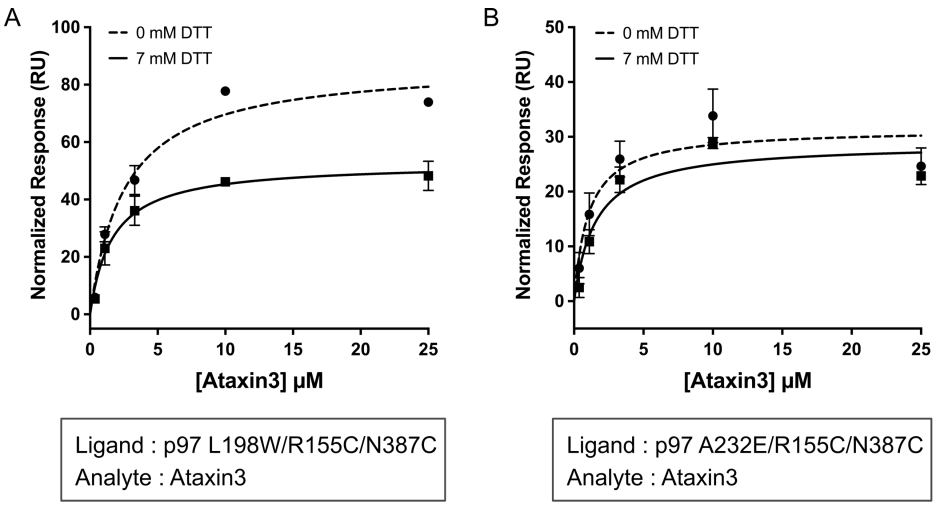

Appendix 2 Supplemental Figure S10. Ataxin3 binds MSP1 versions of the R155C/N387C double mutant. Ataxin3 binds the MSP1 mutant versions of the R155C/N387C double mutant, both in the presence and absence of DTT. Normalized equilibrium binding response for ataxin3 ($n \geq 3$ at each concentration) binding to the **(A)** L198W and **(B)** A232E versions of the R155C/N387C double mutant, with and without 7 mM DTT.

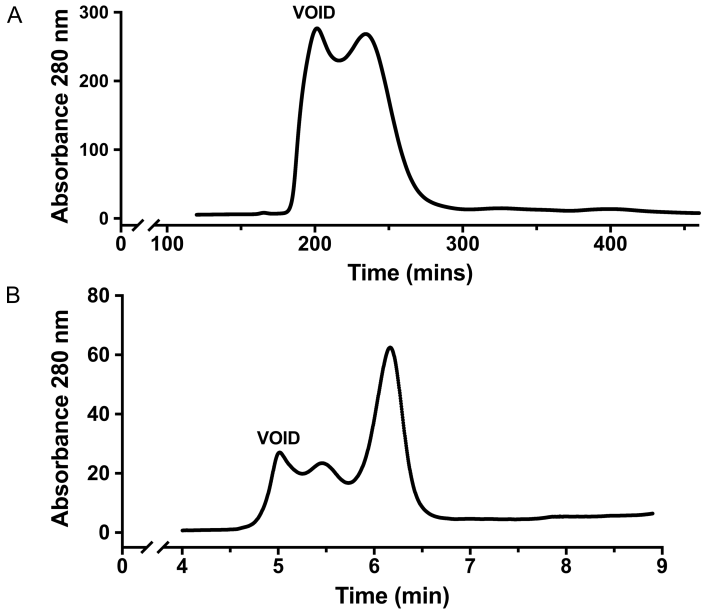

Appendix 2 Supplemental Figure S11. Elution profiles of full-length p97 from size-exclusion chromatography. SEC elution profile of full-length p97 from the **(A)** Sephacryl S-300 preparative column and **(B)** Yarra SEC-3000 column. The void peak in both contains aggregated material. A smaller peak is resolved in (B), eluting between the void and hexamer peaks, and most likely contains higher-order oligomers such as dodecamers and/or small aggregates. The elution profile in (A) is the same as the p97-alone profile shown in Fig. S3*B*.

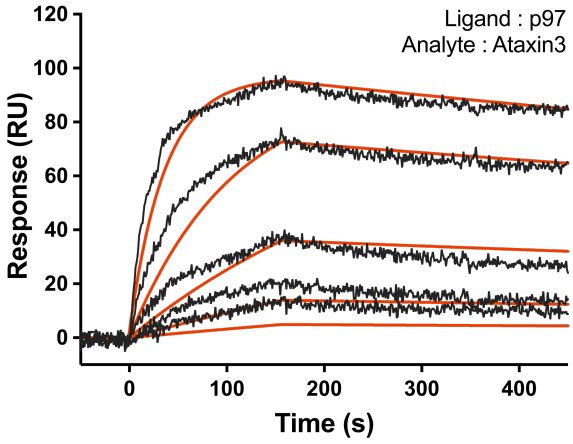

Appendix 2 Supplemental Figure S12. Global 1:1 kinetic analysis of full-length ataxin3 binding to full-length p97. Representative SPR sensorgrams for the binding of full-length ataxin3 to full-length 1D4-tagged p97. Highest ataxin3 concentration = 10 μM; other concentrations obtained by successive 3-fold dilutions. The *orange lines* represent a global fit to a one-site kinetic model. Note that the fit deviates considerably from the sensorgrams, especially at the lower concentrations, and thus reliable kinetic rates cannot be derived. This could either be resolved by fitting to a more complex model or by accounting for surface-induced mass-transport limitations.

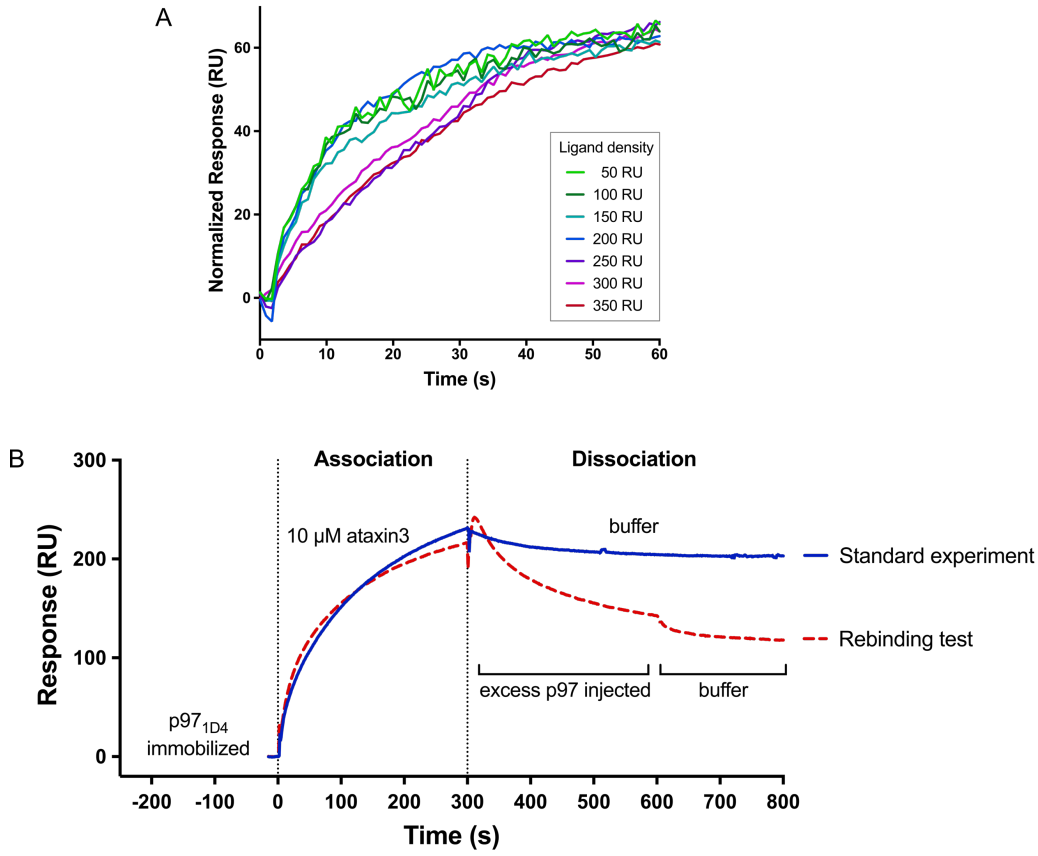

Appendix 2 Supplemental Figure S13. Detecting the presence of mass-transport limitations in the p97-ataxin3 system. (A) Comparison of the association signals from 10 μM ataxin3 binding to different densities (50–350 RU) of the immobilized ligand p97-1D4. The responses are normalized to the density of p97-1D4 on each corresponding surface. Superimposable responses were obtained for surfaces with densities between 50–200 RU; ligand densities greater than 200 RU showed slower association, indicating the presence of mass-transport effects. **(B)** Data showing the association and dissociation between 10 μM ataxin3 analyte and p97-1D4 ligand, obtained under standard experimental conditions *(blue line),* and rebinding test conditions *(dashed red line)*. Rebinding was tested by injecting excess untagged p97 during the dissociation phase (instead of the running buffer alone); the excess p97 serves as a competitor and binds the dissociated ataxin3, preventing its rebinding to the immobilized p97-1D4. Note the significantly faster dissociation under these conditions, indicating that analyte rebinding is occurring under the standard experimental conditions, implying that the true dissociation rate is probably greater than that observed in the standard experiment.

APPENDIX 3: Supplemental Tables and Figures for Chapter 3.

Appendix 3 Tables

Appendix 3 Supplementary Table 1. Expression constructs and primers used to generate the ubiquitin proteins.

Target	Primers (5'-3')	Plasmid Backbone	Cloning Method
Ubiquitin	1: TTTTTTCATATGCAGATCTTCGTGAAGACCC 2: TTTTTTGAATTCTATTACCCACCTCTGAGACGGAGCA	pRSETA	NdeI/EcoR1 ligation
Ubiquitin-His_6	1: TAATACGACTCACTATAGGG 2: TTTTTTCCCGGGACCGCCCCCACCACGGGACGCAGCACCA	pETCH	Xba1/Xma1digestion and ligation

Appendix 3 Supplementary Table 2. Primers used for one-step site-directed mutagenesis of ataxin3 (199). Full-length pETHSUL-ataxin3 was used as templates.

Ataxin3 mutant	Primers (5'-3')
Site 2 mutant (W87K)	1: GCCTTGAAAGTTAAAGGTTTAGAACTAATCCTGTTCAACAGTCCAGAGTATCAGAGG 2: CTAAACCTTTAACTTTCAAGGCATTGCTTATAACCTGAATAGAGAAAAAACCACTGTC
UIM mutant (S236A/S256A)	S236A 1: GGCACTAGCACGCCAAGAAATTGACATGGAAGATGAGGAAGCAG 2: CTTGGCGTGCTAGTGCCAGAGCCCTCTGCAAATCCTCCTC S256A 1: CAGCTAGCAATGCAAGGTAGTTCCAGAAACATATCTCAAGATATG 2: CCTTGCATTGCTAGCTGAATAGCCCTGCGGAGATCTGCTTC

Appendix 3 Supplemental Figures

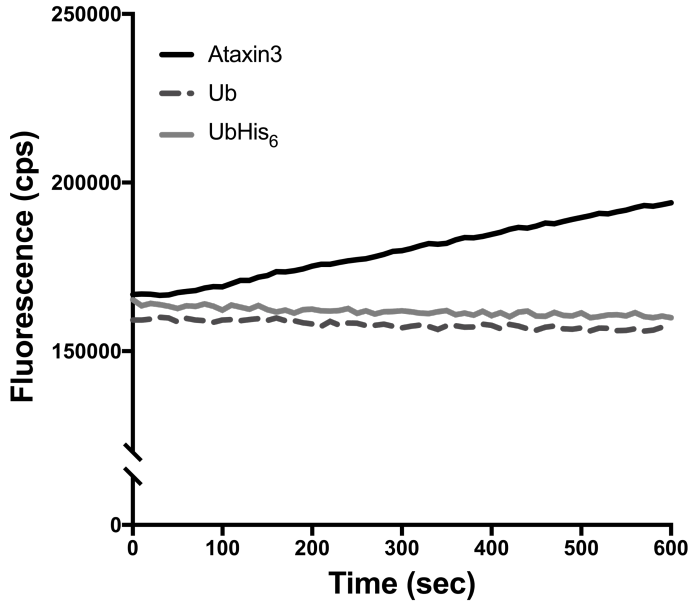

Appendix 3 Supplemental Figure S1. The ubiquitin constructs alone do not contribute fluorescence. Representative plot showing the increase in fluorescence over time for ataxin3 alone *(black line)*, and the control reactions with Ub *(grey dashes)* and $UbHis_6$ *(grey line)* in the absence of the DUB. The ubiquitin constructs do not produce any increase in fluorescence by themselves *($n \geq 3$ for each reaction).*

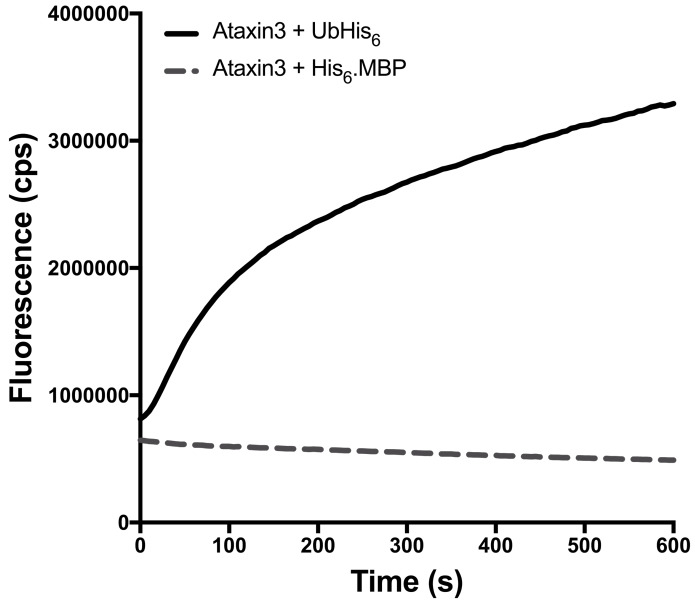

Appendix 3 Supplemental Figure S2. The His_6-tagged MBP control does not stimulate ataxin3 activity. Representative plot showing the increase in fluorescence over time for ataxin3 in the presence of $UbHis_6$ *(black line)*, and His_6-MBP *(grey dashes)* at the same concentration (75 μM). The His_6-MBP control reaction does not show any increase in fluorescence, and thus, His_6-MBP does not stimulate ataxin3 activity *($n \geq 3$ for each reaction).*

List of References

1. Balch, W. E., Morimoto, R. I., Dillin, A., and Kelly, J. W. (2008) Adapting proteostasis for disease intervention. *Science (New York, N.Y.)* **319**, 916-919
2. Hetz, C., and Glimcher, L. H. (2011) Protein homeostasis networks in physiology and disease. *Current opinion in cell biology* **23**, 123-125
3. Voth, W., and Jakob, U. (2017) Stress-Activated Chaperones: A First Line of Defense. *Trends in biochemical sciences*
4. Fernandez-Fernandez, M. R., Gragera, M., Ochoa-Ibarrola, L., Quintana-Gallardo, L., and Valpuesta, J. M. (2017) Hsp70 - a master regulator in protein degradation. *FEBS letters* **591**, 2648-2660
5. Brettschneider, J., Del Tredici, K., Lee, V. M., and Trojanowski, J. Q. (2015) Spreading of pathology in neurodegenerative diseases: a focus on human studies. *Nature reviews. Neuroscience* **16**, 109-120
6. Schneider, K., and Bertolotti, A. (2015) Surviving protein quality control catastrophes--from cells to organisms. *Journal of cell science* **128**, 3861-3869
7. Schreiber, A., and Peter, M. (2014) Substrate recognition in selective autophagy and the ubiquitin-proteasome system. *Biochimica et biophysica acta* **1843**, 163-181
8. Kisselev, A. F., Akopian, T. N., Woo, K. M., and Goldberg, A. L. (1999) The sizes of peptides generated from protein by mammalian 26 and 20 S proteasomes. Implications for understanding the degradative mechanism and antigen presentation. *The Journal of biological chemistry* **274**, 3363-3371
9. Liebl, M. P., and Hoppe, T. (2016) It's all about talking: two-way communication between proteasomal and lysosomal degradation pathways via ubiquitin. *American journal of physiology. Cell physiology* **311**, C166-178
10. Ravikumar, B., Duden, R., and Rubinsztein, D. C. (2002) Aggregate-prone proteins with polyglutamine and polyalanine expansions are degraded by autophagy. *Human molecular genetics* **11**, 1107-1117
11. Mizushima, N. (2011) Autophagy in protein and organelle turnover. *Cold Spring Harbor symposia on quantitative biology* **76**, 397-402
12. Kwon, Y. T., and Ciechanover, A. (2017) The Ubiquitin Code in the Ubiquitin-Proteasome System and Autophagy. *Trends in biochemical sciences*
13. Saeki, Y. (2017) Ubiquitin recognition by the proteasome. *Journal of biochemistry* **161**, 113-124
14. Ciechanover, A. (2006) The ubiquitin proteolytic system: from a vague idea, through basic mechanisms, and onto human diseases and drug targeting. *Neurology* **66**, S7-19
15. Geng, F., Wenzel, S., and Tansey, W. P. (2012) Ubiquitin and proteasomes in transcription. *Annual review of biochemistry* **81**, 177-201
16. Bader, M., and Steller, H. (2009) Regulation of cell death by the ubiquitin-proteasome system. *Current opinion in cell biology* **21**, 878-884
17. Kirkin, V., and Dikic, I. (2007) Role of ubiquitin- and Ubl-binding proteins in cell signaling. *Current opinion in cell biology* **19**, 199-205
18. Yau, R., and Rape, M. (2016) The increasing complexity of the ubiquitin code. *Nature cell biology* **18**, 579-586

19. Komander, D., Clague, M. J., and Urbe, S. (2009) Breaking the chains: structure and function of the deubiquitinases. *Nature reviews. Molecular cell biology* **10**, 550-563
20. Coyne, E. S., and Wing, S. S. (2016) The business of deubiquitination - location, location, location. *F1000Research* **5**
21. Ruggiano, A., Foresti, O., and Carvalho, P. (2014) Quality control: ER-associated degradation: protein quality control and beyond. *The Journal of cell biology* **204**, 869-879
22. Goeckeler, J. L., and Brodsky, J. L. (2010) Molecular chaperones and substrate ubiquitination control the efficiency of endoplasmic reticulum-associated degradation. *Diabetes, obesity & metabolism* **12 Suppl 2**, 32-38
23. Bento, C. F., Renna, M., Ghislat, G., Puri, C., Ashkenazi, A., Vicinanza, M., Menzies, F. M., and Rubinsztein, D. C. (2016) Mammalian Autophagy: How Does It Work? *Annual review of biochemistry* **85**, 685-713
24. Lamark, T., and Johansen, T. (2012) Aggrephagy: selective disposal of protein aggregates by macroautophagy. *International journal of cell biology* **2012**, 736905
25. Ji, C. H., and Kwon, Y. T. (2017) Crosstalk and Interplay between the Ubiquitin-Proteasome System and Autophagy. *Molecules and cells* **40**, 441-449
26. Tang, B., Cai, J., Sun, L., Li, Y., Qu, J., Snider, B. J., and Wu, S. (2014) Proteasome inhibitors activate autophagy involving inhibition of PI3K-Akt-mTOR pathway as an anti-oxidation defense in human RPE cells. *PloS one* **9**, e103364
27. Bao, W., Gu, Y., Ta, L., Wang, K., and Xu, Z. (2016) Induction of autophagy by the MG132 proteasome inhibitor is associated with endoplasmic reticulum stress in MCF7 cells. *Molecular medicine reports* **13**, 796-804
28. Low, P., Varga, A., Pircs, K., Nagy, P., Szatmari, Z., Sass, M., and Juhasz, G. (2013) Impaired proteasomal degradation enhances autophagy via hypoxia signaling in Drosophila. *BMC cell biology* **14**, 29
29. Shen, Y. F., Tang, Y., Zhang, X. J., Huang, K. X., and Le, W. D. (2013) Adaptive changes in autophagy after UPS impairment in Parkinson's disease. *Acta pharmacologica Sinica* **34**, 667-673
30. Waite, K. A., De-La Mota-Peynado, A., Vontz, G., and Roelofs, J. (2016) Starvation Induces Proteasome Autophagy with Different Pathways for Core and Regulatory Particles. *The Journal of biological chemistry* **291**, 3239-3253
31. Bartel, B. (2015) Proteaphagy-Selective Autophagy of Inactive Proteasomes. *Molecular cell* **58**, 970-971
32. Xia, D., Tang, W. K., and Ye, Y. (2016) Structure and function of the AAA+ ATPase p97/Cdc48p. *Gene* **583**, 64-77
33. Doss-Pepe, E. W., Stenroos, E. S., Johnson, W. G., and Madura, K. (2003) Ataxin-3 interactions with rad23 and valosin-containing protein and its associations with ubiquitin chains and the proteasome are consistent with a role in ubiquitin-mediated proteolysis. *Molecular and cellular biology* **23**, 6469-6483
34. Burnett, B., Li, F., and Pittman, R. N. (2003) The polyglutamine neurodegenerative protein ataxin-3 binds polyubiquitylated proteins and has ubiquitin protease activity. *Human molecular genetics* **12**, 3195-3205
35. Ashkenazi, A., Bento, C. F., Ricketts, T., Vicinanza, M., Siddiqi, F., Pavel, M., Squitieri, F., Hardenberg, M. C., Imarisio, S., Menzies, F. M., and Rubinsztein, D.

C. (2017) Polyglutamine tracts regulate beclin 1-dependent autophagy. *Nature* **545**, 108-111

36. Burnett, B. G., and Pittman, R. N. (2005) The polyglutamine neurodegenerative protein ataxin 3 regulates aggresome formation. *Proceedings of the National Academy of Sciences of the United States of America* **102**, 4330-4335
37. Zhong, X., and Pittman, R. N. (2006) Ataxin-3 binds VCP/p97 and regulates retrotranslocation of ERAD substrates. *Human molecular genetics* **15**, 2409-2420
38. Wang, Q., Li, L., and Ye, Y. (2006) Regulation of retrotranslocation by p97-associated deubiquitinating enzyme ataxin-3. *The Journal of cell biology* **174**, 963-971
39. Zhao, M., and Brunger, A. T. (2016) Recent Advances in Deciphering the Structure and Molecular Mechanism of the AAA+ ATPase N-Ethylmaleimide-Sensitive Factor (NSF). *Journal of molecular biology* **428**, 1912-1926
40. Kressler, D., Hurt, E., Bergler, H., and Bassler, J. (2012) The power of AAA-ATPases on the road of pre-60S ribosome maturation--molecular machines that strip pre-ribosomal particles. *Biochimica et biophysica acta* **1823**, 92-100
41. Grimm, I., Erdmann, R., and Girzalsky, W. (2016) Role of AAA(+)-proteins in peroxisome biogenesis and function. *Biochimica et biophysica acta* **1863**, 828-837
42. DeLaBarre, B., and Brunger, A. T. (2003) Complete structure of p97/valosin-containing protein reveals communication between nucleotide domains. *Nature structural biology* **10**, 856-863
43. Banerjee, S., Bartesaghi, A., Merk, A., Rao, P., Bulfer, S. L., Yan, Y., Green, N., Mroczkowski, B., Neitz, R. J., Wipf, P., Falconieri, V., Deshaies, R. J., Milne, J. L., Huryn, D., Arkin, M., and Subramaniam, S. (2016) 2.3 A resolution cryo-EM structure of human p97 and mechanism of allosteric inhibition. *Science (New York, N.Y.)* **351**, 871-875
44. Isaacson, R. L., Pye, V. E., Simpson, P., Meyer, H. H., Zhang, X., Freemont, P. S., and Matthews, S. (2007) Detailed structural insights into the p97-Npl4-Ufd1 interface. *The Journal of biological chemistry* **282**, 21361-21369
45. Davies, J. M., Tsuruta, H., May, A. P., and Weis, W. I. (2005) Conformational changes of p97 during nucleotide hydrolysis determined by small-angle X-Ray scattering. *Structure (London, England : 1993)* **13**, 183-195
46. Peters, J. M., Walsh, M. J., and Franke, W. W. (1990) An abundant and ubiquitous homo-oligomeric ring-shaped ATPase particle related to the putative vesicle fusion proteins Sec18p and NSF. *The EMBO journal* **9**, 1757-1767
47. Zhang, L., Ashendel, C. L., Becker, G. W., and Morre, D. J. (1994) Isolation and characterization of the principal ATPase associated with transitional endoplasmic reticulum of rat liver. *The Journal of cell biology* **127**, 1871-1883
48. Rouiller, I., Butel, V. M., Latterich, M., Milligan, R. A., and Wilson-Kubalek, E. M. (2000) A major conformational change in p97 AAA ATPase upon ATP binding. *Molecular cell* **6**, 1485-1490
49. Zhang, X., Shaw, A., Bates, P. A., Newman, R. H., Gowen, B., Orlova, E., Gorman, M. A., Kondo, H., Dokurno, P., Lally, J., Leonard, G., Meyer, H., van Heel, M., and Freemont, P. S. (2000) Structure of the AAA ATPase p97. *Molecular cell* **6**, 1473-1484

50. Hanzelmann, P., and Schindelin, H. (2017) The Interplay of Cofactor Interactions and Post-translational Modifications in the Regulation of the AAA+ ATPase p97. *Frontiers in molecular biosciences* **4**, 21
51. Dougan, D. A., Mogk, A., Zeth, K., Turgay, K., and Bukau, B. (2002) AAA+ proteins and substrate recognition, it all depends on their partner in crime. *FEBS letters* **529**, 6-10
52. Briggs, L. C., Baldwin, G. S., Miyata, N., Kondo, H., Zhang, X., and Freemont, P. S. (2008) Analysis of nucleotide binding to P97 reveals the properties of a tandem AAA hexameric ATPase. *The Journal of biological chemistry* **283**, 13745-13752
53. Fernandez-Saiz, V., and Buchberger, A. (2010) Imbalances in p97 co-factor interactions in human proteinopathy. *EMBO reports* **11**, 479-485
54. Niwa, H., Ewens, C. A., Tsang, C., Yeung, H. O., Zhang, X., and Freemont, P. S. (2012) The role of the N-domain in the ATPase activity of the mammalian AAA ATPase p97/VCP. *The Journal of biological chemistry* **287**, 8561-8570
55. Arumughan, A., Roske, Y., Barth, C., Forero, L. L., Bravo-Rodriguez, K., Redel, A., Kostova, S., McShane, E., Opitz, R., Faelber, K., Rau, K., Mielke, T., Daumke, O., Selbach, M., Sanchez-Garcia, E., Rocks, O., Panakova, D., Heinemann, U., and Wanker, E. E. (2016) Quantitative interaction mapping reveals an extended UBX domain in ASPL that disrupts functional p97 hexamers. *Nature communications* **7**, 13047
56. Dreveny, I., Kondo, H., Uchiyama, K., Shaw, A., Zhang, X., and Freemont, P. S. (2004) Structural basis of the interaction between the AAA ATPase p97/VCP and its adaptor protein p47. *The EMBO journal* **23**, 1030-1039
57. Pye, V. E., Beuron, F., Keetch, C. A., McKeown, C., Robinson, C. V., Meyer, H. H., Zhang, X., and Freemont, P. S. (2007) Structural insights into the p97-Ufd1-Npl4 complex. *Proceedings of the National Academy of Sciences of the United States of America* **104**, 467-472
58. Kim, S. J., Cho, J., Song, E. J., Kim, S. J., Kim, H. M., Lee, K. E., Suh, S. W., and Kim, E. E. (2014) Structural basis for ovarian tumor domain-containing protein 1 (OTU1) binding to p97/valosin-containing protein (VCP). *The Journal of biological chemistry* **289**, 12264-12274
59. Tang, W. K., Li, D., Li, C. C., Esser, L., Dai, R., Guo, L., and Xia, D. (2010) A novel ATP-dependent conformation in p97 N-D1 fragment revealed by crystal structures of disease-related mutants. *The EMBO journal* **29**, 2217-2229
60. DeLaBarre, B., and Brunger, A. T. (2005) Nucleotide dependent motion and mechanism of action of p97/VCP. *Journal of molecular biology* **347**, 437-452
61. Hanzelmann, P., and Schindelin, H. (2016) Structural Basis of ATP Hydrolysis and Intersubunit Signaling in the AAA+ ATPase p97. *Structure (London, England : 1993)* **24**, 127-139
62. Huang, C., Li, G., and Lennarz, W. J. (2012) Dynamic flexibility of the ATPase p97 is important for its interprotomer motion transmission. *Proceedings of the National Academy of Sciences of the United States of America* **109**, 9792-9797
63. Hanzelmann, P., Buchberger, A., and Schindelin, H. (2011) Hierarchical binding of cofactors to the AAA ATPase p97. *Structure (London, England : 1993)* **19**, 833-843

64. Hanzelmann, P., and Schindelin, H. (2011) The structural and functional basis of the p97/valosin-containing protein (VCP)-interacting motif (VIM): mutually exclusive binding of cofactors to the N-terminal domain of p97. *The Journal of biological chemistry* **286**, 38679-38690
65. Zhao, G., Zhou, X., Wang, L., Li, G., Schindelin, H., and Lennarz, W. J. (2007) Studies on peptide:N-glycanase-p97 interaction suggest that p97 phosphorylation modulates endoplasmic reticulum-associated degradation. *Proceedings of the National Academy of Sciences of the United States of America* **104**, 8785-8790
66. Bulfer, S. L., Chou, T. F., and Arkin, M. R. (2016) p97 Disease Mutations Modulate Nucleotide-Induced Conformation to Alter Protein-Protein Interactions. *ACS chemical biology* **11**, 2112-2116
67. Zhang, X., Gui, L., Zhang, X., Bulfer, S. L., Sanghez, V., Wong, D. E., Lee, Y., Lehmann, L., Lee, J. S., Shih, P. Y., Lin, H. J., Iacovino, M., Weihl, C. C., Arkin, M. R., Wang, Y., and Chou, T. F. (2015) Altered cofactor regulation with disease-associated p97/VCP mutations. *Proceedings of the National Academy of Sciences of the United States of America* **112**, E1705-1714
68. Meyer, H., Bug, M., and Bremer, S. (2012) Emerging functions of the VCP/p97 AAA-ATPase in the ubiquitin system. *Nature cell biology* **14**, 117-123
69. Dantuma, N. P., and Hoppe, T. (2012) Growing sphere of influence: Cdc48/p97 orchestrates ubiquitin-dependent extraction from chromatin. *Trends in cell biology* **22**, 483-491
70. Franz, A., Ackermann, L., and Hoppe, T. (2014) Create and preserve: proteostasis in development and aging is governed by Cdc48/p97/VCP. *Biochimica et biophysica acta* **1843**, 205-215
71. Meyer, H., and Weihl, C. C. (2014) The VCP/p97 system at a glance: connecting cellular function to disease pathogenesis. *Journal of cell science* **127**, 3877-3883
72. Tresse, E., Salomons, F. A., Vesa, J., Bott, L. C., Kimonis, V., Yao, T. P., Dantuma, N. P., and Taylor, J. P. (2010) VCP/p97 is essential for maturation of ubiquitin-containing autophagosomes and this function is impaired by mutations that cause IBMPFD. *Autophagy* **6**, 217-227
73. Krick, R., Bremer, S., Welter, E., Schlotterhose, P., Muehe, Y., Eskelinen, E. L., and Thumm, M. (2010) Cdc48/p97 and Shp1/p47 regulate autophagosome biogenesis in concert with ubiquitin-like Atg8. *The Journal of cell biology* **190**, 965-973
74. Dantuma, N. P., Acs, K., and Luijsterburg, M. S. (2014) Should I stay or should I go: VCP/p97-mediated chromatin extraction in the DNA damage response. *Experimental cell research* **329**, 9-17
75. Ritz, D., Vuk, M., Kirchner, P., Bug, M., Schutz, S., Hayer, A., Bremer, S., Lusk, C., Baloh, R. H., Lee, H., Glatter, T., Gstaiger, M., Aebersold, R., Weihl, C. C., and Meyer, H. (2011) Endolysosomal sorting of ubiquitylated caveolin-1 is regulated by VCP and UBXD1 and impaired by VCP disease mutations. *Nature cell biology* **13**, 1116-1123
76. Meyer, H. H., Wang, Y., and Warren, G. (2002) Direct binding of ubiquitin conjugates by the mammalian p97 adaptor complexes, p47 and Ufd1-Npl4. *The EMBO journal* **21**, 5645-5652

77. Uchiyama, K., and Kondo, H. (2005) p97/p47-Mediated biogenesis of Golgi and ER. *Journal of biochemistry* **137**, 115-119
78. Chapman, E., Fry, A. N., and Kang, M. (2011) The complexities of p97 function in health and disease. *Molecular bioSystems* **7**, 700-710
79. Tang, W. K., and Xia, D. (2016) Mutations in the Human AAA+ Chaperone p97 and Related Diseases. *Frontiers in molecular biosciences* **3**, 79
80. Muller, J. M., Deinhardt, K., Rosewell, I., Warren, G., and Shima, D. T. (2007) Targeted deletion of p97 (VCP/CDC48) in mouse results in early embryonic lethality. *Biochemical and biophysical research communications* **354**, 459-465
81. Nalbandian, A., Llewellyn, K. J., Kitazawa, M., Yin, H. Z., Badadani, M., Khanlou, N., Edwards, R., Nguyen, C., Mukherjee, J., Mozaffar, T., Watts, G., Weiss, J., and Kimonis, V. E. (2012) The homozygote VCP(R(1)(5)(5)H/R(1)(5)(5)H) mouse model exhibits accelerated human VCP-associated disease pathology. *PloS one* **7**, e46308
82. Watts, G. D., Wymer, J., Kovach, M. J., Mehta, S. G., Mumm, S., Darvish, D., Pestronk, A., Whyte, M. P., and Kimonis, V. E. (2004) Inclusion body myopathy associated with Paget disease of bone and frontotemporal dementia is caused by mutant valosin-containing protein. *Nature genetics* **36**, 377-381
83. Schroder, R., Watts, G. D., Mehta, S. G., Evert, B. O., Broich, P., Fliessbach, K., Pauls, K., Hans, V. H., Kimonis, V., and Thal, D. R. (2005) Mutant valosin-containing protein causes a novel type of frontotemporal dementia. *Annals of neurology* **57**, 457-461
84. Kimonis, V. E., and Watts, G. D. (2005) Autosomal dominant inclusion body myopathy, Paget disease of bone, and frontotemporal dementia. *Alzheimer disease and associated disorders* **19 Suppl 1**, S44-47
85. Tang, W. K., and Xia, D. (2012) Structural and functional deviations in disease-associated p97 mutants. *Journal of structural biology* **179**, 83-92
86. Ching, J. K., Elizabeth, S. V., Ju, J. S., Lusk, C., Pittman, S. K., and Weihl, C. C. (2013) mTOR dysfunction contributes to vacuolar pathology and weakness in valosin-containing protein associated inclusion body myopathy. *Human molecular genetics* **22**, 1167-1179
87. Weihl, C. C., Miller, S. E., Hanson, P. I., and Pestronk, A. (2007) Transgenic expression of inclusion body myopathy associated mutant p97/VCP causes weakness and ubiquitinated protein inclusions in mice. *Human molecular genetics* **16**, 919-928
88. Caccamo, A., Majumder, S., Deng, J. J., Bai, Y., Thornton, F. B., and Oddo, S. (2009) Rapamycin rescues TDP-43 mislocalization and the associated low molecular mass neurofilament instability. *The Journal of biological chemistry* **284**, 27416-27424
89. Hubbers, C. U., Clemen, C. S., Kesper, K., Boddrich, A., Hofmann, A., Kamarainen, O., Tolksdorf, K., Stumpf, M., Reichelt, J., Roth, U., Krause, S., Watts, G., Kimonis, V., Wattjes, M. P., Reimann, J., Thal, D. R., Biermann, K., Evert, B. O., Lochmuller, H., Wanker, E. E., Schoser, B. G., Noegel, A. A., and Schroder, R. (2007) Pathological consequences of VCP mutations on human striated muscle. *Brain : a journal of neurology* **130**, 381-393

90. Halawani, D., and Latterich, M. (2006) p97: The cell's molecular purgatory? *Molecular cell* **22**, 713-717
91. Manno, A., Noguchi, M., Fukushi, J., Motohashi, Y., and Kakizuka, A. (2010) Enhanced ATPase activities as a primary defect of mutant valosin-containing proteins that cause inclusion body myopathy associated with Paget disease of bone and frontotemporal dementia. *Genes to cells : devoted to molecular & cellular mechanisms* **15**, 911-922
92. Huyton, T., Pye, V. E., Briggs, L. C., Flynn, T. C., Beuron, F., Kondo, H., Ma, J., Zhang, X., and Freemont, P. S. (2003) The crystal structure of murine p97/VCP at 3.6A. *Journal of structural biology* **144**, 337-348
93. Eletr, Z. M., and Wilkinson, K. D. (2014) Regulation of proteolysis by human deubiquitinating enzymes. *Biochimica et biophysica acta* **1843**, 114-128
94. Burrows, J. F., and Johnston, J. A. (2012) Regulation of cellular responses by deubiquitinating enzymes: an update. *Frontiers in bioscience (Landmark edition)* **17**, 1184-1200
95. Reyes-Turcu, F. E., Ventii, K. H., and Wilkinson, K. D. (2009) Regulation and cellular roles of ubiquitin-specific deubiquitinating enzymes. *Annual review of biochemistry* **78**, 363-397
96. Soboleva, T. A., and Baker, R. T. (2004) Deubiquitinating enzymes: their functions and substrate specificity. *Current protein & peptide science* **5**, 191-200
97. Ventii, K. H., and Wilkinson, K. D. (2008) Protein partners of deubiquitinating enzymes. *The Biochemical journal* **414**, 161-175
98. Chow, M. K., Mackay, J. P., Whisstock, J. C., Scanlon, M. J., and Bottomley, S. P. (2004) Structural and functional analysis of the Josephin domain of the polyglutamine protein ataxin-3. *Biochemical and biophysical research communications* **322**, 387-394
99. Weeks, S. D., Grasty, K. C., Hernandez-Cuebas, L., and Loll, P. J. (2011) Crystal structure of a Josephin-ubiquitin complex: evolutionary restraints on ataxin-3 deubiquitinating activity. *The Journal of biological chemistry* **286**, 4555-4565
100. Tzvetkov, N., and Breuer, P. (2007) Josephin domain-containing proteins from a variety of species are active de-ubiquitination enzymes. *Biological chemistry* **388**, 973-978
101. Chai, Y., Berke, S. S., Cohen, R. E., and Paulson, H. L. (2004) Poly-ubiquitin binding by the polyglutamine disease protein ataxin-3 links its normal function to protein surveillance pathways. *The Journal of biological chemistry* **279**, 3605-3611
102. Nicastro, G., Masino, L., Esposito, V., Menon, R. P., De Simone, A., Fraternali, F., and Pastore, A. (2009) Josephin domain of ataxin-3 contains two distinct ubiquitin-binding sites. *Biopolymers* **91**, 1203-1214
103. Li, X., Liu, H., Fischhaber, P. L., and Tang, T. S. (2015) Toward therapeutic targets for SCA3: Insight into the role of Machado-Joseph disease protein ataxin-3 in misfolded proteins clearance. *Progress in neurobiology* **132**, 34-58
104. Ramani, B., Harris, G. M., Huang, R., Seki, T., Murphy, G. G., Costa Mdo, C., Fischer, S., Saunders, T. L., Xia, G., McEachin, R. C., and Paulson, H. L. (2015) A knockin mouse model of spinocerebellar ataxia type 3 exhibits prominent aggregate pathology and aberrant splicing of the disease gene transcript. *Human molecular genetics* **24**, 1211-1224

105. Boy, J., Schmidt, T., Schumann, U., Grasshoff, U., Unser, S., Holzmann, C., Schmitt, I., Karl, T., Laccone, F., Wolburg, H., Ibrahim, S., and Riess, O. (2010) A transgenic mouse model of spinocerebellar ataxia type 3 resembling late disease onset and gender-specific instability of CAG repeats. *Neurobiology of disease* **37**, 284-293
106. Goti, D., Katzen, S. M., Mez, J., Kurtis, N., Kiluk, J., Ben-Haiem, L., Jenkins, N. A., Copeland, N. G., Kakizuka, A., Sharp, A. H., Ross, C. A., Mouton, P. R., and Colomer, V. (2004) A mutant ataxin-3 putative-cleavage fragment in brains of Machado-Joseph disease patients and transgenic mice is cytotoxic above a critical concentration. *The Journal of neuroscience : the official journal of the Society for Neuroscience* **24**, 10266-10279
107. Kawaguchi, Y., Okamoto, T., Taniwaki, M., Aizawa, M., Inoue, M., Katayama, S., Kawakami, H., Nakamura, S., Nishimura, M., Akiguchi, I., and et al. (1994) CAG expansions in a novel gene for Machado-Joseph disease at chromosome 14q32.1. *Nature genetics* **8**, 221-228
108. Costa Mdo, C., and Paulson, H. L. (2012) Toward understanding Machado-Joseph disease. *Progress in neurobiology* **97**, 239-257
109. Matos, C. A., de Macedo-Ribeiro, S., and Carvalho, A. L. (2011) Polyglutamine diseases: the special case of ataxin-3 and Machado-Joseph disease. *Progress in neurobiology* **95**, 26-48
110. Goto, J., Watanabe, M., Ichikawa, Y., Yee, S. B., Ihara, N., Endo, K., Igarashi, S., Takiyama, Y., Gaspar, C., Maciel, P., Tsuji, S., Rouleau, G. A., and Kanazawa, I. (1997) Machado-Joseph disease gene products carrying different carboxyl termini. *Neuroscience research* **28**, 373-377
111. Donaldson, K. M., Li, W., Ching, K. A., Batalov, S., Tsai, C. C., and Joazeiro, C. A. (2003) Ubiquitin-mediated sequestration of normal cellular proteins into polyglutamine aggregates. *Proceedings of the National Academy of Sciences of the United States of America* **100**, 8892-8897
112. Araujo, J., Breuer, P., Dieringer, S., Krauss, S., Dorn, S., Zimmermann, K., Pfeifer, A., Klockgether, T., Wuellner, U., and Evert, B. O. (2011) FOXO4-dependent upregulation of superoxide dismutase-2 in response to oxidative stress is impaired in spinocerebellar ataxia type 3. *Human molecular genetics* **20**, 2928-2941
113. Boeddrich, A., Gaumer, S., Haacke, A., Tzvetkov, N., Albrecht, M., Evert, B. O., Muller, E. C., Lurz, R., Breuer, P., Schugardt, N., Plassmann, S., Xu, K., Warrick, J. M., Suopanki, J., Wullner, U., Frank, R., Hartl, U. F., Bonini, N. M., and Wanker, E. E. (2006) An arginine/lysine-rich motif is crucial for VCP/p97-mediated modulation of ataxin-3 fibrillogenesis. *The EMBO journal* **25**, 1547-1558
114. Evert, B. O., Araujo, J., Vieira-Saecker, A. M., de Vos, R. A., Harendza, S., Klockgether, T., and Wullner, U. (2006) Ataxin-3 represses transcription via chromatin binding, interaction with histone deacetylase 3, and histone deacetylation. *The Journal of neuroscience : the official journal of the Society for Neuroscience* **26**, 11474-11486
115. Mao, Y., Senic-Matuglia, F., Di Fiore, P. P., Polo, S., Hodsdon, M. E., and De Camilli, P. (2005) Deubiquitinating function of ataxin-3: insights from the solution structure of the Josephin domain. *Proceedings of the National Academy of Sciences of the United States of America* **102**, 12700-12705

116. Satoh, T., Sumiyoshi, A., Yagi-Utsumi, M., Sakata, E., Sasakawa, H., Kurimoto, E., Yamaguchi, Y., Li, W., Joazeiro, C. A., Hirokawa, T., and Kato, K. (2014) Mode of substrate recognition by the Josephin domain of ataxin-3, which has an endo-type deubiquitinase activity. *FEBS letters* **588**, 4422-4430
117. Winborn, B. J., Travis, S. M., Todi, S. V., Scaglione, K. M., Xu, P., Williams, A. J., Cohen, R. E., Peng, J., and Paulson, H. L. (2008) The deubiquitinating enzyme ataxin-3, a polyglutamine disease protein, edits Lys63 linkages in mixed linkage ubiquitin chains. *The Journal of biological chemistry* **283**, 26436-26443
118. Nicastro, G., Todi, S. V., Karaca, E., Bonvin, A. M., Paulson, H. L., and Pastore, A. (2010) Understanding the role of the Josephin domain in the PolyUb binding and cleavage properties of ataxin-3. *PloS one* **5**, e12430
119. Berke, S. J., Chai, Y., Marrs, G. L., Wen, H., and Paulson, H. L. (2005) Defining the role of ubiquitin-interacting motifs in the polyglutamine disease protein, ataxin-3. *The Journal of biological chemistry* **280**, 32026-32034
120. Todi, S. V., Winborn, B. J., Scaglione, K. M., Blount, J. R., Travis, S. M., and Paulson, H. L. (2009) Ubiquitination directly enhances activity of the deubiquitinating enzyme ataxin-3. *The EMBO journal* **28**, 372-382
121. Thrower, J. S., Hoffman, L., Rechsteiner, M., and Pickart, C. M. (2000) Recognition of the polyubiquitin proteolytic signal. *The EMBO journal* **19**, 94-102
122. Nicastro, G., Menon, R. P., Masino, L., Knowles, P. P., McDonald, N. Q., and Pastore, A. (2005) The solution structure of the Josephin domain of ataxin-3: structural determinants for molecular recognition. *Proceedings of the National Academy of Sciences of the United States of America* **102**, 10493-10498
123. Scaglione, K. M., Zavodszky, E., Todi, S. V., Patury, S., Xu, P., Rodriguez-Lebron, E., Fischer, S., Konen, J., Djarmati, A., Peng, J., Gestwicki, J. E., and Paulson, H. L. (2011) Ube2w and ataxin-3 coordinately regulate the ubiquitin ligase CHIP. *Molecular cell* **43**, 599-612
124. Hubener, J., Vauti, F., Funke, C., Wolburg, H., Ye, Y., Schmidt, T., Wolburg-Buchholz, K., Schmitt, I., Gardyan, A., Driessen, S., Arnold, H. H., Nguyen, H. P., and Riess, O. (2011) N-terminal ataxin-3 causes neurological symptoms with inclusions, endoplasmic reticulum stress and ribosomal dislocation. *Brain : a journal of neurology* **134**, 1925-1942
125. Rodrigues, A. J., Neves-Carvalho, A., Teixeira-Castro, A., Rokka, A., Corthals, G., Logarinho, E., and Maciel, P. (2011) Absence of ataxin-3 leads to enhanced stress response in C. elegans. *PloS one* **6**, e18512
126. Kuhlbrodt, K., Janiesch, P. C., Kevei, E., Segref, A., Barikbin, R., and Hoppe, T. (2011) The Machado-Joseph disease deubiquitylase ATX-3 couples longevity and proteostasis. *Nature cell biology* **13**, 273-281
127. Elsasser, S., and Finley, D. (2005) Delivery of ubiquitinated substrates to protein-unfolding machines. *Nature cell biology* **7**, 742-749
128. Mueller, B., Klemm, E. J., Spooner, E., Claessen, J. H., and Ploegh, H. L. (2008) SEL1L nucleates a protein complex required for dislocation of misfolded glycoproteins. *Proceedings of the National Academy of Sciences of the United States of America* **105**, 12325-12330

129. Verma, R., Oania, R., Graumann, J., and Deshaies, R. J. (2004) Multiubiquitin chain receptors define a layer of substrate selectivity in the ubiquitin-proteasome system. *Cell* **118**, 99-110
130. Li, F., Macfarlan, T., Pittman, R. N., and Chakravarti, D. (2002) Ataxin-3 is a histone-binding protein with two independent transcriptional corepressor activities. *The Journal of biological chemistry* **277**, 45004-45012
131. Sacco, J. J., Yau, T. Y., Darling, S., Patel, V., Liu, H., Urbe, S., Clague, M. J., and Coulson, J. M. (2014) The deubiquitylase Ataxin-3 restricts PTEN transcription in lung cancer cells. *Oncogene* **33**, 4265-4272
132. Reina, C. P., Nabet, B. Y., Young, P. D., and Pittman, R. N. (2012) Basal and stress-induced Hsp70 are modulated by ataxin-3. *Cell stress & chaperones* **17**, 729-742
133. Bonanomi, M., Mazzucchelli, S., D'Urzo, A., Nardini, M., Konarev, P. V., Invernizzi, G., Svergun, D. I., Vanoni, M., Regonesi, M. E., and Tortora, P. (2014) Interactions of ataxin-3 with its molecular partners in the protein machinery that sorts protein aggregates to the aggresome. *The international journal of biochemistry & cell biology* **51**, 58-64
134. Wang, H., Ying, Z., and Wang, G. (2012) Ataxin-3 regulates aggresome formation of copper-zinc superoxide dismutase (SOD1) by editing K63-linked polyubiquitin chains. *The Journal of biological chemistry* **287**, 28576-28585
135. Tsou, W. L., Ouyang, M., Hosking, R. R., Sutton, J. R., Blount, J. R., Burr, A. A., and Todi, S. V. (2015) The deubiquitinase ataxin-3 requires Rad23 and DnaJ-1 for its neuroprotective role in Drosophila melanogaster. *Neurobiology of disease* **82**, 12-21
136. Menzies, F. M., Huebener, J., Renna, M., Bonin, M., Riess, O., and Rubinsztein, D. C. (2010) Autophagy induction reduces mutant ataxin-3 levels and toxicity in a mouse model of spinocerebellar ataxia type 3. *Brain : a journal of neurology* **133**, 93-104
137. Nascimento-Ferreira, I., Santos-Ferreira, T., Sousa-Ferreira, L., Auregan, G., Onofre, I., Alves, S., Dufour, N., Colomer Gould, V. F., Koeppen, A., Deglon, N., and Pereira de Almeida, L. (2011) Overexpression of the autophagic beclin-1 protein clears mutant ataxin-3 and alleviates Machado-Joseph disease. *Brain : a journal of neurology* **134**, 1400-1415
138. Seidel, K., den Dunnen, W. F., Schultz, C., Paulson, H., Frank, S., de Vos, R. A., Brunt, E. R., Deller, T., Kampinga, H. H., and Rub, U. (2010) Axonal inclusions in spinocerebellar ataxia type 3. *Acta neuropathologica* **120**, 449-460
139. Orr, H. T. (2001) Beyond the Qs in the polyglutamine diseases. *Genes & development* **15**, 925-932
140. Warrick, J. M., Morabito, L. M., Bilen, J., Gordesky-Gold, B., Faust, L. Z., Paulson, H. L., and Bonini, N. M. (2005) Ataxin-3 suppresses polyglutamine neurodegeneration in Drosophila by a ubiquitin-associated mechanism. *Molecular cell* **18**, 37-48
141. Warrick, J. M., Paulson, H. L., Gray-Board, G. L., Bui, Q. T., Fischbeck, K. H., Pittman, R. N., and Bonini, N. M. (1998) Expanded polyglutamine protein forms nuclear inclusions and causes neural degeneration in Drosophila. *Cell* **93**, 939-949
142. Sutton, J. R., Blount, J. R., Libohova, K., Tsou, W. L., Joshi, G. S., Paulson, H. L., Costa, M. D. C., Scaglione, K. M., and Todi, S. V. (2017) Interaction of the

polyglutamine protein ataxin-3 with Rad23 regulates toxicity in Drosophila models of Spinocerebellar Ataxia Type 3. *Human molecular genetics* **26**, 1419-1431

143. Hubener, J., and Riess, O. (2010) Polyglutamine-induced neurodegeneration in SCA3 is not mitigated by non-expanded ataxin-3: conclusions from double-transgenic mouse models. *Neurobiology of disease* **38**, 116-124
144. Meusser, B., Hirsch, C., Jarosch, E., and Sommer, T. (2005) ERAD: the long road to destruction. *Nature cell biology* **7**, 766-772
145. Christianson, J. C., and Ye, Y. (2014) Cleaning up in the endoplasmic reticulum: ubiquitin in charge. *Nature structural & molecular biology* **21**, 325-335
146. Stolz, A., and Wolf, D. H. (2010) Endoplasmic reticulum associated protein degradation: a chaperone assisted journey to hell. *Biochimica et biophysica acta* **1803**, 694-705
147. Ye, Y., Shibata, Y., Yun, C., Ron, D., and Rapoport, T. A. (2004) A membrane protein complex mediates retro-translocation from the ER lumen into the cytosol. *Nature* **429**, 841-847
148. Lilley, B. N., and Ploegh, H. L. (2004) A membrane protein required for dislocation of misfolded proteins from the ER. *Nature* **429**, 834-840
149. Oda, Y., Okada, T., Yoshida, H., Kaufman, R. J., Nagata, K., and Mori, K. (2006) Derlin-2 and Derlin-3 are regulated by the mammalian unfolded protein response and are required for ER-associated degradation. *The Journal of cell biology* **172**, 383-393
150. Lilley, B. N., and Ploegh, H. L. (2005) Multiprotein complexes that link dislocation, ubiquitination, and extraction of misfolded proteins from the endoplasmic reticulum membrane. *Proceedings of the National Academy of Sciences of the United States of America* **102**, 14296-14301
151. Neuber, O., Jarosch, E., Volkwein, C., Walter, J., and Sommer, T. (2005) Ubx2 links the Cdc48 complex to ER-associated protein degradation. *Nature cell biology* **7**, 993-998
152. Schuberth, C., and Buchberger, A. (2005) Membrane-bound Ubx2 recruits Cdc48 to ubiquitin ligases and their substrates to ensure efficient ER-associated protein degradation. *Nature cell biology* **7**, 999-1006
153. Ye, Y., Shibata, Y., Kikkert, M., van Voorden, S., Wiertz, E., and Rapoport, T. A. (2005) Recruitment of the p97 ATPase and ubiquitin ligases to the site of retrotranslocation at the endoplasmic reticulum membrane. *Proceedings of the National Academy of Sciences of the United States of America* **102**, 14132-14138
154. Kikkert, M., Doolman, R., Dai, M., Avner, R., Hassink, G., van Voorden, S., Thanedar, S., Roitelman, J., Chau, V., and Wiertz, E. (2004) Human HRD1 is an E3 ubiquitin ligase involved in degradation of proteins from the endoplasmic reticulum. *The Journal of biological chemistry* **279**, 3525-3534
155. Bays, N. W., and Hampton, R. Y. (2002) Cdc48-Ufd1-Npl4: stuck in the middle with Ub. *Current biology : CB* **12**, R366-371
156. Ye, Y., Meyer, H. H., and Rapoport, T. A. (2003) Function of the p97-Ufd1-Npl4 complex in retrotranslocation from the ER to the cytosol: dual recognition of nonubiquitinated polypeptide segments and polyubiquitin chains. *The Journal of cell biology* **162**, 71-84

157. Park, S., Isaacson, R., Kim, H. T., Silver, P. A., and Wagner, G. (2005) Ufd1 exhibits the AAA-ATPase fold with two distinct ubiquitin interaction sites. *Structure (London, England : 1993)* **13**, 995-1005
158. Dai, R. M., and Li, C. C. (2001) Valosin-containing protein is a multi-ubiquitin chain-targeting factor required in ubiquitin-proteasome degradation. *Nature cell biology* **3**, 740-744
159. Claessen, J. H., Kundrat, L., and Ploegh, H. L. (2012) Protein quality control in the ER: balancing the ubiquitin checkbook. *Trends in cell biology* **22**, 22-32
160. Laco, M. N., Cortes, L., Travis, S. M., Paulson, H. L., and Rego, A. C. (2012) Valosin-containing protein (VCP/p97) is an activator of wild-type ataxin-3. *PloS one* **7**, e43563
161. Liu, S., Fu, Q. S., Zhao, J., and Hu, H. Y. (2013) Structural and mechanistic insights into the arginine/lysine-rich peptide motifs that interact with P97/VCP. *Biochimica et biophysica acta* **1834**, 2672-2678
162. Almeida, B., Abreu, I. A., Matos, C. A., Fraga, J. S., Fernandes, S., Macedo, M. G., Gutierrez-Gallego, R., Pereira, P. J., Carvalho, A. L., and Macedo-Ribeiro, S. (2015) SUMOylation of the brain-predominant Ataxin-3 isoform modulates its interaction with p97. *Biochimica et biophysica acta* **1852**, 1950-1959
163. Bodnar, N. O., and Rapoport, T. A. (2017) Molecular Mechanism of Substrate Processing by the Cdc48 ATPase Complex. *Cell* **169**, 722-735.e729
164. Liu, Y., and Ye, Y. (2012) Roles of p97-associated deubiquitinases in protein quality control at the endoplasmic reticulum. *Current protein & peptide science* **13**, 436-446
165. Kuhlbrodt, K., Mouysset, J., and Hoppe, T. (2005) Orchestra for assembly and fate of polyubiquitin chains. *Essays in biochemistry* **41**, 1-14
166. Ackermann, L., Schell, M., Pokrzywa, W., Kevei, E., Gartner, A., Schumacher, B., and Hoppe, T. (2016) E4 ligase-specific ubiquitination hubs coordinate DNA double-strand-break repair and apoptosis. *Nature structural & molecular biology* **23**, 995-1002
167. Fujita, K., Nakamura, Y., Oka, T., Ito, H., Tamura, T., Tagawa, K., Sasabe, T., Katsuta, A., Motoki, K., Shiwaku, H., Sone, M., Yoshida, C., Katsuno, M., Eishi, Y., Murata, M., Taylor, J. P., Wanker, E. E., Kono, K., Tashiro, S., Sobue, G., La Spada, A. R., and Okazawa, H. (2013) A functional deficiency of TERA/VCP/p97 contributes to impaired DNA repair in multiple polyglutamine diseases. *Nature communications* **4**, 1816
168. Rao, M. V., Williams, D. R., Cocklin, S., and Loll, P. J. (2017) Interaction between the AAA(+) ATPase p97 and its cofactor ataxin3 in health and disease: Nucleotide-induced conformational changes regulate cofactor binding. *The Journal of biological chemistry* **292**, 18392-18407
169. Ogura, T., and Wilkinson, A. J. (2001) AAA+ superfamily ATPases: common structure--diverse function. *Genes to cells : devoted to molecular & cellular mechanisms* **6**, 575-597
170. Baek, G. H., Cheng, H., Choe, V., Bao, X., Shao, J., Luo, S., and Rao, H. (2013) Cdc48: a swiss army knife of cell biology. *Journal of amino acids* **2013**, 183421
171. Bug, M., and Meyer, H. (2012) Expanding into new markets--VCP/p97 in endocytosis and autophagy. *Journal of structural biology* **179**, 78-82

172. Dargemont, C., and Ossareh-Nazari, B. (2012) Cdc48/p97, a key actor in the interplay between autophagy and ubiquitin/proteasome catabolic pathways. *Biochimica et biophysica acta* **1823**, 138-144
173. Kim, H. J., Kim, N. C., Wang, Y. D., Scarborough, E. A., Moore, J., Diaz, Z., MacLea, K. S., Freibaum, B., Li, S., Molliex, A., Kanagaraj, A. P., Carter, R., Boylan, K. B., Wojtas, A. M., Rademakers, R., Pinkus, J. L., Greenberg, S. A., Trojanowski, J. Q., Traynor, B. J., Smith, B. N., Topp, S., Gkazi, A. S., Miller, J., Shaw, C. E., Kottlors, M., Kirschner, J., Pestronk, A., Li, Y. R., Ford, A. F., Gitler, A. D., Benatar, M., King, O. D., Kimonis, V. E., Ross, E. D., Weihl, C. C., Shorter, J., and Taylor, J. P. (2013) Mutations in prion-like domains in hnRNPA2B1 and hnRNPA1 cause multisystem proteinopathy and ALS. *Nature* **495**, 467-473
174. Watts, G. D., Thomasova, D., Ramdeen, S. K., Fulchiero, E. C., Mehta, S. G., Drachman, D. A., Weihl, C. C., Jamrozik, Z., Kwiecinski, H., Kaminska, A., and Kimonis, V. E. (2007) Novel VCP mutations in inclusion body myopathy associated with Paget disease of bone and frontotemporal dementia. *Clinical genetics* **72**, 420-426
175. Locke, M., Toth, J. I., and Petroski, M. D. (2014) Lys11- and Lys48-linked ubiquitin chains interact with p97 during endoplasmic-reticulum-associated degradation. *The Biochemical journal* **459**, 205-216
176. Chou, T. F., Brown, S. J., Minond, D., Nordin, B. E., Li, K., Jones, A. C., Chase, P., Porubsky, P. R., Stoltz, B. M., Schoenen, F. J., Patricelli, M. P., Hodder, P., Rosen, H., and Deshaies, R. J. (2011) Reversible inhibitor of p97, DBeQ, impairs both ubiquitin-dependent and autophagic protein clearance pathways. *Proceedings of the National Academy of Sciences of the United States of America* **108**, 4834-4839
177. Magnaghi, P., D'Alessio, R., Valsasina, B., Avanzi, N., Rizzi, S., Asa, D., Gasparri, F., Cozzi, L., Cucchi, U., Orrenius, C., Polucci, P., Ballinari, D., Perrera, C., Leone, A., Cervi, G., Casale, E., Xiao, Y., Wong, C., Anderson, D. J., Galvani, A., Donati, D., O'Brien, T., Jackson, P. K., and Isacchi, A. (2013) Covalent and allosteric inhibitors of the ATPase VCP/p97 induce cancer cell death. *Nature chemical biology* **9**, 548-556
178. Wojcik, C., Rowicka, M., Kudlicki, A., Nowis, D., McConnell, E., Kujawa, M., and DeMartino, G. N. (2006) Valosin-containing protein (p97) is a regulator of endoplasmic reticulum stress and of the degradation of N-end rule and ubiquitin-fusion degradation pathway substrates in mammalian cells. *Molecular biology of the cell* **17**, 4606-4618
179. Wojcik, C., Yano, M., and DeMartino, G. N. (2004) RNA interference of valosin-containing protein (VCP/p97) reveals multiple cellular roles linked to ubiquitin/proteasome-dependent proteolysis. *Journal of cell science* **117**, 281-292
180. Jarosch, E., Taxis, C., Volkwein, C., Bordallo, J., Finley, D., Wolf, D. H., and Sommer, T. (2002) Protein dislocation from the ER requires polyubiquitination and the AAA-ATPase Cdc48. *Nature cell biology* **4**, 134-139
181. Nishikori, S., Yamanaka, K., Sakurai, T., Esaki, M., and Ogura, T. (2008) p97 Homologs from Caenorhabditis elegans, CDC-48.1 and CDC-48.2, suppress the aggregate formation of huntingtin exon1 containing expanded polyQ repeat. *Genes to cells : devoted to molecular & cellular mechanisms* **13**, 827-838

182. Song, C., Wang, Q., and Li, C. C. (2007) Characterization of the aggregation-prevention activity of p97/valosin-containing protein. *Biochemistry* **46**, 14889-14898
183. Xu, S., Peng, G., Wang, Y., Fang, S., and Karbowski, M. (2011) The AAA-ATPase p97 is essential for outer mitochondrial membrane protein turnover. *Molecular biology of the cell* **22**, 291-300
184. Kobayashi, T., Manno, A., and Kakizuka, A. (2007) Involvement of valosin-containing protein (VCP)/p97 in the formation and clearance of abnormal protein aggregates. *Genes to cells : devoted to molecular & cellular mechanisms* **12**, 889-901
185. van den Boom, J., Wolf, M., Weimann, L., Schulze, N., Li, F., Kaschani, F., Riemer, A., Zierhut, C., Kaiser, M., Iliakis, G., Funabiki, H., and Meyer, H. (2016) VCP/p97 Extracts Sterically Trapped Ku70/80 Rings from DNA in Double-Strand Break Repair. *Molecular cell* **64**, 189-198
186. Ballar, P., Pabuccuoglu, A., and Kose, F. A. (2011) Different p97/VCP complexes function in retrotranslocation step of mammalian ER-associated degradation (ERAD). *The international journal of biochemistry & cell biology* **43**, 613-621
187. Franz, A., Ackermann, L., and Hoppe, T. (2016) Ring of Change: CDC48/p97 Drives Protein Dynamics at Chromatin. *Frontiers in genetics* **7**, 73
188. Jentsch, S., and Rumpf, S. (2007) Cdc48 (p97): a "molecular gearbox" in the ubiquitin pathway? *Trends in biochemical sciences* **32**, 6-11
189. Buchberger, A., Schindelin, H., and Hanzelmann, P. (2015) Control of p97 function by cofactor binding. *FEBS letters* **589**, 2578-2589
190. Onofre, I., Mendonca, N., Lopes, S., Nobre, R., de Melo, J. B., Carreira, I. M., Januario, C., Goncalves, A. F., and de Almeida, L. P. (2016) Fibroblasts of Machado Joseph Disease patients reveal autophagy impairment. *Scientific reports* **6**, 28220
191. Schmitt, I., Linden, M., Khazneh, H., Evert, B. O., Breuer, P., Klockgether, T., and Wuellner, U. (2007) Inactivation of the mouse Atxn3 (ataxin-3) gene increases protein ubiquitination. *Biochemical and biophysical research communications* **362**, 734-739
192. Chai, Y., Koppenhafer, S. L., Shoesmith, S. J., Perez, M. K., and Paulson, H. L. (1999) Evidence for proteasome involvement in polyglutamine disease: localization to nuclear inclusions in SCA3/MJD and suppression of polyglutamine aggregation in vitro. *Human molecular genetics* **8**, 673-682
193. Yang, H., Li, J. J., Liu, S., Zhao, J., Jiang, Y. J., Song, A. X., and Hu, H. Y. (2014) Aggregation of polyglutamine-expanded ataxin-3 sequesters its specific interacting partners into inclusions: implication in a loss-of-function pathology. *Scientific reports* **4**, 6410
194. Hirabayashi, M., Inoue, K., Tanaka, K., Nakadate, K., Ohsawa, Y., Kamei, Y., Popiel, A. H., Sinohara, A., Iwamatsu, A., Kimura, Y., Uchiyama, Y., Hori, S., and Kakizuka, A. (2001) VCP/p97 in abnormal protein aggregates, cytoplasmic vacuoles, and cell death, phenotypes relevant to neurodegeneration. *Cell death and differentiation* **8**, 977-984

195. Hanzelmann, P., and Schindelin, H. (2016) Characterization of an Additional Binding Surface on the p97 N-Terminal Domain Involved in Bipartite Cofactor Interactions. *Structure (London, England : 1993)* **24**, 140-147
196. Yeung, H. O., Kloppsteck, P., Niwa, H., Isaacson, R. L., Matthews, S., Zhang, X., and Freemont, P. S. (2008) Insights into adaptor binding to the AAA protein p97. *Biochemical Society transactions* **36**, 62-67
197. Schuetz, A. K., and Kay, L. E. (2016) A Dynamic molecular basis for malfunction in disease mutants of p97/VCP. *eLife* **5**
198. Weeks, S. D., Drinker, M., and Loll, P. J. (2007) Ligation independent cloning vectors for expression of SUMO fusions. *Protein expression and purification* **53**, 40-50
199. Zheng, L., Baumann, U., and Reymond, J. L. (2004) An efficient one-step site-directed and site-saturation mutagenesis protocol. *Nucleic acids research* **32**, e115
200. Locatelli-Hoops, S. C., Gorshkova, I., Gawrisch, K., and Yeliseev, A. A. (2013) Expression, surface immobilization, and characterization of functional recombinant cannabinoid receptor CB2. *Biochimica et biophysica acta* **1834**, 2045-2056
201. Molday, L. L., and Molday, R. S. (2014) 1D4: a versatile epitope tag for the purification and characterization of expressed membrane and soluble proteins. *Methods in molecular biology (Clifton, N.J.)* **1177**, 1-15
202. Norby, J. G. (1988) Coupled assay of Na+,K+-ATPase activity. *Methods in enzymology* **156**, 116-119
203. Ludtke, S. J., Baldwin, P. R., and Chiu, W. (1999) EMAN: semiautomated software for high-resolution single-particle reconstructions. *Journal of structural biology* **128**, 82-97
204. Scheres, S. H. (2012) RELION: implementation of a Bayesian approach to cryo-EM structure determination. *Journal of structural biology* **180**, 519-530
205. Scheres, S. H. (2012) A Bayesian view on cryo-EM structure determination. *Journal of molecular biology* **415**, 406-418
206. Lim, J. J., Lee, Y., Ly, T. T., Kang, J. Y., Lee, J. G., An, J. Y., Youn, H. S., Park, K. R., Kim, T. G., Yang, J. K., Jun, Y., and Eom, S. H. (2016) Structural insights into the interaction of p97 N-terminus domain and VBM in rhomboid protease, RHBDL4. *The Biochemical journal* **473**, 2863-2880
207. Stapf, C., Cartwright, E., Bycroft, M., Hofmann, K., and Buchberger, A. (2011) The general definition of the p97/valosin-containing protein (VCP)-interacting motif (VIM) delineates a new family of p97 cofactors. *The Journal of biological chemistry* **286**, 38670-38678
208. Buchberger, A., Howard, M. J., Proctor, M., and Bycroft, M. (2001) The UBX domain: a widespread ubiquitin-like module. *Journal of molecular biology* **307**, 17-24
209. Chou, T. F., Bulfer, S. L., Weihl, C. C., Li, K., Lis, L. G., Walters, M. A., Schoenen, F. J., Lin, H. J., Deshaies, R. J., and Arkin, M. R. (2014) Specific inhibition of p97/VCP ATPase and kinetic analysis demonstrate interaction between D1 and D2 ATPase domains. *Journal of molecular biology* **426**, 2886-2899
210. Tang, W. K., and Xia, D. (2013) Altered intersubunit communication is the molecular basis for functional defects of pathogenic p97 mutants. *The Journal of biological chemistry* **288**, 36624-36635

211. Erzurumlu, Y., Kose, F. A., Gozen, O., Gozuacik, D., Toth, E. A., and Ballar, P. (2013) A unique IBMPFD-related P97/VCP mutation with differential binding pattern and subcellular localization. *The international journal of biochemistry & cell biology* **45**, 773-782
212. Askanas, V., and Engel, W. K. (2012) *Muscle Aging : Inclusion-Body Myositis and Myopathies*, Wiley-Blackwell
213. Kondo, H., Rabouille, C., Newman, R., Levine, T. P., Pappin, D., Freemont, P., and Warren, G. (1997) p47 is a cofactor for p97-mediated membrane fusion. *Nature* **388**, 75-78
214. Ewens, C. A., Kloppsteck, P., Forster, A., Zhang, X., and Freemont, P. S. (2010) Structural and functional implications of phosphorylation and acetylation in the regulation of the AAA+ protein p97. *Biochemistry and cell biology = Biochimie et biologie cellulaire* **88**, 41-48
215. Macedo-Ribeiro, S., Cortes, L., Maciel, P., and Carvalho, A. L. (2009) Nucleocytoplasmic shuttling activity of ataxin-3. *PloS one* **4**, e5834
216. Blythe, E. E., Olson, K. C., Chau, V., and Deshaies, R. J. (2017) Ubiquitin- and ATP-dependent unfoldase activity of P97/VCP*NPLOC4*UFD1L is enhanced by a mutation that causes multisystem proteinopathy. *Proceedings of the National Academy of Sciences of the United States of America* **114**, E4380-e4388
217. Raasi, S., Orlov, I., Fleming, K. G., and Pickart, C. M. (2004) Binding of polyubiquitin chains to ubiquitin-associated (UBA) domains of HHR23A. *Journal of molecular biology* **341**, 1367-1379
218. Richly, H., Rape, M., Braun, S., Rumpf, S., Hoege, C., and Jentsch, S. (2005) A series of ubiquitin binding factors connects CDC48/p97 to substrate multiubiquitylation and proteasomal targeting. *Cell* **120**, 73-84
219. Wright, J. D., Mace, P. D., and Day, C. L. (2016) Noncovalent Ubiquitin Interactions Regulate the Catalytic Activity of Ubiquitin Writers. *Trends in biochemical sciences* **41**, 924-937
220. Schnell, J. D., and Hicke, L. (2003) Non-traditional functions of ubiquitin and ubiquitin-binding proteins. *The Journal of biological chemistry* **278**, 35857-35860
221. Dikic, I., Wakatsuki, S., and Walters, K. J. (2009) Ubiquitin-binding domains - from structures to functions. *Nature reviews. Molecular cell biology* **10**, 659-671
222. Hurley, J. H., Lee, S., and Prag, G. (2006) Ubiquitin-binding domains. *The Biochemical journal* **399**, 361-372
223. Hicke, L., Schubert, H. L., and Hill, C. P. (2005) Ubiquitin-binding domains. *Nature reviews. Molecular cell biology* **6**, 610-621
224. Miller, S. L., Malotky, E., and O'Bryan, J. P. (2004) Analysis of the role of ubiquitin-interacting motifs in ubiquitin binding and ubiquitylation. *The Journal of biological chemistry* **279**, 33528-33537
225. Fisher, R. D., Wang, B., Alam, S. L., Higginson, D. S., Robinson, H., Sundquist, W. I., and Hill, C. P. (2003) Structure and ubiquitin binding of the ubiquitin-interacting motif. *The Journal of biological chemistry* **278**, 28976-28984
226. Song, A. X., Zhou, C. J., Peng, Y., Gao, X. C., Zhou, Z. R., Fu, Q. S., Hong, J., Lin, D. H., and Hu, H. Y. (2010) Structural transformation of the tandem ubiquitin-interacting motifs in ataxin-3 and their cooperative interactions with ubiquitin chains. *PloS one* **5**, e13202

227. Prag, G., Misra, S., Jones, E. A., Ghirlando, R., Davies, B. A., Horazdovsky, B. F., and Hurley, J. H. (2003) Mechanism of ubiquitin recognition by the CUE domain of Vps9p. *Cell* **113**, 609-620
228. Polo, S., Sigismund, S., Faretta, M., Guidi, M., Capua, M. R., Bossi, G., Chen, H., De Camilli, P., and Di Fiore, P. P. (2002) A single motif responsible for ubiquitin recognition and monoubiquitination in endocytic proteins. *Nature* **416**, 451-455
229. Amerik, A. Y., and Hochstrasser, M. (2004) Mechanism and function of deubiquitinating enzymes. *Biochimica et biophysica acta* **1695**, 189-207
230. Nijman, S. M., Luna-Vargas, M. P., Velds, A., Brummelkamp, T. R., Dirac, A. M., Sixma, T. K., and Bernards, R. (2005) A genomic and functional inventory of deubiquitinating enzymes. *Cell* **123**, 773-786
231. Yao, T., Song, L., Jin, J., Cai, Y., Takahashi, H., Swanson, S. K., Washburn, M. P., Florens, L., Conaway, R. C., Cohen, R. E., and Conaway, J. W. (2008) Distinct modes of regulation of the Uch37 deubiquitinating enzyme in the proteasome and in the Ino80 chromatin-remodeling complex. *Molecular cell* **31**, 909-917
232. Sahtoe, D. D., and Sixma, T. K. (2015) Layers of DUB regulation. *Trends in biochemical sciences* **40**, 456-467
233. Meray, R. K., and Lansbury, P. T., Jr. (2007) Reversible monoubiquitination regulates the Parkinson disease-associated ubiquitin hydrolase UCH-L1. *The Journal of biological chemistry* **282**, 10567-10575
234. Seki, T., Gong, L., Williams, A. J., Sakai, N., Todi, S. V., and Paulson, H. L. (2013) JosD1, a membrane-targeted deubiquitinating enzyme, is activated by ubiquitination and regulates membrane dynamics, cell motility, and endocytosis. *The Journal of biological chemistry* **288**, 17145-17155
235. Miura, T., Klaus, W., Gsell, B., Miyamoto, C., and Senn, H. (1999) Characterization of the binding interface between ubiquitin and class I human ubiquitin-conjugating enzyme 2b by multidimensional heteronuclear NMR spectroscopy in solution. *Journal of molecular biology* **290**, 213-228
236. Pruneda, J. N., Littlefield, P. J., Soss, S. E., Nordquist, K. A., Chazin, W. J., Brzovic, P. S., and Klevit, R. E. (2012) Structure of an E3:E2~Ub complex reveals an allosteric mechanism shared among RING/U-box ligases. *Molecular cell* **47**, 933-942
237. Kumar, A., Chaugule, V. K., Condos, T. E. C., Barber, K. R., Johnson, C., Toth, R., Sundaramoorthy, R., Knebel, A., Shaw, G. S., and Walden, H. (2017) Parkin-phosphoubiquitin complex reveals cryptic ubiquitin-binding site required for RBR ligase activity. *Nature structural & molecular biology* **24**, 475-483
238. Brzovic, P. S., Lissounov, A., Christensen, D. E., Hoyt, D. W., and Klevit, R. E. (2006) A UbcH5/ubiquitin noncovalent complex is required for processive BRCA1-directed ubiquitination. *Molecular cell* **21**, 873-880
239. Wang, J., Li, B. X., Ge, P. P., Li, J., Wang, Q., Gao, G. F., Qiu, X. B., and Liu, C. H. (2015) Mycobacterium tuberculosis suppresses innate immunity by coopting the host ubiquitin system. *Nature immunology* **16**, 237-245
240. Saric, T., Muller, D., Seitz, H. J., and Pavelic, K. (2003) Non-covalent interaction of ubiquitin with insulin-degrading enzyme. *Molecular and cellular endocrinology* **204**, 11-20

241. Schmidt, T., Landwehrmeyer, G. B., Schmitt, I., Trottier, Y., Auburger, G., Laccone, F., Klockgether, T., Volpel, M., Epplen, J. T., Schols, L., and Riess, O. (1998) An isoform of ataxin-3 accumulates in the nucleus of neuronal cells in affected brain regions of SCA3 patients. *Brain pathology (Zurich, Switzerland)* **8**, 669-679
242. Todi, S. V., Laco, M. N., Winborn, B. J., Travis, S. M., Wen, H. M., and Paulson, H. L. (2007) Cellular turnover of the polyglutamine disease protein ataxin-3 is regulated by its catalytic activity. *The Journal of biological chemistry* **282**, 29348-29358
243. Studier, F. W. (2005) Protein production by auto-induction in high density shaking cultures. *Protein expression and purification* **41**, 207-234
244. Ohno, A., Jee, J., Fujiwara, K., Tenno, T., Goda, N., Tochio, H., Kobayashi, H., Hiroaki, H., and Shirakawa, M. (2005) Structure of the UBA domain of Dsk2p in complex with ubiquitin molecular determinants for ubiquitin recognition. *Structure (London, England : 1993)* **13**, 521-532
245. Hicke, L., and Dunn, R. (2003) Regulation of membrane protein transport by ubiquitin and ubiquitin-binding proteins. *Annual review of cell and developmental biology* **19**, 141-172
246. Masino, L., Nicastro, G., Calder, L., Vendruscolo, M., and Pastore, A. (2011) Functional interactions as a survival strategy against abnormal aggregation. *FASEB journal : official publication of the Federation of American Societies for Experimental Biology* **25**, 45-54
247. Hofmann, K., and Falquet, L. (2001) A ubiquitin-interacting motif conserved in components of the proteasomal and lysosomal protein degradation systems. *Trends in biochemical sciences* **26**, 347-350
248. Traut, T. (2008) *Allosteric Regulatory Enzymes*, Springer, New York
249. Osz, J., Bodo, G., Branca, R. M., and Bagyinka, C. (2005) Theoretical calculations on hydrogenase kinetics: explanation of the lag phase and the enzyme concentration dependence of the activity of hydrogenase uptake. *Biophysical journal* **89**, 1957-1964
250. Kamata, K., Mitsuya, M., Nishimura, T., Eiki, J., and Nagata, Y. (2004) Structural basis for allosteric regulation of the monomeric allosteric enzyme human glucokinase. *Structure (London, England : 1993)* **12**, 429-438
251. Bowler, J. M., Hervert, K. L., Kearley, M. L., and Miller, B. G. (2013) Small-Molecule Allosteric Activation of Human Glucokinase in the Absence of Glucose. *ACS medicinal chemistry letters* **4**
252. Vugmeyster, Y., Borodovsky, A., Maurice, M. M., Maehr, R., Furman, M. H., and Ploegh, H. L. (2002) The ubiquitin-proteasome pathway in thymocyte apoptosis: caspase-dependent processing of the deubiquitinating enzyme USP7 (HAUSP). *Molecular immunology* **39**, 431-441
253. Shen, C., Ye, Y., Robertson, S. E., Lau, A. W., Mak, D. O., and Chou, M. M. (2005) Calcium/calmodulin regulates ubiquitination of the ubiquitin-specific protease TRE17/USP6. *The Journal of biological chemistry* **280**, 35967-35973
254. Wada, K., and Kamitani, T. (2006) UnpEL/Usp4 is ubiquitinated by Ro52 and deubiquitinated by itself. *Biochemical and biophysical research communications* **342**, 253-258

255. Fernandez-Montalvan, A., Bouwmeester, T., Joberty, G., Mader, R., Mahnke, M., Pierrat, B., Schlaeppi, J. M., Worpenberg, S., and Gerhartz, B. (2007) Biochemical characterization of USP7 reveals post-translational modification sites and structural requirements for substrate processing and subcellular localization. *The FEBS journal* **274**, 4256-4270
256. Nicastro, G., Habeck, M., Masino, L., Svergun, D. I., and Pastore, A. (2006) Structure validation of the Josephin domain of ataxin-3: conclusive evidence for an open conformation. *Journal of biomolecular NMR* **36**, 267-277
257. Grasso, G., Tuszynski, J. A., Morbiducci, U., Licandro, G., Danani, A., and Deriu, M. A. (2017) Thermodynamic and kinetic stability of the Josephin Domain closed arrangement: evidences from replica exchange molecular dynamics. *Biology direct* **12**, 2
258. Deriu, M. A., Grasso, G., Tuszynski, J. A., Gallo, D., Morbiducci, U., and Danani, A. (2016) Josephin Domain Structural Conformations Explored by Metadynamics in Essential Coordinates. *PLoS computational biology* **12**, e1004699
259. Masino, L., Musi, V., Menon, R. P., Fusi, P., Kelly, G., Frenkiel, T. A., Trottier, Y., and Pastore, A. (2003) Domain architecture of the polyglutamine protein ataxin-3: a globular domain followed by a flexible tail. *FEBS letters* **549**, 21-25
260. Beal, R., Deveraux, Q., Xia, G., Rechsteiner, M., and Pickart, C. (1996) Surface hydrophobic residues of multiubiquitin chains essential for proteolytic targeting. *Proceedings of the National Academy of Sciences of the United States of America* **93**, 861-866
261. Sloper-Mould, K. E., Jemc, J. C., Pickart, C. M., and Hicke, L. (2001) Distinct functional surface regions on ubiquitin. *The Journal of biological chemistry* **276**, 30483-30489
262. Rumpf, S., and Jentsch, S. (2006) Functional division of substrate processing cofactors of the ubiquitin-selective Cdc48 chaperone. *Molecular cell* **21**, 261-269
263. Jelinsky, S. A., Estep, P., Church, G. M., and Samson, L. D. (2000) Regulatory networks revealed by transcriptional profiling of damaged Saccharomyces cerevisiae cells: Rpn4 links base excision repair with proteasomes. *Molecular and cellular biology* **20**, 8157-8167
264. Verma, R., Aravind, L., Oania, R., McDonald, W. H., Yates, J. R., 3rd, Koonin, E. V., and Deshaies, R. J. (2002) Role of Rpn11 metalloprotease in deubiquitination and degradation by the 26S proteasome. *Science (New York, N.Y.)* **298**, 611-615
265. Wang, Y., Satoh, A., Warren, G., and Meyer, H. H. (2004) VCIP135 acts as a deubiquitinating enzyme during p97-p47-mediated reassembly of mitotic Golgi fragments. *The Journal of cell biology* **164**, 973-978
266. Sowa, M. E., Bennett, E. J., Gygi, S. P., and Harper, J. W. (2009) Defining the human deubiquitinating enzyme interaction landscape. *Cell* **138**, 389-403
267. Ernst, R., Mueller, B., Ploegh, H. L., and Schlieker, C. (2009) The otubain YOD1 is a deubiquitinating enzyme that associates with p97 to facilitate protein dislocation from the ER. *Molecular cell* **36**, 28-38
268. Schuck, P., and Zhao, H. (2010) The role of mass transport limitation and surface heterogeneity in the biophysical characterization of macromolecular binding processes by SPR biosensing. *Methods in molecular biology (Clifton, N.J.)* **627**, 15-54

269. Le, L. T., Kang, W., Kim, J. Y., Le, O. T., Lee, S. Y., and Yang, J. K. (2016) Structural Details of Ufd1 Binding to p97 and Their Functional Implications in ER-Associated Degradation. *PloS one* **11**, e0163394
270. Lee, J. J., Park, J. K., Jeong, J., Jeon, H., Yoon, J. B., Kim, E. E., and Lee, K. J. (2013) Complex of Fas-associated factor 1 (FAF1) with valosin-containing protein (VCP)-Npl4-Ufd1 and polyubiquitinated proteins promotes endoplasmic reticulum-associated degradation (ERAD). *The Journal of biological chemistry* **288**, 6998-7011